بِسْمِ اللَّهِ الرَّحْمَٰنِ الرَّحِيمِ

الجمهورية الجزائرية الديمقراطية الشعبية

République Algérienne Démocratique et Populaire

Ministère de L'Enseignement Supérieur et de la Recherche Scientifique

Université Ferhat ABBAS Sétif 1

UNIVERSITÉ FERHAT ABBAS - SETIF1

INSTITUT D'OPTIQUE ET MÉCANIQUE DE PRÉCISION

THÈSE

Présentée Au Département D'Optique Pour L'Obtention Du Diplôme De

DOCTORAT

Domaine : Sciences et Technologie

Filière : Optique et Mécanique de Précision

Option : Optique et Photonique Appliquée

Par

BENDADA Hana

THÈME

Exploitation Du Formalisme De Stokes-Mueller Pour La Caractérisation Des Propriétés Optiques Et Structurales Des Matériaux

Soutenue le 19/02/2025 devant le Jury :

MANALLAH Aissa	**Professeur**	**Univ. Ferhat Abbas Sétif 1**	**Président**
BAKHOUCHE Belkacem	**Professeur**	**Univ. Ferhat Abbas Sétif 1**	**Directeur de thèse**
BENCHEIKH Abdelhalim	**Professeur**	**Univ. Mohamed El Bachir El-Ibrahim Bordj Bou Arréridj**	**Examinateur**
NOURI Abdelhak	**M.C.A.**	**Univ. Ferhat Abbas Sétif 1**	**Examinateur**

قطعا لا نرتقي الى تلك العلياء و لكن:

الى **فلسطين** الشهيدة

Contents

Acknowledgments

In the Name of "الله", the Most Gracious, the Most Merciful.

I would like to express my deepest gratitude to **Pr. Belkacem Bakhouche**, my supervisor, mentor, and guide throughout this journey. From the moment he accepted me as his student, he welcomed me with open arms, not just as a scholar but as a daughter. His high morals, kindness, and unwavering support have been a source of inspiration to me. Whenever I faced difficulties, his door was always open, offering not only guidance but also comfort in my darkest moments. Pr. Bakhouche's constant encouragement gave me the strength to persevere, and his profound wisdom shaped me as both a researcher and a person. It is impossible to overstate how much I have learned from him—not just academically but in the ways of patience, humility, and generosity. His gentle and corrective nature made this journey a meaningful one, and I consider myself incredibly fortunate to have had such a mentor. As we reach the end of this beautiful chapter, I find myself saddened by the thought of no longer walking this path together. Pr. Bakhouche has been more than a supervisor; he has been a father figure who guided me with care and compassion. Though this partnership comes to a close, the lessons I have learned and the respect I hold for him will remain with me always.

I owe my deepest gratitude to Dr. Oriol Arteaga, whose guidance and support have been invaluable throughout this journey. The nine months I spent in his lab were, without a doubt, the most fruitful and enriching period of my work on this thesis. I am incredibly grateful for the warm welcome he extended, the freedom he allowed me to explore and experiment with his equipment, and the patience he showed through all the mistakes I made along the way. I also can't forget to thank him for all the lunches he so generously treated me to. Above all, I cherish the wealth of knowledge I gained during my time in his lab, which has been an inspiration throughout this thesis.

As this journey draws to a close with my PhD defence approaching, I wish to express my deepest gratitude to the esteemed jury members: Professor MANALLAH Aissa as the Jury president, Professor BENCHEIKH Abdelhalim, Professor BOUCHERIT Sebti and Doctor NOURI Abdelhak. I am truly indebted to them for graciously offering their valuable time to evaluate my work. Their insightful feedback and guidance will not only help refine my research but also provide me with the professional direction I need as I move forward into the next chapter of my life.

My acknowledgement, though never enough, to my beloved mother; she is the sun that has illuminated every shadowed corner of my life. Her endless love is the softness that has filled my soul, even in moments of doubt. Her whispered prayers have been my compass, guiding me through the stormiest seas. Every success of mine reflects her unyielding strength; every step forward is a tribute to her gentle hands that carried me when I could not stand. In the quiet strength of her sacrifice and the warmth of her embrace, I have found the courage to dream. To the one whose heart beats in harmony with mine, I owe everything.

To my dear father, the rock upon which I have built the foundation of my dreams. His wisdom has been the steady wind beneath my wings, and his quiet endurance, my shield against the trials of life. With every word of encouragement, you have sown seeds of belief within me, and through your unwavering support, those seeds have blossomed into the heights I now reach. Your silent strength has been the silent roar that has driven me forward, and for that, I am eternally grateful.

I am profoundly grateful to my sister Soundous, who stood by my side through every moment. She wiped away my tears, took on all the responsibilities of the home, and gifted me the precious time I needed to complete this journey. She spoke words of kindness and encouragement that no one else ever has, uplifting me when I needed it most. For all the moments of selflessness, for the endless support she gave, and for making me strong simply by being there, I owe her my deepest thanks. My gratitude extends to my dear brothers, Sifeddine, Rahim and Raouf, who have been unwavering pillars of support throughout this journey. Their constant presence has been a source of strength, and they have always made me feel the immense pride they carry for me. For being the shield that protects me through every challenge.

During my journey, I found myself in a foreign land, but I was fortunate never to be alone. Two remarkable and extraordinary women, Khalti Fatima and Fadella, were there for me, offering unwavering financial and emotional support. They spared no effort in helping me, becoming like second mothers, and for that, I am deeply grateful.

This work is a culmination of 7 years of study, and an acknowledgement must be addressed to all the colleagues who saved no effort to help me, and to give me the impetus to carry on my studies; Among many Subiao, Huihui, Sarrah, Dale, Islam, the kindest persons ever: Imane Mayouf, Tahar Aouissi and Bekis Hocine. In addition to Slimi Younes, a dear friend who gave me the opportunity to have been to Germany and offered me to join him as a colleague.

I extend my heartfelt thanks to everyone who supported me, whether from near or afar, throughout my PhD journey. Your encouragement, guidance, and belief in me—whether through words, actions, or simply your presence—have been invaluable, and for that, I am deeply grateful.

Introduction

Polarimetry, the study of the polarization of light and its interaction with matter, has a rich history spanning over two centuries. Its roots can be traced back to the early 19th century when French astronomer François Arago employed a prismatic device with a birefringent crystal to observe celestial objects [1]. This primitive polariscope is regarded as one of the first polarimeters used for scientific purposes. Shortly after, Jean-Baptiste Biot built upon Arago's work by applying polarimetric methods to the study of optical rotation, most notably in sugary solutions. Biot's findings laid the groundwork for the development of the polarimetric saccharimeter, a device that remains essential in determining the concentration of optically active substances [2, 3].

Around the mid-19th century, Sir George Gabriel Stokes made a significant advancement in the understanding of polarization. His empirical work resulted in the definition of four measurable quantities now known as Stokes parameters, which provide a comprehensive description of the polarization state of light [4]. While these parameters marked a major milestone in polarization optics, Stokes' work was underappreciated for nearly a century. It was not until the mid-20th century that his contributions gained the recognition they deserved, thanks to the coupling of his empirical approach with the then-maturing mathematical matrix calculus developed by R.C. Jones in 1941 and Hans Mueller in 1948[5, 6]. This synthesis of ideas culminated in the Stokes-Mueller formalism, a robust mathematical framework that provides a complete description of light polarization states and allows for the detailed characterization of materials' optical properties.

Interferometry, a technique historically intertwined with the study of light polarization, has also played a critical role in advancing polarimetric methods. In 1817, the interferomitrist Thomas Young proposed the transverse nature of light waves as an interpretation of the work's result of the polarimetrists Arago and Augustin-Jean Fresnel while studying the interference of polarized light [7]. This discovery laid the foundation for understanding the wave nature of light and its interaction with materials. More than a century later, in 1956, Indian physicist S. Pancharatnam, again, while studying the interference of polarized

light, identified the geometric phase—an additional phase shift that depends on the path traversed by polarization on the Poincaré sphere[8]. This concept of the geometric phase, later expanded by M.V. Berry in the context of quantum mechanics [9], revolutionized the design of optical devices, leading to the creation of advanced photonic devices with unparalleled precision and performance.

In the last three decades, the rapid advancement of technology has led to the development of new optical materials and devices, expanding the scope of polarimetric techniques. Polarimetry has kept pace with these developments, emerging as a powerful tool for the fast and precise characterization of materials with diverse properties. In fields ranging from biology and chemistry to material science and physics, polarimetry has proven to be indispensable, offering unique insights into the optical properties of substances.

Building on this historical foundation, polarimetry continues to evolve with new methods and techniques. The introduction of structured light, which involves controlling the spatial, phase, and polarization properties of light, has opened up new avenues for research. Geometric phase optical elements, for example, can manipulate the wavefront structure of light in ways that were previously unattainable. This control, achieved through birefringent effects, offers potential applications in areas such as microscopy, imaging, and telecommunications.

Another significant area of advancement is spectral domain polarimetry, where polarization information is stored in the spectral domain. The development of techniques like channeled polarimetry allows for the extraction of polarization information from the Fourier transform of light's intensity as a function of wavenumber, offering a novel approach to analyzing polarization [10]. While traditional time-modulated systems remain dominant, spectral domain analysis presents a compact, fast, and cost-effective alternative for specific applications. For instance, measuring optical rotation in highly diluted solutions or investigating birefringence in complex materials are areas where this method shows particular promise.

The combination of historical achievements, technological advancements, and the development of new analytical methods underscores the enduring significance of polarimetry. It remains a cornerstone of optical characterization, offering unparalleled precision and versatility in the analysis of materials. As researchers continue to explore the boundaries of light-matter interactions, polarimetric techniques will undoubtedly play a central role in uncovering new phenomena and enabling the development of next-generation optical devices.

Organization

The present manuscript has been structured to cover the work undertaken to address the Stokes-Mueller formalism's utility for the optical and structural characterization of materials of various natures. As traditionally has been the case, it contains two major parts: Theory and Contribution.

Part I: divided into two theoretical segments. the first one delves, as an opening text, into ***the historical evolution of light polarization and polarimetry***. A story that might seem long and boring, but it gives a deep conscience of the importance of patience while conducting scientific research and evokes a strong sense of duty as the young new generation of researchers. The second segment has been considered as ***Chapter 1***. It takes a complete account of the bifurcated theory of Stokes-Mueller Polarimetry that has been, to some extent, adapted to encompass the ad hoc studies undertaken along the rest of the manuscript.

Part II: comprises three chapters. ***Chapter 2*** is dedicated to establishing a novel proposed method to extract optical properties from the modified calculated Mueller matrix. The principles and calculations of this method are extendedly detailed. ***Chapter 3*** focuses on the polarimetric evaluation of the Geometric Phase optics without resorting to interferometry. Principles of working, experiments, and interpretations of results are included. As a subject of scientific publication, ***Chapter 4*** describes the spectral polarimetry with wavelength domain analysis without resorting to Fourier transform. The methodology of investigation, the offered features, and the development of this new method, all along with its application to small optical rotation measurements, are detailed within this last chapter.

Conclusions and Future Perspectives were the concluding text writing of this PhD thesis entitled: **Exploitation of Stokes-Mueller Formalism for the Characterization of Optical and Structural Properties of Materials.**

Part I

Background:
History and Basics

State of the art:

landmarks in the woven history of polarized light

The study of polarization is deeply intertwined with the development of the wave theory of light. This theory presents a cornerstone of modern optics, and it has successfully interpreted and explained various optical phenomena that captivated scientists for centuries. While a comprehensive review of the entire history is beyond the scope of this thesis, this section will examine the key milestones and contributions that shaped our current understanding of light's wave nature and, therefore, our understanding of the light polarization phenomenon.

To establish a foundation for our own research contribution, this brief history delves into some discoveries and scientific theories related to light polarization's explanation, geometrical presentations, and mathematical calculations; we will provide a more detailed analysis of these pivotal advancements. A concise overview of other relevant developments will be presented. For clarity and coherence, this section is divided into two distinct periods, delineated by Fresnel's establishment of the wave theory of light in 1821.

- **Corpuscular or Wave, Longitudinal or Transverse: Polarization Battles**

Pinpointing the exact date of "light polarization" manifestation as an optical concept for the first time is a bit challenging. The scientific understanding of the phenomenon itself developed gradually over time. Through inspection of various research materials reviewing light polarization and\or polarimetry, it was clear that the first documented physical observation related to this optical phenomenon was in:

1669 by ***Erasmus Bartholinus***, the Danish physician who published an accurate description of the double refraction of a ray of light by Iceland spar (calcite), in which he

used for the first time an everlasting utilized terms in optical physics: **the ordinary and extraordinary refraction** [11].
although he could not find the true cause of birefringence, his observations allowed it to be discovered in:

1677 by ***Christiaan Huygens***, Dutch physicist and astronomer, He presented one of the strongest arguments supporting the wave theory of light in his "Treatise on Light," through his **construction of propagating wavefronts**. Huygens' law asserts that at any point within a crystal, the light disturbance generates two wavefronts: a spherical one for the ordinary ray and a spheroidal one for the extraordinary ray, with every point on a wavefront acting as a source of tiny wavelets. The original French title of Huygens's first publication on the properties of light, completed in 1678 and published in **1960**, is "*Traité de la Lumière: Où sont expliquées les causes de ce qui luy arrive dans la reflexion et dans la refraction. Et particulièrement dans l'étrange refraction du cristal d'Islande.*" Additionally, he made a significant experimental observation that doubly diffracted rays behaved differently from regular light when entering a second crystal. Unfortunately, this experiment lacked a satisfactory interpretation, leading to Huygens's work being discredited for over a century. [7, 12].

Based on an alternate description of atomism, in:

1704 ***Isaac Newton***, an English polymath, published "Newton's Opticks" which was considered the definitive text on the subject throughout the 18th century. In it, Newton set out his **corpuscular or emission theory**, whereby light consists of molecules emitted by luminous bodies. This idea explained rays of light insofar as these corpuscles were said to travel in straight lines. He favored this paradigm to explain the phenomenon of Newton's rings, which are colored rings observed when a curved surface touches a flat surface very closely. He used a concept called the "method of fits". This theory suggested light particles cycled between states that were more likely to reflect or be transmitted when encountering a surface. Thicker air gaps caused the light to be in a state prone to reflection, while thinner parts allowed transmission. According to Newton's theory, color

was generated uniquely at the second reflecting surface of the thin films. This treatise also contained many of the basic principles of the wave theory of light; therefore, we can see that Newton embraced simultaneously features of two opposite theories [3, 13, 14].

by the turn of the century, the wave theory was revived in:

1801 by ***Thomas Young***, an English former physician. He conducted the now-famous **double-slit experiment** with light. This experiment provided strong evidence for the wave theory of light and demonstrated the phenomenon of light wave interference. Young's work on wave theory provided a framework for understanding double refraction, so that, In **1802**, following Young's proposal, *William Hyde Wollaston* conducted experimental investigations into the validity of Huygens' construction for the extraordinary ray. His findings showed remarkable consistency, despite the fact that the phenomenon of two rays emerging from a single material was not yet fully comprehended. [7].

The early nineteenth century was a pivotal period in the history of optics, marked by intense debate between the Newtonian corpuscular theory and the Huygenian undulatory theory. While the corpuscular theory initially held more sway, this era also saw significant advancements in optical science due to a concerted effort to integrate mathematics with experimental physics. In France, a flourishing research environment emerged as the scientific society initiated a program to mathematize experimental physics. This program was driven by a new generation of highly trained physicists in laboratory techniques and mathematical theory. This dual emphasis on theory and practice laid the groundwork for several groundbreaking discoveries in optical science.
In the decade before Fresnel's work, the corpuscular theory of light was actively used in the interpretation of new data, and from which the **corpuscular theory of polarization** derived in:

1808 by ***Étienne Louis Malus*** , the French engineer who has conducted a study that had two significant implications for the history of polarization. First, he confirmed and expanded Huygens's seventeenth-century Law regarding the direction of the extraor-

dinary ray in Iceland spar, extending its applicability to other doubly refracting crystals. Second, one evening, Malus observed variations in the intensities of double-refracted images when a calcite crystal was rotated, leading to the formulation of Malus's Law. This law asserts that the transmitted light intensity through a polarizer is proportional to the cosine squared of the angle between the polarizer's transmission axis and the polarization direction of the incident light.($I = I_0 \cos^2(\theta)$). Malus's discovery of light **polarization by reflection** supported the corpuscular theory of light, hypothesizing that just like magnetic **poles** cause magnetic materials to align in a particular direction, the reflection process causes the light corpuscles to align in a specific way, and based on that he coined, inaugurally, the term **"Polarization"** and suggested that a completely polarized beam being formed of molecules with identically oriented poles [1, 7, 15–17].

Malus observed that natural light reflected by a transparent glass surface at an angle close to 57°could be completely extinguished when viewed through a crystal. He suggested that natural light consists of mutually perpendicular s- and p-polarizations but did not establish the relationship between material properties and polarizing angles. it was with more persistence that in:

1811 ***David Brewster***, the Scottish physicist, He discovered the law that bears his name, which relates to polarization caused by reflection. Which he revealed in a paper form **1815**. He measured the polarizing angle for various materials and unravelled that maximum light polarization occurs at a specific angle of incidence, now known as **Brewster's angle**, where the reflected and refracted rays are perpendicular. **Brewster's Law** states that the tangent of this angle equals the material's refractive index, resulting in complete polarization of the reflected light [18].

Several physicists worked extensively on polarization in the years immediately following Malus's discovery of light polarization by reflection. Notably, the subsequent era was marked by a productive scientific rivalry between two distinguished physicists, viz., *Arago* and Biot. Both possessed exceptional intellectual insight and experimental skills. As we will demonstrate later, their competitive pursuit of light polarization-related study

significantly contributed to establishing the wave theory of light. To start in

1811 ***Dominique-François-Jean Arago***, the physicist, mathematician, and astronomer, better known simply as *François Arago*, discovered a series of polarization phenomena, collectively termed "**Polarisation Colorée**", best translated as “chromatic polarization”, which he detailed in his notable paper delivered on August 11, 1811. While verifying telescope components, Arago investigated the effects of fully polarized light on Newton’s rings and the potential for improving objective lens design through polarized light properties.
Arago used a lunette prismatic with a double-refracting prism, likely a Rochon prism, to observe celestial objects. This device also served as a double-refracting analyzer in a modified Newton rings setup. By inserting a thin mica sheet, he observed that polarized light produced complementary colors in the images formed by the analyzer, a phenomenon he termed **chromatic polarization**. He incorporated this principle into a polarimeter, discovering that moonlight was polarized. Additionally, Arago noted that the intensity of the complementary colors varied with the rotation of the mica sheet or the analyzer, identifying this modification as "**depolarization**". He found similar effects with other birefringent materials like gypsum but not with quartz plates cut perpendicular to their axis. In quartz, polarized light showed no birefringence along the axis but exhibited color and polarization effects after analysis, indicating **circular polarization**.

Arago’s experiments led to the first observations of **optical rotation** and **optical rotatory dispersion**, though he did not fully distinguish between rotatory and chromatic polarization. This distinction was later clarified by Biot, who conducted a comprehensive study of these phenomena [1–3, 19, 20].

A rift over this discovery was placed between colleagues, co-workers, and even close friends, Arago and Biot; this latter tried to claim credit for himself as a priority. However, Arago protested that Biot pre-empted his discovery and proved it by citing his own prior observations documented in laboratory notebooks. A feud began because of this incident. Historians and contemporaries have seen Biot’s quick and possibly heavy-handed

approach to the field Arago had opened as an improper takeover of a novel-uncovered subject. Arago's discovery was developed starting from:

1812 ***Jean-Baptiste Biot***, Arago's fiercest competitor, significantly advanced the field of optics with his discovery of **rotatory polarization** during a series of presentations to the Académie des Sciences between November 30, 1812, and May 31, 1813, later published in 1814. Biot observed that quartz plates cut perpendicular to the axis induced a wavelength-dependent rotation of the plane of polarized light. **He distinguished between chromatic polarization, which manifested as color changes, and rotary polarization, which resulted in a varying rotation angle**, with shorter wavelengths experiencing larger rotations. Biot further demonstrated that by using a calibrating factor and Newton's table, he could **estimate the tint of the observed ray**. He applied a modified version of Malus's sine-squared formalism to rotary polarization, deriving formulas for the intensities of the colored images. His experiments revealed that quartz plates could produce either **dextro-rotation** or **levo-rotation** (the plane of polarization rotated in respectively clockwise or counterclockwise direction), with the rotation's magnitude directly proportional to the plate's thickness, and that an equally thick plate could cancel out the effects of one rotational direction with the opposite direction. Biot, a proponent of the corpuscular theory, explained these polarization effects through the hypothesis of oscillating light molecules, known as the theory of "mobile polarization" [1–3, 21–23].

Also, an entirely new field of research was opened up in:

1815 by ***Biot***, when he made the significant discovery of the **rotatory power of certain liquids** such as turpentines or solutions of natural occurring solids such as camphor. **Cane sugar (sucrose)** was recorded to be among the list, all along with other sugary liquids, later in **1818** [20].

A significant shift in the debate over wave theory occurred when Arago, previously a supporter of corpuscular theory, changed his stance. The results of a series of exper-

iments that he had conducted refuted his earlier corpuscular conclusions on gaseous refraction with Biot. By 1815, Arago became a proponent of wave theory, aligning himself with Augustin Jean Fresnel, whom he strongly supported at the Institut de France. So that, in:

1816 ***Augustin Jean Fresnel***, A french civil engineer with remarkable mathematical prowess and practical ingenuity, together with Arago, investigated the interference of polarized rays of light and found that, in every case, While two rays polarized in the same direction can interfere if they come from the same polarized source, two beams with perpendicular polarizations do not exhibit interference, and their total intensity remains constant when reunited, regardless of path differences. This finding forms one of **the Arago-Fresnel laws of polarization.**

During a visit to Young in 1816, Arago shared with him the new discovery he had with Fresnel, which provided crucial evidence supporting the wave theory of light. In:

1817 ***Thomas Young***, through a letter to Arago and an article for the Encyclopaedia Britannica, he discovered the missing piece of the puzzle and initially suggested the crucial **link between the undulatory theory of light and polarization phenomena: "the transversality of light vibrations."**

By that time, Fresnel was devoting his time to work on diffraction; he made an experimental and theoretical study of it, which he was emboldened enough to present to the French Academy of Sciences in:

1818 ***Fresnel*** described light as consisting of waves and introduced the **concept of wavelength** as a fundamental characteristic of these waves.

Next year, Arago conveyed Young's ideas to Fresnel, who quickly recognized them as the primary explanation for their experimental results and all known polarization phenomena at that time. Working on this brilliant, controversial idea, Fresnel turned

his attention to the study of birefringent crystals, focusing on double refraction and polarization. In

1821 ***Fresnel*** developed the theory of double refraction in uniaxial and biaxial crystals, culminating in what is considered his crowning achievement, published in a memoir and supplements between **November 1821 and March 1822**. Fresnel quickly **interpreted natural light as a superposition of waves polarized in all possible directions, viewing polarization as a manifestation of wave transversality.** He considered direct light to be a rapid succession of waves polarized in various directions. In this context, **polarization involves decomposing the transverse motions into fixed directions and separating the components, allowing the oscillatory motions in each component to occur in the same plane.** This transversality allowed him to demonstrate how a **transverse wave striking an isotropic medium divides into a reflected and a refracted beam, with each beam being partially polarized.**. By early 1822, Fresnel's **wave theory of light**, based on simple principles such as transversality, interference, wavelength dependence, and the conservation of energy, provided a comprehensive explanation for a wide range of optical phenomena, namely, reflection, refraction, double refraction, polarization, diffraction, and interference [1, 3, 7, 24–26].

The foundation of the wave theory in France is indebted to Arago's encouragement as much as it is to Fresnel's experimental insight. This foundation marked a turning point in investigating light polarization-related phenomena, especially in the mathematical realm, which succeeded greatly, as we detail in what follows.

- ## Mathematical framing of polarization and polarimetry

Based on the wave nature of light, as understood from the earlier work of Thomas Young and Augustin-Jean Fresnel, dating in:

1852 ***Sir George Gabriel Stokes***, British mathematician and physicist, published a paper in which he established a mathematical formalism ideal for describing the state of

polarization of any light beam. He stated that "**the optical properties of any mixture of independent polarized light streams are entirely determined by four constants. These constants are functions of the intensities, azimuths, and eccentricities of the ellipses characterizing the individual streams.**". Stokes studied the behavior of polarized light, particularly how it interacted with different materials and surfaces. His work was purposefully empirical and resulted in the development of observable quantities of phenomenological polarization optics [4, 25].

The significance of this work remained obscure and underappreciated, failing to receive the recognition it deserved for more than seventy years. Stokes's paper was rediscovered by the Nobel laureate ***Subrahmanyan Chandrasekhar*** in **1947** while writing his fundamental papers on radiative transfer [27]. Chandrasekhar had a prestigious and well-established position in the scientific community, and thereby Stokes's work became well-known. Soon after Chandrasekhar's publications on radiative transfer, ***Ugo Fano*** demonstrated that the Stokes parameters serve as an excellent analytical method for addressing polarization issues in both classical optics and quantum mechanics [25].
By bringing together the work that had been done by brilliant physicists, in particular, **Faraday's law of induction**. In:

1861 ***James Clerk Maxwell*** the Scottish theoretical physicist and mathematician formulated the theory of electromagnetism, culminating in Maxwell's equations, which describe the interactions and propagation of electric and magnetic fields. He demonstrated that electromagnetic waves travel at a speed shown to be the known speed of light, concluding that **light is an electromagnetic wave**. Maxwell's work confirmed the transverse nature of light waves, as only transverse components arise in free space. He explained that **Light waves are composed of oscillating electric and magnetic fields that are mutually perpendicular and also perpendicular to the direction of wave propagation. By concentrating on the electric field—given that varying electric fields generate comparatively weaker magnetic fields Maxwell's theory could successfully explain the properties and behavior of polarized light**.

Maxwell's theory was verified by direct experiments in **1888** by the German physicist ***Heinrich Hertz*** [7, 25, 28].

Not clear whether building upon Stokes parameters or not being aware of them, in a text from:

1892 ***Jules Henri Poincaré*** mapped all polarization states onto the surface of a sphere, which is now known as **the Poincaré sphere**. This mapping allowed for a comprehensive understanding of various polarization states, including elliptical polarization. The center of the sphere corresponds to natural light, whereas the surface corresponds to totally polarized light, and within it lies the partially polarized light. Poincaré **represented changes in polarization as rotations on the sphere** [25].

Before the iconic work of R. S. Chandrasekhar, the Stokes parameters reappeared through their re-introduction, application, and further development by other two prominent scientists: P. Soleillet and F. Perrin. In:

1929 ***Paul Soleillet***, a French physicist, was the first to revive the Stokes parameters theory in his PhD dissertation entitled: "SUR LES PARAMETRES CARACTERISANT LA POLARISATION PARTIELLE DE LA LUMIERE DANS LES PHENOMENES DE FLUORESCENCE". He highlighted that **the relationship between the Stokes parameters of an incident light beam (S_i) and those of the transmitted or scattered beam (S_i') must be linear**. He observed that **the intensity and polarization state of the emergent beam depend on those of the incident beam**. In the case of two independent incident beams, if the process is linear, the emergent beam will be the superposition of the two emergent beams corresponding to the individual incident beams, without interference [25, 29, 30].

1936 ***Ramanathan Sivaramakrishnan Krishnan***, an Indian physicist, published his work on **the depolarization of scattered light**. His research provided critical insights into how the polarization of light changes when scattered by different materials, which was

instrumental in furthering the understanding of molecular and crystal structures. In **1938**, He identified the reciprocity relation concerning the intensity of horizontally polarized incident light that is scattered with vertical polarization and vice versa, irrespective of the nature of the colloidal particles. This became known as **the Krishnan reciprocity Effect** [31, 32].

It is worthwhile to note that leveraging the contributions of Soleillet and Krishnan that in:

1942 ***Francis Perrin***, a French physicist and mathematician who was a friend of Soleillet; he first noted Soleillet's observations and expanded upon the reciprocity theory of Krishnan in his later work, which led him to the radical understanding that the **transformation of polarization states through optical systems could be represented by a set of linear equations characterized by 16 coefficients.** These coefficients essentially describe the optical system's effect on the light's polarization state. Perrin subsequently quantified the number of nonzero (independent) coefficients for various media, demonstrating that the linear relationships could be expressed in a 4×4 matrix format. It is noteworthy that he addressed the Stokes polarization parameters and their connection to the Poincaré sphere without any preliminary introduction or background. [25, 29, 33].

Extrapolating from Stokes work in addition to Soleillet and Perrin's contributions to it, in:

1943 ***Hens Mueller***, a professor of physics at the Massachusetts Institute of Technology (MIT), advanced the integration of Stokes vectors with 4x4 matrix representations. He recognized that the state of polarization of light, described by Stokes parameters, could be systematically transformed as light passed through different optical elements, which led him To formalise this process by **associating each optical element with an individual 4x4 matrix**. This matrix describes how the Stokes parameters of the incident light are altered by the optical system. The Mueller formalism comes from experimental

considerations of the intensity measurements of polarized light. Mueller kept improving his formalism in the subsequent years, which appeared in a now declassified report and course notes of lectures at MIT (to refer M-26, M-27, and M-28 in the reference material [34]) [25, 34, 35].

Around the same time, another description of the state of polarization of a light beam in a standard manner, through an elementary process of matrix algebra, was developed and appeared in:

1941 by ***Robert Clark Jones***, an American physicist who had recently completed his PhD at Harvard University, published the first of eight articles in his renowned series titled "A New Calculus for the Treatment of Optical Systems." Like Mueller's approach, Jones described the incident light beam with a vector and the optical system with a matrix, enabling the determination of the outgoing light beam through matrix-vector multiplication. The key differences in Jones's calculus lie in its derivation from electromagnetic wave theory, which **retains information about the absolute phase**. Additionally, it utilizes a smaller 2×2 **matrix with complex elements**, and it is specifically applicable to optical systems that do not exhibit depolarization. In essence, Jones introduced his formalism for characterizing completely polarized light and the transformations that occur between any two completely polarized light beams. [5, 25, 34].

It is to Professor Mueller's successors that we owe the final, brilliant synthesis—integrating Mueller and Jones's diverse insights into a cohesive and powerful theoretical toolset that has significantly advanced our current grasp of light polarization and polarimetry. Back in:

1948 ***Nathan Grier Parke III***, a student of Mueller's, made significant contributions, particularly through his **PhD thesis** titled "**Matrix Optics**", suggested and guided by Mueller himself, completed in 1948 at MIT. Parke explored **the applicability of the Mueller calculus to unpolarized light** and succeeded in relating it rigorously to the electromagnetic theory. He was the first to name the Mueller and Jones calculi after

their inventors' names and the first to set **the algebraic process to relating the Jones matrices and Maxwell vectors to the corresponding complex Mueller matrices and Stokes vectors** [25, 34, 35].

To our understanding, that was the first public appearance of the Stokes-Mueller formalism applied to matter characterization with a polarimetric method. This excerpt from centuries of unstoppable ingenious scientific advancement is what this thesis revolves around.

Chapter 1

Polarization Brief Theory

"In the theoretical part of science, those who are most active can make the most progress in the shortest time."

– Henri Poincaré

Main Objectif

The preceding historical section has illuminated many intricate concepts surrounding light polarization and its interaction with matter. Additionally, a wealth of information on the subject is readily available in both digital and print sources. Consequently, this concise theoretical section will lay the foundational principles essential for the forthcoming contributions. We will focus on specific concepts and the associated Stokes-Mueller mathematics that will be pivotal in the detailed analysis and developments presented in the contribution part.

1.1 Introduction to Light Polarization

Q: What is light polarization?

A: Light polarization arises when the vibration vectors of the electric field in an electromagnetic wave (light) become aligned in a specific direction, rather than oscillating in all directions perpendicular to the wave's propagation. The process of converting unpolarized light into polarized light is referred to as **polarization**. [25, 36].

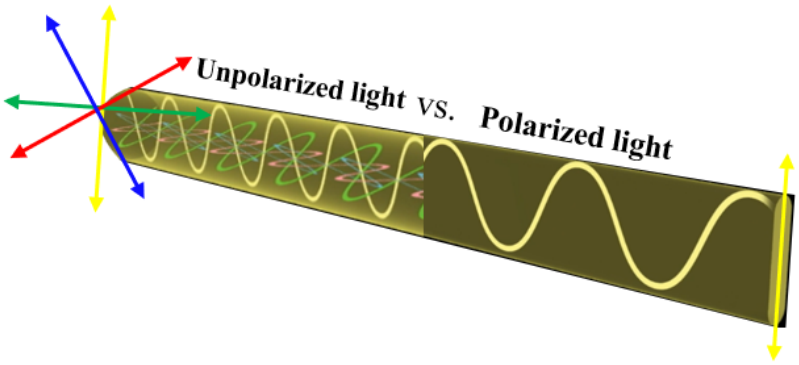

Figure 1.1: Unpolarized light vs. Polarized light

Q: How does it occur?

A: Light can become polarized in several ways. In each process, the light waves become oriented in a specific manner, either fully or partially polarized, depending on the conditions and the medium involved, as listed and illustrated in Figure (1.2).

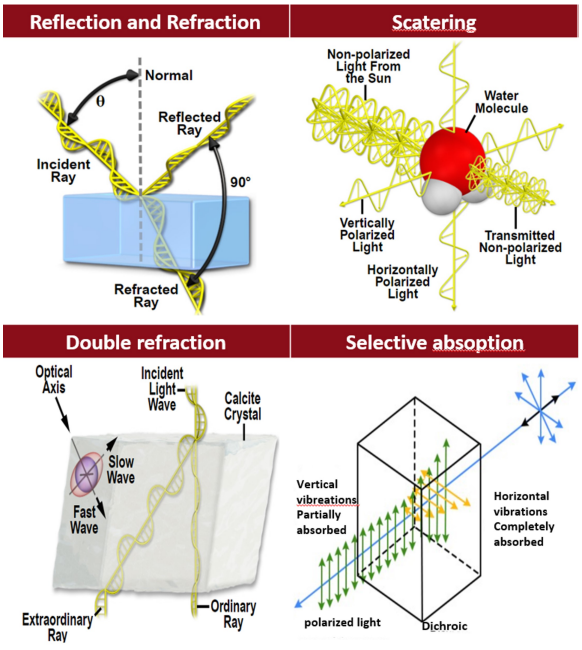

Figure 1.2: Ways of light polarization occurring [37]

Q: Why is it important?

A: The polarization of light plays a critical role in a wide array of scientific and technological applications. It directly influences the focusing characteristics of laser beams, determining beam shape and intensity, which is crucial in high-precision tasks such as material processing and medical surgery. Additionally, polarization affects the cut-off wavelengths of optical filters, enabling precise control over the spectral properties of light in imaging systems and optical communication.

Moreover, controlling polarization is vital to minimizing unwanted back reflections in optical systems, a key consideration in the design of sensitive instruments like telescopes and interferometers. In metrology, polarization-based techniques are indispensable for stress analysis in transparent materials such as glass or plastic, where they help detect internal stresses that could lead to structural failures. In the pharmaceutical industry, polarization analysis is employed to identify and quantify ingredients, ensuring the consistency and safety of drugs. In biological microscopy, polarized light enhances contrast and reveals structural details that are otherwise invisible, enabling deeper insights into cellular and tissue structures.

Beyond these applications, the differential absorption of light polarization by materials is fundamental to technologies such as LCD screens, where it controls the display of images and the creation of immersive experiences in 3D movies. Polarization is also harnessed in the design of glare-reducing sunglasses, which selectively block polarized light reflected from surfaces like water or roads, enhancing visual comfort and safety. Additionally, geometric phase elements, which manipulate the phase of light through its polarization, are increasingly used in advanced optical systems to achieve novel functionalities like beam shaping and light steering [38].

These diverse applications underscore the importance of understanding and controlling light polarization, which has become a cornerstone in fields ranging from material science and pharmaceuticals to optics, consumer electronics, and beyond.

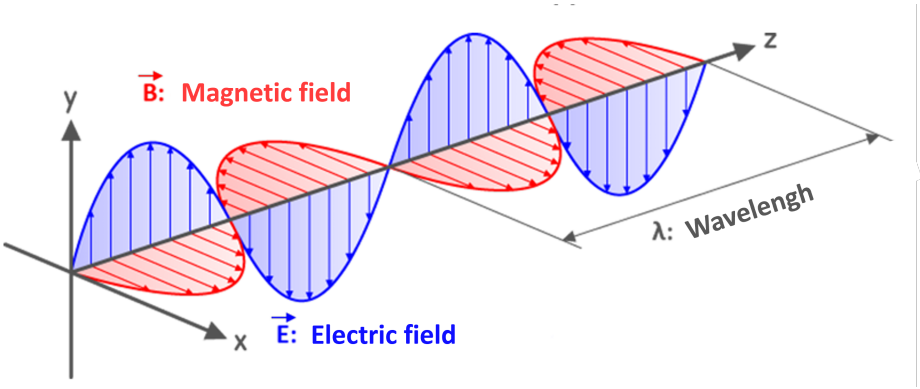

Figure 1.3: Representation of an electromagnetic wave propagating in the Z-direction. Extracted from [39].

1.2 Understanding Polarimetry

The two era-maker works concerning the light-wave nature established by Fresnel (theory of transversality in 1821) and Maxwell (theory of electromagnetism in 1861) were pivotal in elucidating the complex and initially mysterious behaviour of light polarization. However, the application of polarization for measurement purposes predates these seminal theories. One of the earliest known uses of polarization for measurement, and perhaps the first, was conducted by Arago, as discussed in the preceding historical section. Arago employed a rudimentary polarimetric setup involving a polarizer and analyzer, akin to modern polarimetric techniques, to investigate the polarization of moonlight. By measuring the changes in light intensity as he rotated the analyzer, Arago captured a key aspect of polarimetric analysis, marking a significant early contribution to the Polarimetric field.

Polarimetry, as the term suggests, encompasses the various techniques and methodologies for measuring and analyzing the physical properties associated with light polarization and its alteration by material media. This involves examining the orientation, amplitude, and phase of the electric field vector in a light wave after its interaction with matter [40]. A comprehensive understanding of polarimetry requires familiarity with three fundamental concepts: the polarization ellipse, Stokes-Mueller and Jones calculi, and the Poincaré Sphere. These concepts form the basis for analyzing and interpreting polarization-related phenomena.

1.2.1 The Polarization Ellipse

Generally, the microscopic forces exerted by the electric field of a wave on matter are significantly stronger than those produced by the magnetic field. Consequently, the temporal behavior of the electric field is taken as the primary representation of the characteristic known as polarization. For waves of arbitrary shape, the polarization state is defined in relation to a local Cartesian coordinate system XYZ. Consider the temporal evolution of the endpoint of the electric field vector $\vec{E}(z,t)$ of a monochromatic electromagnetic wave, characterized by an angular frequency ω and wavelength λ, propagating along the Z-axis (the direction of propagation). The wave vector $\mathbf{k}$ aligns with the propagation direction, and its magnitude is given by $k = \frac{2\pi}{\lambda}$. This vector can be decomposed in the wave plane into the sum of two components along two arbitrarily selected perpendicular directions, X and Y, situated within a local plane Π known as the *polarization plane*, as illustrated below.

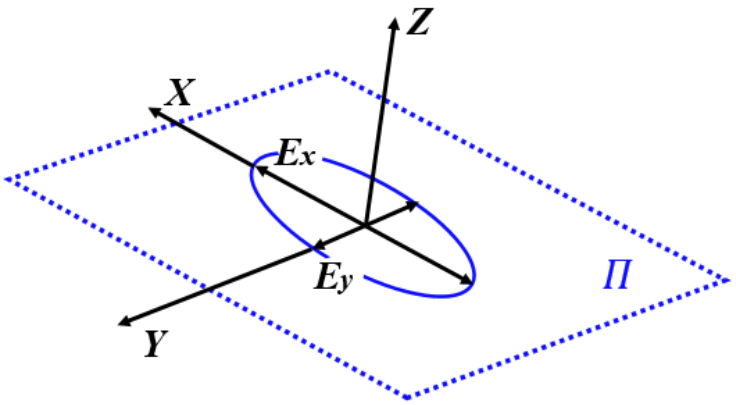

Figure 1.4: The electric field progresses within a fixed plane Π, with the direction of propagation aligned along the Z-axis, which is perpendicular to the polarization plane. The polarization state is defined concerning the local coordinate system, comprising the Z-axis and a pair of XY axes situated on the local polarization plane Π, tangent to the wavefront [40].

The real components of the vector $\vec{E}$(z, t) are expressed as:

$$E_x(z,t) = E_{0x}\cos(kz - \omega t + \delta_x)\,, \tag{1.1a}$$

$$E_y(z,t) = E_{0y}\cos(kz - \omega t + \delta_y)\,, \tag{1.1b}$$

where E_{0x} and E_{0y} are respectively the amplitudes of the electric field components in the

x and y directions, while δ_x and δ_y are the phases of these components at the origin. The term $kz - \omega t$ is called the propagator; by its elimination, we remove the time and spatial dependence, allowing us to focus on the relative phases and amplitudes of the electric field components. Thus, we obtain the following relationship [25]:

$$\left(\frac{E_x}{E_{0x}}\right)^2 + \left(\frac{E_y}{E_{0y}}\right)^2 - 2\frac{E_x}{E_{0x}}\frac{E_y}{E_{0y}}\cos\delta = \sin^2\delta\,, \tag{1.2}$$

where $\delta = \delta_y - \delta_x$ ($0 \leq \delta < 2\pi$) corresponds to the phase shift between the two components E_x and E_y. Conventionally, this phase shift is included in the interval $[-\pi, +\pi]$. The equation (1.2) is identified as the equation of an ellipse and demonstrates that, at any given moment, the electric field's locus of points as it travels takes the shape of an ellipse.

1.2.1.1 Instantaneous Polarization Ellipse and Quasi-monochromaticity condition

A significant factor affecting the polarization ellipse is the spectral width of the light wave. Light, represented as a strictly monochromatic wave with zero spectral width, serves as an ideal theoretical scenario. In this case, the coherence time τ is infinite, resulting in complete polarization. Thus, for a monochromatic light wave, the endpoint of the electric field vector traces a fixed elliptical shape within a stable plane (polarization plane) as it propagates. However, in practical scenarios, light waves are typically quasi-monochromatic, which can be viewed as a combination of mutually incoherent monochromatic light beams with frequencies distributed within a narrow bandwidth $\delta\omega$ around a central frequency ω_0. This variation leads to gradual fluctuations in the amplitudes and phases of the electric fields. These fluctuations account for why the ellipse described by Equation (1.2) is commonly referred to as the *instantaneous polarization ellipse*; conventionally, for a quasi-monochromatic wave, Equation (1.2) is expressed as:

$$\frac{\langle E_x^2\rangle}{E_{0x}^2} + \frac{\langle E_y^2\rangle}{E_{0y}^2} - 2\frac{\langle E_x E_y\rangle}{E_{0x}E_{0y}}\cos\delta = \sin^2\delta\,, \tag{1.3}$$

The angle brackets $\langle\ldots\rangle$ denote a time average and are introduced to account for the previously discussed fluctuations of a quasi-monochromatic light. In this instance, for evaluating the polarization of quasi-monochromatic light waves, three temporal scales need to be taken into consideration:

- Measurement time **T**, defined as the response time of the detector, typically takes values in the optical range of $T > 10^{-4}$ s.
- Mean natural period $\mathbf{T}_0 = \frac{1}{\omega_0}$, which represents the time needed for the endpoint of the electric field vector to complete one full ellipse. This period is generally on the order of 10^{-15} s, leading to the designation of waves as *"instantaneous"*.
- Polarization time τ_p, the average duration during which the polarization ellipse remains stable. Its lower limit is given by $\tau = \frac{1}{\delta\omega}$.

Accordingly, the following cases are distinguished:

- Totally polarized states: For a measurement time **T**, the field variables of a quasi-monochromatic wave exhibit slow fluctuations relative to the mean natural period T_0. Thus, the shape of the polarization ellipse remains constant during the polarization time τ_p, which encompasses many natural cycles (i.e., $\tau_p > T$, case a) in Figure 1.5).
- Partially polarized quasi-monochromatic states: In this scenario, the shape of the polarization ellipse changes over the measurement time **T**, while the plane Π containing it remains stable (case b) in Figure 1.5).
- Unpolarized states: This situation arises when the shape of the polarization pattern evolves randomly, even though it remains within a stable plane Π.

A quasi-monochromatic wave behaves like a monochromatic wave for times much shorter than the coherence time of the wave. Within this limit, the description of the polarization states of the quasi-monochromatic wave remains valid, similar to that of a monochromatic one [40, 41].

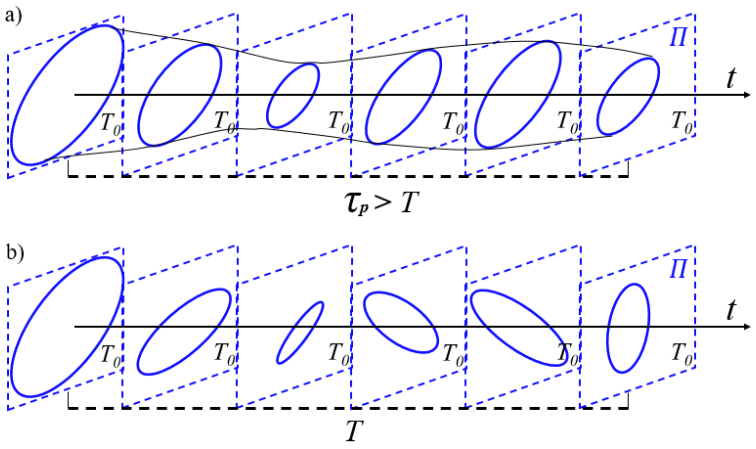

Figure 1.5: Quasi-monochromatic wave's polarization ellipse's slow fluctuations in time: a) totally polarized state, b) partially polarized state [40].

1.2.1.2 Degenerated Forms Of The Polarization Ellipse

While light is generally elliptically polarized, the polarization can be simplified under certain conditions into more specific forms. These specific degenerate forms of the polarization ellipse are frequently encountered in the study of polarized light. Due to their significance, these special degenerate forms and the special conditions of their appearance will be presented hereafter.

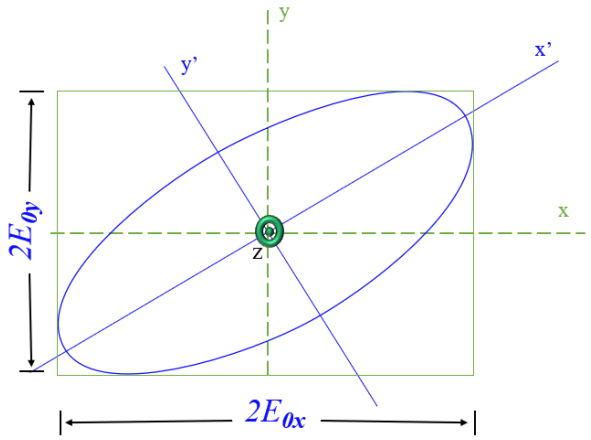

Figure 1.6: Sectional drawing of the polarization ellipse for an elliptically polarized wave. The ellipse is depicted inscribed within a rectangle, with the sides of the rectangle aligned parallel to the coordinate axes and having lengths of $2E_{0x}$ and $2E_{0y}$. The original axes are denoted by x and y, while the rotated axes are represented by x' and y' [40].

The overall cross-sectional shape (the most familiar), for an observer looking at an oncoming optical quasi-monochromatic beam, its polarization ellipse can be characterized using two different sets of parameters: (i) the terms defined in Figure (1.6), which determine the area of the ellipse and describe its specific forms under particular conditions, and (ii) the angular parameters outlined in Figure (1.7). Both sets of parameters will be considered in the following discussion.

(i) According to Dennis H. Goldstein [25], the polarization ellipse is of an area of:

$$A = \pi E_{0x} E_{0y} sin\delta \,. \tag{1.4}$$

The area of the polarization ellipse is defined by the magnitudes of the semi-axes denoted as E_{0x} and E_{0y}, along with the phase shift δ between the orthogonal transverse components. Depending on specific values of these magnitudes and the phase shift δ, the equation (1.4) may describe:

- A linearly polarized light (vertically, horizontally, +45°, -45°)
- A circularly polarized light (right-handed (clockwise), left-handed (counterclockwise))
- An elliptically polarized light (standard ellipse, right-handed, left-handed)

All potential degenerate forms are illustrated in Figure (1.8), along with the special conditions of their appearance.

(ii) It is worthwhile to note that the sheer scope of polarimetry is grounded in the concept of "*Elliptical parameters of the polarization ellipse*", which is detailed below.

Recall that the equation (1.2):

$$\left(\frac{E_x}{E_{0x}}\right)^2 + \left(\frac{E_y}{E_{0y}}\right)^2 - 2\frac{E_x}{E_{0x}}\frac{E_y}{E_{0y}}\cos\delta = \sin^2\delta, \tag{1.2}$$

stands for an equation of an ellipse, including the cross term ($E_x E_y$) in this equation indicates that the polarisation ellipse is generally rotated. This characteristic is illustrated in Figure (1.7), where the ellipse is depicted to be rotated by an angle ϕ.

Thus, a completely polarized state can be fully characterized by the parameters of the polarization ellipse, which include the azimuth ϕ and the ellipticity angle χ, along with an

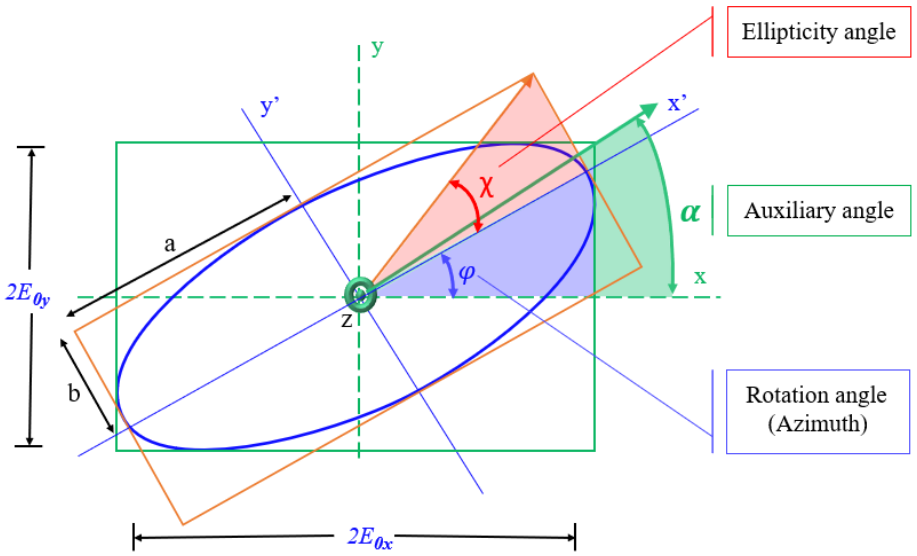

Figure 1.7: The rotated polarization ellipse characterized by the semi-axes a and b, together with the rotation angle ϕ and the ellipticity angle χ [40, 42].

auxiliary angle α, whereby:

$$tan\alpha = \frac{E_{0y}}{E_{0x}}\,, \qquad 0 \leq \alpha \leq \frac{\pi}{2}\,, \tag{1.5}$$

$$tan\chi = \frac{\pm b}{a}\,, \qquad -\frac{\pi}{4} \leq \chi \leq \frac{\pi}{4}\,. \tag{1.6}$$

In addition, since the two sets of parameters, i.e., (i) E_{0x}, E_{0y} and δ, and (ii) the rotation angle ϕ and the ellipticity angle χ, are describing the same ellipse, conventionally, they are connected by the following equations [25]:

$$\begin{aligned} tan2\phi &= \frac{2E_{0x}E_{0y}}{E_{0x}^2 - E_{0y}^2}\, cos\delta \\ &= tan2\alpha\, cos\delta\,, \end{aligned} \tag{1.7}$$

where: $0 \leq \phi \leq \pi$

$$\begin{aligned} sin2\chi &= \frac{2E_{0x}E_{0y}}{E_{0x}^2 + E_{0y}^2}\, sin\delta \\ &= sin2\alpha\, sin\delta\,. \end{aligned} \tag{1.8}$$

A common concept in describing the shape of the polarization ellipse is the ellipticity, denoted by ϵ. While closely related to the ellipticity angle, these two are distinct. Ellipticity, defined as the ratio $\frac{a}{b}$ of the semi-major to the semi-minor axes, quantifies the shape of

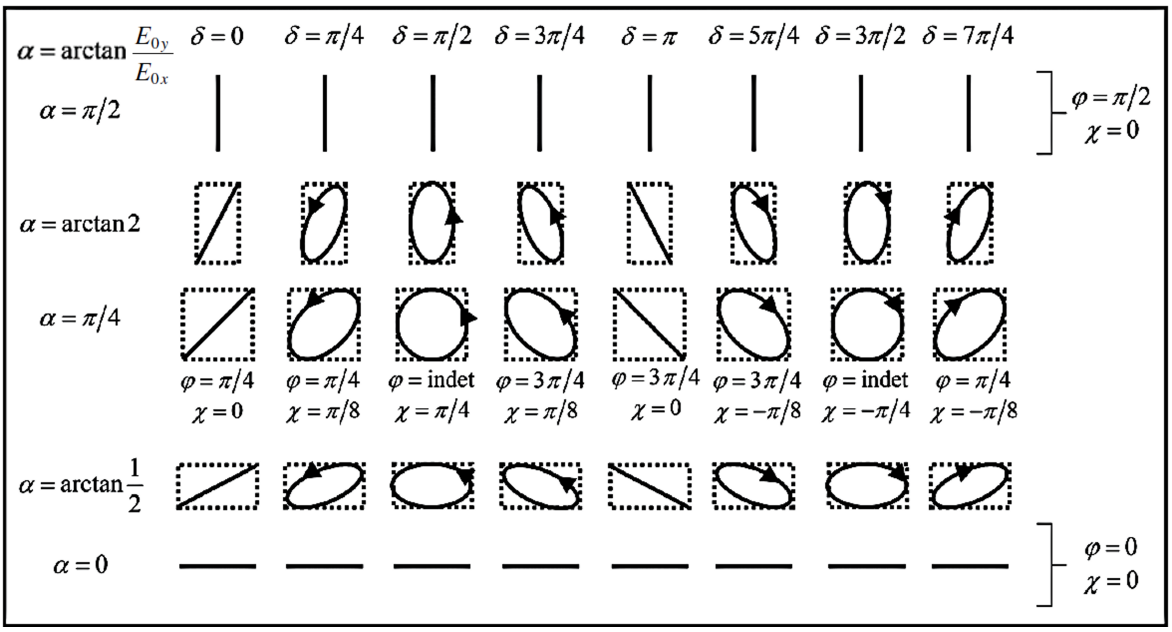

Figure 1.8: Appearance of different polarization states as determined by specific values of the angular parameters of the polarization ellipse [40].

the ellipse. The ellipticity angle, on the other hand, is an angular measure whose tangent corresponds to the ellipticity (as given by equation (1.5)). Although both convey the same information, the ellipticity angle is often more convenient for mathematical descriptions and analyses. Again, All potential degenerate forms are illustrated in Figure (1.8).

In addition to naturally emerging as special cases of the polarization ellipse, these degenerate states hold significant importance due to their relative ease of generation in an optical laboratory. These states can be utilized to establish 'null-intensity' conditions, which are critical for operating polarization instruments. Often designed around null-intensity principles, such instruments allow for highly precise measurements [40].

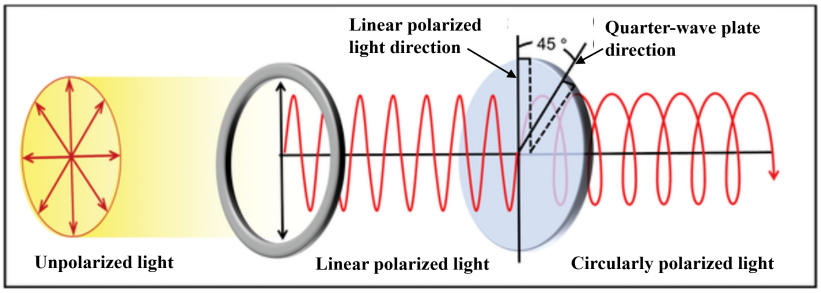

Figure 1.9: Controlling polarization states from unpolarized light to linearly then circularly polarized light, image copied from [43].

1.2.2 Stokes, Jones, and Mueller Polarimetric Calculi

These individually or combined calculi provide a comprehensive Analysis of Polarization Descriptions.

1.2.2.1 Stokes parameters

In his famous article, George Stokes developed a formalism to describe not only totally polarized light but also partially polarized and completely depolarized light. Instead of using a description based on the amplitude and phase of the light wave, he developed a description based on light intensity, a quantity that is easily measurable and observable. The electric field vector describes the polarization ellipse within a time interval on the order of 10^{-15} seconds. However, there is no detector with a response time T short enough to follow the trace of the polarization ellipse. Only the light intensity I, which is proportional to the time-averaged square of the magnitude of the electric field $\vec{E}$, is detectable. Stokes demonstrated that any state of polarization can be described using four measurable quantities corresponding to light intensities. These parameters, known as the Stokes parameters, can be obtained from the time average of the equation (1.3). Thus, the time-averaged transverse components of the electric field yield [4, 25, 44]:

$$\langle E_x \rangle = \frac{1}{2} E_{0x}^2 \,, \tag{1.9}$$

$$\langle E_y \rangle = \frac{1}{2} E_{0y}^2 \,, \tag{1.10}$$

$$\langle E_x E_y \rangle = \frac{1}{2} E_{0x} E_{oy} \cos\delta \,. \tag{1.11}$$

Using equations (1.9, 1.10, and 1.11), equation (1.3) can be rewritten in the following form:

$$(E_{0x}^2 + E_{0y}^2)^2 - (E_{0x}^2 - E_{0y}^2)^2 - (2E_{0x}E_{0y}\cos\delta)^2 = (2E_{0x}E_{0y}\sin\delta)^2 \,. \tag{1.12}$$

The quantities within parentheses are light intensities corresponding to the Stokes parameters denoted as S_i $(0 \leq i \leq 3)$:

$$S_0 = E_{0x}^2 + E_{0y}^2 \,, \tag{1.13}$$

$$S_1 = E_{0x}^2 - E_{0y}^2 \,, \tag{1.14}$$

$$S_2 = 2E_{0x}E_{0y}\cos\delta \;\;, \tag{1.15}$$

$$S_3 = 2E_{0x}E_{0y}\sin\delta \,. \tag{1.16}$$

Thus, equation (1.12) can simply be written as follows:

$$S_0^2 = S_1^2 + S_2^2 + S_3^2 \,. \tag{1.17}$$

The first parameter S_0 corresponds to the total intensity of the light, while the other three parameters S_1, S_2, and S_3 characterize the state of polarization. When the light is partially polarized or completely depolarized, equation (1.17) becomes an inequality:

$$S_0^2 \geq S_1^2 + S_2^2 + S_3^2 \,. \tag{1.18}$$

A handy property of the Stokes parameters is that they allow the evaluation of the Degree of Polarization (DOP) of a light wave [4, 25, 44]:

$$DOP = \frac{\sqrt{S_1^2 + S_2^2 + S_3^2}}{S_0} \,, \qquad\qquad 0 \leq DOP \leq 1 \,. \tag{1.19}$$

For fully polarized light, the DOP is equal to 1. It is less than 1 for partially polarized light and equal to 0 for completely depolarized light.

The four Stokes parameters can be combined into a column vector called the "Stokes vector," which characterizes the state of polarization such as:

$$\vec{S} = \begin{bmatrix} S_0 \\ S_1 \\ S_2 \\ S_3 \end{bmatrix} = \begin{bmatrix} E_{0x}^2 + E_{0y}^2 \\ E_{0x}^2 - E_{0y}^2 \\ 2E_{0x}E_{0y}\cos\delta \\ 2E_{0x}E_{0y}\sin\delta \end{bmatrix} \,. \tag{1.20}$$

They can also be obtained from multiple intensity measurements such as:

$$\vec{S} = \begin{bmatrix} S_0 \\ S_1 \\ S_2 \\ S_3 \end{bmatrix} = \begin{bmatrix} I_H + I_V \\ I_H - I_V \\ I_{45} + I_{-45} \\ I_R + I_L \end{bmatrix} \,, \tag{1.21}$$

where I_H, I_V, I_{+45}, and I_{-45} are the intensities corresponding to the contributions to the linearly polarized wave in the horizontal, vertical, $+45°$, and $-45°$ directions, respectively. I_R and I_L are the intensities corresponding to the contributions to the circularly polarized wave in the right and left directions, respectively. The parameter S_1 describes the electric field portion with horizontal or vertical linear polarization. The parameter S_2 describes the electric field part with linear polarization oriented at $+45°$ or $-45°$. Finally, the parameter S_3 characterizes the part of the electric field with right or left circular polarization.
Giving that $I_H + I_V = I_{45} + I_{-45} = I_R + I_L$, the Stokes vector can be obtained with only four intensity measurements [4, 25, 41]:

$$\vec{S} = \begin{bmatrix} I_H + I_V \\ I_H - I_V \\ 2I_{45} - (I_H + I_V) \\ 2I_R - (I_H + I_V) \end{bmatrix} . \tag{1.22}$$

In general, the Stokes vector is normalized with respect to the S_0 parameter, which corresponds to the total intensity:

$$\vec{S} = \begin{bmatrix} 1 \\ \frac{S_1}{S_0} \\ \frac{S_2}{S_0} \\ \frac{S_3}{S_0} \end{bmatrix} . \tag{1.23}$$

Finally, it is pertinent to highlight that the angular parameters of the polarization ellipse discussed in the previous section can be derived from the Stokes parameters. The expressions for these angular parameters are given as follows [45]:

$$\chi = \frac{1}{2} \arctan\left(\frac{S_2}{S_1}\right) , \tag{1.24}$$

$$\phi = \frac{1}{2} \arcsin\left(\frac{S_3}{S_0}\right) , \tag{1.25}$$

$$\alpha = \frac{1}{2} \arctan\left(\frac{S_3}{\sqrt{S_1^2 + S_2^2}}\right) . \tag{1.26}$$

Having established a foundational understanding of Stokes parameters and their role in describing the state of polarization, we now turn our attention to more advanced mathematical frameworks—namely the Jones and Mueller calculi, and the Poincaré sphere. These

tools not only build upon the principles introduced by Stokes parameters but also provide more comprehensive methods for analyzing and manipulating polarized light [4, 25, 41].

1.2.2.2 Jones mathematical representation of totally polarized light

The Jones formalism offers a straightforward approach for describing polarized light and its alterations. Introduced by American physicist R. Clark Jones in 1941 [5], the Jones vector is formulated by recognizing that the equation of a plane wave can be expressed as a column vector, such as:

$$E(z,t) = \begin{bmatrix} E_{0x}\exp[i(\omega t - kz + \delta_x)] \\ E_{0y}\exp[i(\omega t - kz + \delta_y)] \end{bmatrix} = \exp[i(\omega t - kz)] \begin{bmatrix} E_{0x}e^{i\delta_x} \\ E_{0y}e^{i\delta_y} \end{bmatrix} . \tag{1.27}$$

In practice, the term $\exp[i(\omega t - kz)]$ as explained in the section (1.2.1) is typically omitted, leading to a simplified expression:

$$\mathbf{E}(z,t) = \begin{bmatrix} E_x \\ E_y \end{bmatrix} , \tag{1.28}$$

where E_x and E_y are complex amplitudes:

$$E_x = E_{0x}e^{i\delta_x} , \tag{1.29a}$$

$$E_y = E_{0y}e^{i\delta_y} . \tag{1.29b}$$

The Jones vector represents a monochromatic, uniform, and transverse-electric plane wave, encapsulating the complete information about the field's amplitudes and phases and, hence, the wave's polarization. However, in reality, light is often quasi-monochromatic (see section 1.2.1.1); nevertheless, for time intervals shorter than the coherence time, the Jones vector remains a valid description of polarization states in quasi-monochromatic light.
The intensity of the light can be calculated by multiplying the Jones vector $\mathbf{E}$ with its Hermitian adjoint $\mathbf{E}^\dagger$ (The Hermitian adjoint of a matrix is the complex conjugate of the transpose of the matrix, thus $\mathbf{E}^\dagger$ is a row vector) [5, 25, 40, 44]:

$$I = \mathbf{E}^\dagger\mathbf{E} = E_x^* E_x + E_y^* E_y . \tag{1.30}$$

The interaction of light with a medium or optical system can be characterized by a 2×2 complex matrix denoted as the Jones matrix:

$$\begin{bmatrix} E'_x \\ E'_y \end{bmatrix} = \mathbf{J} \begin{bmatrix} E_x \\ E_y \end{bmatrix} , \tag{1.31}$$

with $E_{x,y}$, $E'_{x,y}$ referring to the incident and outgoing electric field components, respectively.

The Jones matrix $\mathbf{J}$ consists of four generally complex elements, requiring eight independent real parameters to be completely defined. A collection of Jones matrices for standard optical components is readily available in resources like Wikipedia or, more specifically, scholarly sources like [34].

The Jones matrix describing a sequence of optical elements is obtained by multiplying the individual Jones matrices of each component. If we consider the incident and emergent plane waves, the cumulative effect of a cascade of N optical elements can be represented as:

$$\mathbf{E}_0 = \mathbf{J}_N \mathbf{J}_{N-1} \dots \mathbf{J}_{II} \mathbf{J}_I \mathbf{E}_i = \mathbf{J}_{\text{comb}} \mathbf{E}_i \, . \tag{1.32}$$

It is worth noting that the incident plane wave interacts with I optical element first, then element II, et cetera.

In cases where the polarization element rotates by an angle θ while maintaining a constant angle of incidence, the resulting Jones matrix is:

$$\mathbf{J}_\theta = \mathbf{R}(\theta) \mathbf{J} \mathbf{R}(-\theta) \, , \quad \text{where} \quad \mathbf{R}(\theta) = \begin{bmatrix} \cos\theta & \sin\theta \\ -\sin\theta & \cos\theta \end{bmatrix} . \tag{1.33}$$

Here, θ is positive for counter-clockwise rotation as viewed against the direction of propagation.

Quasi-monochromatic radiation is not always fully polarized and can be partially polarized or unpolarized. In practical situations, partially polarized light is commonly encountered. The Jones formalism is limited to completely polarized light. For partially polarized or unpolarized radiation, a different approach, which will be introduced in the following section, is required [5, 25, 40, 44].

1.2.2.3 Stokes-Mueller Formalism

A Mueller matrix $\mathbf{M}$ is a 4×4 matrix comprising 16 real elements, which relates the input and output Stokes vectors following the interaction of electromagnetic radiation with an optical medium [6, 29]:

$$\mathbf{S}^{\text{out}} = \mathbf{M}\mathbf{S}^{\text{in}} \,. \tag{1.34}$$

The Mueller matrix of an optical system composed of elements in series is the product of the Mueller matrices of these elements, arranged in the reverse order of how the incident beam encounters them. Analogy to Jones calculus interpreted by equation (1.32), the cumulative effect of a series of N optical elements is translated into:

$$\mathbf{E}_0 = \mathbf{M}_N \mathbf{M}_{N-1} \ldots \mathbf{M}_{II} \mathbf{M}_I \mathbf{E}_i = \mathbf{M}_{\text{comb}} \mathbf{E}_i \,. \tag{1.35}$$

A comprehensive list of Mueller matrices corresponding to standard optical components is available on Wikipedia and for more mathematical details see Chapter 06 in reference [25]

.

Suppose the polarization element described by the Mueller matrix undergoes rotation by an angle θ (positive for counter-clockwise rotation when viewed against the propagation direction). In that case, the resulting matrix can be expressed as[6, 29, 34]:

$$\mathbf{M}' = \mathbf{R}(-\theta)\mathbf{M}\mathbf{R}(\theta) \,, \quad \text{where} \quad \mathbf{R}(\theta) = \begin{bmatrix} 1 & 0 & 0 & 0 \\ 0 & \cos 2\theta & \sin 2\theta & 0 \\ 0 & -\sin 2\theta & \cos 2\theta & 0 \\ 0 & 0 & 0 & 1 \end{bmatrix} . \tag{1.36}$$

This is analogous to the rotation of Jones matrices described in equation (1.33)

The inequality in equation (1.18) plays a significant role because it enables the classification of the nature of light-medium interaction. For fully polarized incident light, if the Stokes vector of the output light satisfies Equation (1.18) as equality, the medium is termed non-depolarizing, meaning the emerging beam remains completely polarized.

Every Jones matrix has a corresponding Mueller matrix. To highlight this connection, such Mueller matrices derived from Jones matrices are called "Mueller-Jones" matrices. The Mueller-Jones matrix corresponding to any given Jones matrix can be calculated using the

following expression[35, 40, 44]:

$$\mathbf{M} = \mathbf{A}(\mathbf{J} \otimes \mathbf{J}^*)\mathbf{A}^{-1}\,, \tag{1.37}$$

where $\otimes$ denotes the Kronecker product and $\mathbf{A}$ is given by:

$$\mathbf{A} = \frac{1}{\sqrt{2}} \begin{bmatrix} 1 & 0 & 0 & 0 \\ 1 & 0 & 0 & -1 \\ 0 & 1 & 1 & 0 \\ 0 & i & -i & 0 \end{bmatrix}. \tag{1.38}$$

A general Jones matrix comprises 8 independent parameters. However, during the transition to a Mueller-Jones matrix, absolute phase information is forfeited, resulting in only 7 independent elements within the Mueller-Jones matrix. In essence, this conversion diminishes the independent parameters from 8 to 7. Thus, while the Jones matrix delivers a more comprehensive depiction (including phase), the Mueller matrix provides a wider yet somewhat less detailed account of the light's polarization state [29, 40]. The capacity of a medium to transform depolarized light into polarized light is referred to as *polarizance*. When the incoming light is entirely depolarized, the polarization state of the emitted light is completely characterized by the first column of the Mueller matrix. [46]:

$$\begin{bmatrix} M_{00} \\ M_{10} \\ M_{20} \\ M_{30} \end{bmatrix} = \begin{bmatrix} M_{00} & M_{01} & M_{02} & M_{03} \\ M_{10} & M_{11} & M_{12} & M_{13} \\ M_{20} & M_{21} & M_{22} & M_{23} \\ M_{30} & M_{31} & M_{32} & M_{33} \end{bmatrix} \begin{bmatrix} 1 \\ 0 \\ 0 \\ 0 \end{bmatrix}. \tag{1.39}$$

The polarizance P corresponds to the degree of polarization (DOP) of the emerging beam, and the equation gives it:

$$\mathbf{P} = \frac{1}{M_{00}}\sqrt{M_{10}^2 + M_{20}^2 + M_{30}^2}\,, \qquad 0 \leq \mathbf{P} \leq 1\,. \tag{1.40}$$

Having explored how Jones and Mueller matrices individually account for the various elements contributing to polarization, we now shift our focus to the polarization effects induced by these elements. This transition will enable us to complete our understanding of the Stokes-Mueller formalism, solidifying its role as a widely utilized mathematical framework in the study of light polarization.

1.2.2.4 Polarization effects of Polarimetric elements

Polarization effects refer to the modifications in the polarization state of light as it interacts with various materials or optical elements. These changes can be categorized into different types vis.

Dichroism

It refers to the differential absorption of light depending on its polarization state, the reason why it is referred to as Selective absorption.In anisotropic materials exhibiting dichroism, different polarization components of light are absorbed to different extents, leading to variations in the transmitted intensity. Thus, the intensity transmission coefficient T is intrinsically linked to dichroism, reflecting how the material's differential absorption alters the overall transmitted light intensity. Dichroism can be further classified into:

- *Linear Dichroism*: it occurs when a material absorbs different amounts of light depending on the linear polarization direction of the incident light.
  An example of a linear dichroic element is a polarizer that absorbs light differently for two orthogonal linear polarization directions. case a) in the Figure (1.10). For linear polarizer with Axis of Transmission at Angle θ, the Jones matrix can be expressed as:
  $$J_{LP_\theta} = \begin{pmatrix} \cos^2(\theta) & \cos(\theta)\sin(\theta) \\ \cos(\theta)\sin(\theta) & \sin^2(\theta) \end{pmatrix} . \tag{1.41}$$
- *Circular Dichroism:* involves the differential absorption of right- and left-circularly polarized light. cases b) and c) in the Figure (1.10). The responsible polarization element is a circular polarizer or optical material with differential absorption properties for right- and left-circularly polarized light. For circular polarizers, the Jones matrices are[44, 47]:
  $$\text{For Right Circular Polarizer:} \quad J_{RCP} = \frac{1}{2}\begin{pmatrix} 1 & i \\ -i & 1 \end{pmatrix} , \tag{1.42}$$
  $$\text{For Left Circular Polarizer:} \quad J_{LCP} = \frac{1}{2}\begin{pmatrix} 1 & -i \\ i & 1 \end{pmatrix} . \tag{1.43}$$

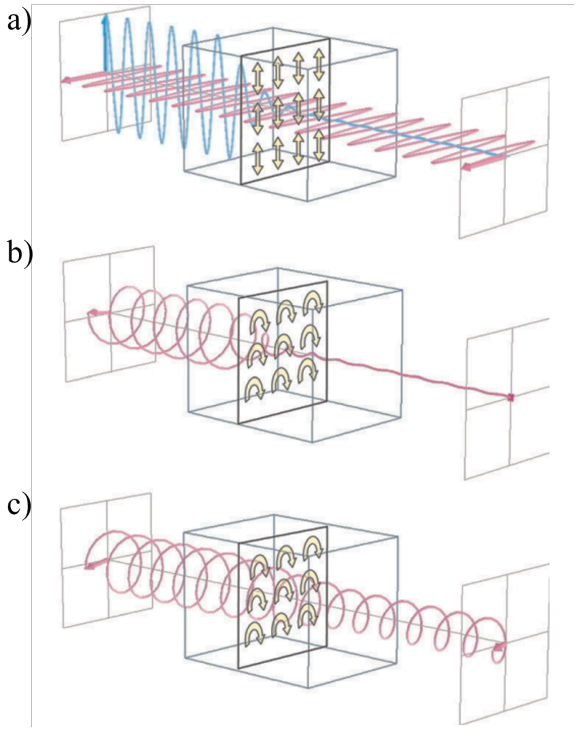

Figure 1.10: The concept of dichroism. The small arrows indicate the varying absorption based on the polarization direction. **a)** Linear dichroism: a horizontally polarized wave traverses the medium, while the vertically polarized wave is significantly diminished and nearly entirely absorbed. **b)** A medium exhibiting right-handed dichroism absorbs a right-handed circularly polarized wave. **c)** A left-handed circularly polarized wave moves through the medium with minimal absorption [47].

Retardance

Birefringence is a property of anisotropic materials (anisotropy describes the variation of properties in different directions within a material) where the refractive index varies with the polarization and propagation direction of light. This leads to a phase difference between the ordinary and extraordinary rays traveling through the material. The phase difference induced by birefringence is referred to as **retardance**. Although the terms "double refraction" and "birefringence" are often used interchangeably to describe the capability of an anisotropic crystal to split incident light into ordinary and extraordinary rays, these terms actually denote different aspects of the same phenomenon. The process of double refraction involves the splitting of a light beam into two distinct rays, each bending at a unique

angle. On the other hand, birefringence pertains to the underlying cause of this splitting, which is a directional variation in the refractive index within a structurally ordered material. The disparity in the refractive indices between the extraordinary and ordinary rays passing through an anisotropic crystal is quantifiable and can be represented as an absolute value using the following formula [37, 44, 48]:

$$\text{Birefringence (B)} = |n_e - n_o|\,, \tag{1.44}$$

the phase retardance δ, which is the phase difference introduced between the ordinary and extraordinary rays due to birefringence, depends on both the birefringence and the physical thickness d of the material through which the light travels.

$$\delta = \frac{2\pi B d}{\lambda} \tag{1.45}$$

. Just like the dichroism, Birefringence can be further classified into:

- *Linear Birefringence*: Media characterized by two refractive indices associated with two orthogonal polarization directions are known as linear birefringent materials. Only linear polarizations parallel to these two directions, referred to as "eigen axes," can propagate without alteration. The lower and higher indices are respectively called the fast index n_{fast} and the slow index n_{slow} because the phase velocity v_ϕ is inversely proportional to the refractive index seen by the wave ($v_\phi = \frac{c}{n}$, where c is the speed of light in a vacuum and n is the refractive index). The two linear polarization states corresponding to the eigenaxes are called the "eigenstates of polarization" of the medium. The index anisotropy, characterized by the linear birefringence of the medium $B_L = n_{slow} - n_{fast}$, leads to a phase shift δ_L between the eigenstates during light propagation through a medium of thickness d [37, 44, 48]:

$$\delta_L = \frac{2\pi}{\lambda} B_L d \tag{1.46}$$

  .

  Materials exhibiting linear birefringence are called **linear retarders** or **phase shifters**. Among anisotropic materials, crystals known as "uniaxial" have two different refractive indices. Calcite and quartz are examples of such crystals. There

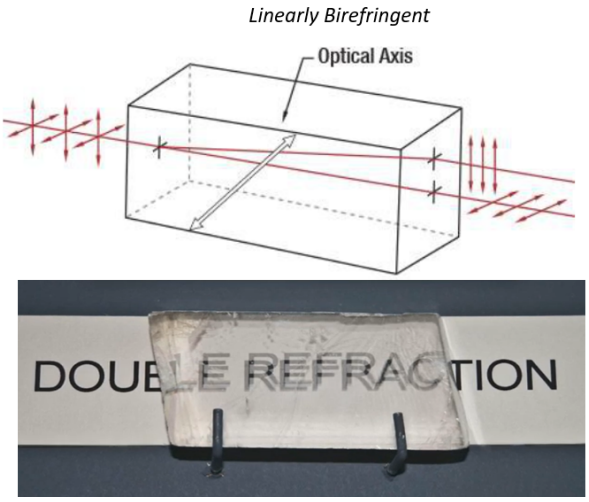

Figure 1.11: Linear Birefringence: scientific illustration and live manifestation

are also biaxial crystals like mica, which have three different refractive indices [37, 48]. Using these materials, elements called **wave plates** or **phase plates** are made, whose function is to create a well-defined linear phase retardation. **The two most commonly used types of wave plates are the half-wave plate** $(\delta_L = \pi)$ **and the quarter-wave plate** $(\delta_L = \frac{\pi}{2})$**.**

- *Circular birefringence*: causes a change in the azimuthal angle of the polarization ellipse, which corresponds to a rotation of the incident polarization state. The rotation angle, also known as optical rotation, is proportional to the value of the circular birefringence, the thickness of the medium traversed, and inversely proportional to the wavelength [44, 48]:

$$\phi = \frac{\pi}{\lambda} B_c d = \frac{\delta_c}{2} \quad \text{with: } \delta_c = \frac{2\pi}{\lambda} B_c d \tag{1.47}$$

.

For a general retarder with overall retardance $T = \sqrt{L^2 + C^2}$, where L and C represent the linear and circular retardancies, respectively, its associated Jones matrix is [44]:

$$J_{gR} = \begin{pmatrix} \cos\frac{T}{2} - \frac{iL}{T}\sin\frac{T}{2} & \frac{C}{T}\sin\frac{T}{2} \\ -\frac{C}{T}\sin\frac{T}{2} & \cos\frac{T}{2} + \frac{iL}{T}\sin\frac{T}{2} \end{pmatrix} . \tag{1.48}$$

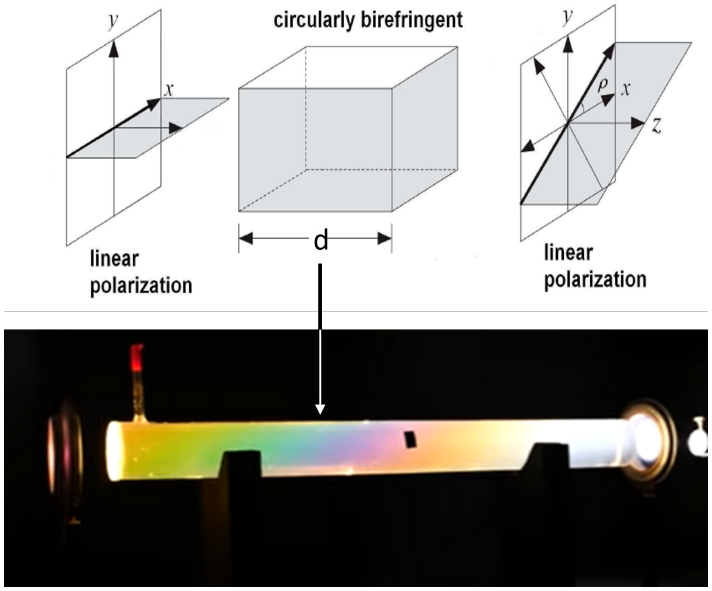

Figure 1.12: Circular Birefringence: scientific illustration and live manifestation [44, 49].

Depolarization

A depolarizing element has the ability to reduce the degree of polarization (DOP) of a light wave. For completely depolarized light, the measured intensities I_H, I_V, I_{45}, I_{-45}, I_R, and I_L are equal. The Stokes parameters S_1, S_2, and S_3, each corresponding to the difference between two of these intensities, are therefore zero. The Stokes vector can thus be written as follows: $\vec{S} = \begin{bmatrix} 1 & 0 & 0 & 0 \end{bmatrix}^T$.
scattering elements are depolarizers and biological tissues are also another example of depolarizing elements [44].

1.2.3 Poincaré Sphere and Relative Geometric Phase concept

The physicist and mathematician Henri Poincaré introduced a three-dimensional model for representing polarization states. Each state is represented by a point P on or inside a unit sphere known as the "Poincaré sphere." The angular coordinates of point P correspond to two parameters of the polarization ellipse: the ellipticity angle χ, which defines the ellipse's shape, and the azimuth ϕ, which determines its orientation. Additionally, the position of point P can be expressed using the Stokes parameters. The triad $OS_1S_2S_3$, illustrated in

Figure (1.13), forms a Cartesian coordinate system with the origin at point O. The coordinates of point P (depicted as a yellow ball) are the Stokes parameters S_1, S_2, and S_3, normalized by S_0, where S_0 (with $0 \leq S_0 \leq 1$) represents the distance from point P to the sphere's center. The Stokes parameters are linked to the ellipticity angle χ and azimuth ϕ of the polarization ellipse through the following equations: [48, 50]:

$$S_1 = \cos 2\chi \cos 2\phi \,, \tag{1.49}$$

$$S_2 = \cos 2\chi \sin 2\phi \,, \tag{1.50}$$

$$S_3 = \sin 2\chi \,. \tag{1.51}$$

Specific polarization states are represented by various positions on the Poincaré sphere:

- The equator ($2\chi = 0$) signifies linear polarization states;
- The south pole ($2\chi = -\pi/2$) and north pole ($2\chi = +\pi/2$) indicate left and right circular polarization, respectively;
- Points along the same parallel correspond to ellipses with identical ellipticity but varying azimuths, reflecting different orientations;
- Points along the same meridian represent polarization states with a consistent azimuth but differing ellipticities [48, 50].

The distance OP indicates the degree of polarization of the light. Partially polarized light is represented by a point P situated within the sphere. When point P aligns with the center O, the light is entirely depolarized.
The Poincaré sphere connects any two polarization states via an arc, facilitating the calculation of their differences in azimuth and ellipticity through spherical trigonometry. This method streamlines the prediction of a light beam's polarization after it interacts with a polarizing element, as well as the determination of the necessary parameters of that element to achieve a desired polarization state.

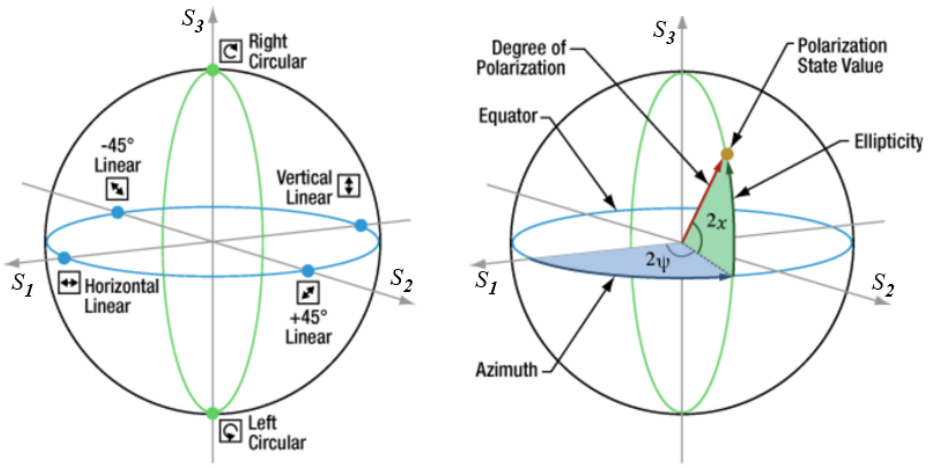

Figure 1.13: Poincare Sphere pictorial: left) all potential polarization states visualization on the sphere, right) polarization states are mapped to the sphere using azimuthal and ellipticity angles [50].

Optical Geometric phase

An optical geometric phase, commonly known as the Pancharatnam-Berry phase (or Berry phase in polarization contexts), represents an extra phase shift that occurs when the polarization state of light experiences a cyclic and adiabatic (slow) change. Unlike the dynamic phase, which depends on the physical path length and refractive index, the geometric phase arises solely from the geometry of the trajectory in the polarization state space, such as on the Poincaré sphere. As demonstrated by Pancharatnam, this additional phase shift corresponds to half the solid angle enclosed by the path. An illustrative figure (1.14) provides a clear visual representation and geometrical explanation of this concept.[51].

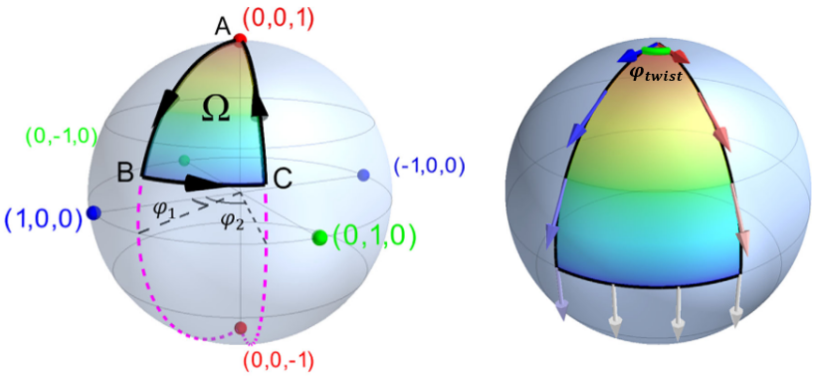

Figure 1.14: The geometric phase ϕ_1 is equivalent to half the solid angle Ω subtended by the loop. The left sphere illustrates the total phase twist ϕ_{twist} resulting from a parallel displacement along the surface of the sphere, returning to the original point [51].

1.3 Conclusion

The first part of this thesis was opened with an extended historical tracing of light polarization over 300 past years; from the initial observations in 1669 to significant advancements by 1948, the field of light polarization has undergone extensive scientific development. Early studies laid the groundwork for understanding polarization phenomena, which gradually led to the establishment of the mathematical frameworks that are fundamental to modern optics. This historical progression can be likened to assembling a complex puzzle, where each scientific discovery contributed a vital piece, ultimately creating a comprehensive understanding of polarization. The brief theory was subsequently established and concisely focused on the fundamental scientific notions and mathematical background that frames the contribution part. In the last 70 years, technological advancements have shifted the focus of polarization studies from theoretical foundations to data-driven practical applications, opening a new chapter in classical polarization research that we have witnessed and had the opportunity to contribute to.

Part II

Contribution

Chapter 2

Mueller Polarimeter Based On Modified Vacuum Matrix

"Even vacuum is complicated!"

– Holger Bech Nielsen

Measurement is a cornerstone of scientific practice, particularly in optics, where polarimetric methods have proven highly effective across various applications. Notably, the Stokes-Mueller formalism has significantly advanced the characterization of polarization since the mid-19th century.
Following this tradition, while current methods have proven effective and reliable, exploring new approaches can uncover additional features and open up new areas of investigation. This chapter introduces a novel method that advances polarimetric techniques by offering unique features not previously explored.

Main objectif

The primary aim is to establish the principles and calculations of this new approach and prove its effectiveness.

2.1 Mueller polarimeter with dual rotating quarter-wave plates

This classical Polarimeter consists of a polarization state generating system (PSG) and polarization state analyzing system (PSA), which together allow the obtaining of the optical system's Mueller matrix. The PSG, see (Fig. 2.1), is composed of a fixed linear polarizer, followed by a rotating quarter wave plate, while the PSA comprises the same elements but in reverse order. The input polarizer is oriented vertically (system's reference), while the output polarizer is oriented horizontally. The orientations of the quarter-wave plates are identified respectively by the angles θ and θ', which the fast axes make to the vertical. Thus,

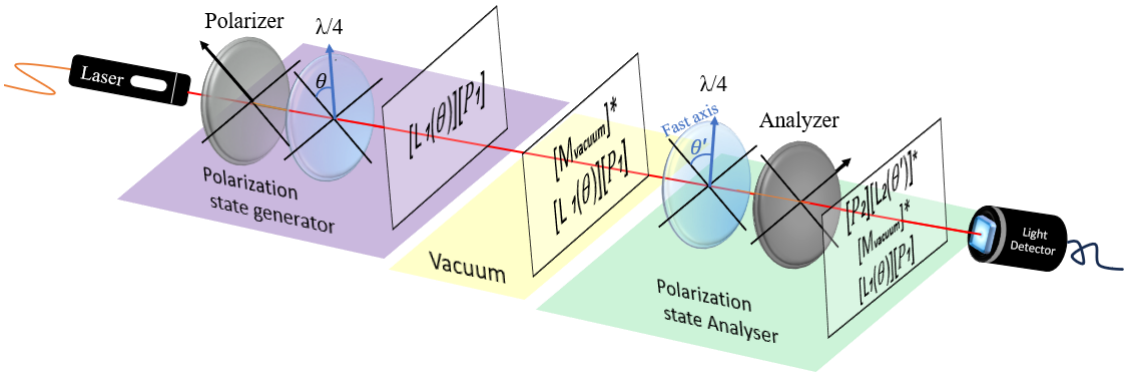

Figure 2.1: the functioning principle of the Mueller polarimeter with two rotating quarter wave plates labeled as $\lambda/4$

at the output of this assembly, the out-coming Stokes vector $\overrightarrow{S'}$ is obtained by means of the Stokes-Mueller calculus, which is presented as:

$$\overrightarrow{S'} = [P_2] \cdot [L_2(\theta')] \cdot [M] \cdot [L_1(\theta)] \cdot [P_1] \cdot \overrightarrow{S} \,, \tag{2.1}$$

where $[P_1]$, $[P_2]$, $[L_1(\theta)]$, $[L_2(\theta')]$, and $\overrightarrow{S}$ are respectively the well-known Mueller matrices of the crossed input and output polarizers, first and second quarter-wave plates, and lastly, the input Stokes vector.

Also, [M] denotes the Mueller matrix of the medium under investigation, such as:

$$[M] = \begin{bmatrix} M_{00} & M_{01} & M_{02} & M_{03} \\ M_{10} & M_{11} & M_{12} & M_{13} \\ M_{20} & M_{21} & M_{22} & M_{23} \\ M_{30} & M_{31} & M_{32} & M_{33} \end{bmatrix}, \tag{2.2}$$

For improved clarity and flow in the subsequent mathematical development, the Mueller matrix of the quarter-wave plate, with its fast axis oriented at an angle (θ) to the system's vertical, is:

$$[L(\theta)] = \begin{bmatrix} 1 & 0 & 0 & 0 \\ 0 & C^2 & CS & -S \\ 0 & CS & S^2 & C \\ 0 & S & -C & 0 \end{bmatrix}, \tag{2.3}$$

viz. C = cos(2θ), S = sin(2θ), and the same equation for the second quarter-wave plate, but in a different orientation with C'= cos(2θ') and S'= sin(2θ').

The luminous intensity I arriving at the detector is entirely contained in the term S'_0 of the Stokes vector leaving the system $\overrightarrow{S'}$, the development of Eq.(2.1) pursuant to S'_0 gives:

$$\begin{aligned} S'_0(\theta,\theta') = I(\theta,\theta') = {} & M_{00} + M_{01}C^2 + M_{02}CS + M_{03}S \\ & + (M_{10} + M_{11}C^2 + M_{12}CS + M_{13}S)(-C'^2) \\ & + (M_{20} + M_{21}C^2 + M_{22}CS + M_{23}S)(-C'S') \\ & + (M_{30} + M_{31}C^2 + M_{32}CS + M_{33}S)(S') \,. \end{aligned} \tag{2.4}$$

While the Mueller matrix is inherently a 4×4 matrix, it can be represented as a 16×1 vector for specific mathematical manipulations. In this case, it can be reshaped into:
$M_{vec} = [M_{00}; M_{01}; M_{02}; M_{03}; M_{10}; M_{11}; M_{12}; M_{13}; M_{20}; M_{21}; M_{22}; M_{23}; M_{30}; M_{31}; M_{32}; M_{33}]$.
All elements M_{ij} of the vacuum matrix to be determined arise in the output intensity expression I, which can then be written as:

$$I(\theta,\theta') = \sum_{N=0}^{15} M_N A_N(\theta,\theta') \,, \tag{2.5}$$

where A_N are coefficients depending on θ and θ'. To solve for the sixteen Mueller matrix elements, sixteen equations of this form with sixteen combinations (θ,θ') are required,

assuming the coefficients are known. The set of sixteen measurements can be written as follows:

$$\begin{bmatrix} I_0 \\ \vdots \\ I_{15} \end{bmatrix} = \begin{bmatrix} A_{0,0} & \dots & A_{0,15} \\ \vdots & \ddots & \vdots \\ A_{15,0} & \dots & A_{15,15} \end{bmatrix} \begin{bmatrix} M_{00} \\ \vdots \\ M_{33} \end{bmatrix} . \tag{2.6}$$

By choosing sixteen combinations (θ, θ'), to prevent that the matrix $[A_{m,n}]$ would be singular (non-invertible), the M_{ij} terms are immediately recovered by:

$$[M_{ij}] = [A^N_{m,n}]^{-1}[I_N] . \tag{2.7}$$

Worth noting is that the Mueller matrix of vacuum $[M_v]$ is theoretically the identity matrix (a square matrix with all diagonal elements equal to 1 and off-diagonal ones equal to 0).

2.2 Mueller Polarimeter based on Modifying Vacuum Matrix (MP-MVM)

2.2.1 Description of the proposed set-up

In this study, a polarimeter with a modifying vacuum matrix is utilized to concurrently determine the phase shift (δ) and the ellipticities (ϵ, -ϵ) of eigenstates, along with the orientation of the fast and slow axes of a birefringent medium. For this purpose, the method described in Section (2.1), which allows the determination of the vacuum Mueller matrix, is applied. However, in this instance, the second quarter-wave plate is replaced by the medium under study, as illustrated in Figure (2.2). Consequently, the alterations observed in the vacuum matrix reveal the sought-after information.

2.2.2 Output Intensity of the Modified Polarimeter

The measurement principle of this method focuses on determining the 16 elements of the modified Mueller matrix of the vacuum $[M_{vmod}]$, achieved by substituting the quarter-wave plate with the birefringent medium. A critical factor enabling this process is the output light intensity, which contains the information necessary to extract the targeted properties. In this regard, the output Stokes vector $\overrightarrow{S'}$ is related to the input vector $\overrightarrow{S}$ through the

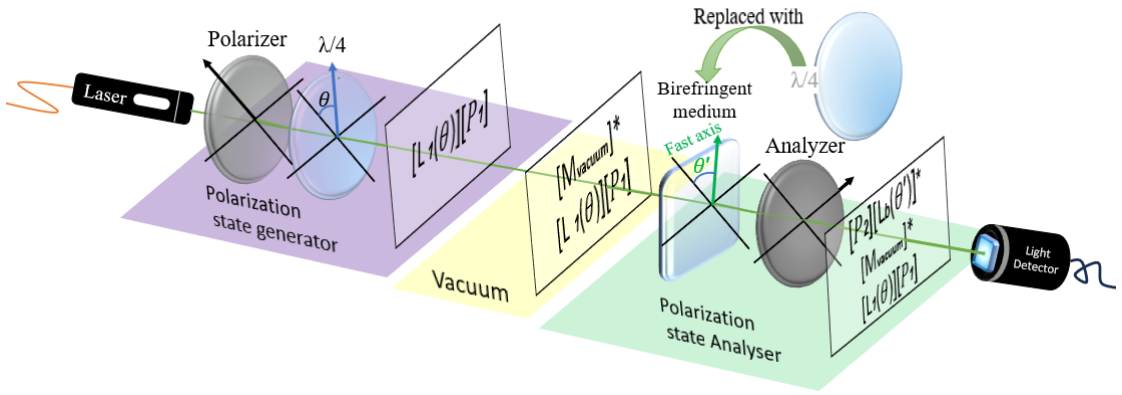

Figure 2.2: schematic of the proposed experimental set-up of an MPMVM

following matrix relationship:

$$\overrightarrow{S'} = [P_2] \cdot [L_b(\theta')] \cdot [M_v] \cdot [L_1(\theta)] \cdot [P_1] \cdot \overrightarrow{S}\,, \tag{2.8}$$

where: $[P_1]$, $[P_2]$, $[L_1]$, $[L_b]$, are respectively, the Mueller matrices of the input and output polarizers, the quarter-wave plate and the birefringent plate under investigation. Regarding this latter, its Mueller matrix is characterized by a phase shift (δ), the ellipticity (ϵ), and the orientation angle (θ'). It is expressed as comes [52]:

$$[L_b(\delta,\epsilon,\theta')] = \begin{bmatrix} 1 & 0 & 0 & 0 \\ 0 & b_1^2 - b_2^2 - b_3^2 + b_4^2 & 2(b_1b_2 + b_3b_4) & -2(b_1b_3 + b_2b_4) \\ 0 & 2(b_1b_2 - b_3b_4) & -b_1^2 + b_2^2 - b_3^2 + b_4^2 & 2(b_1b_4 - b_2b_3) \\ 0 & -2(b_1b_3 - b_2b_4) & -2(b_1b_4 + b_2b_3) & -b_1^2 - b_2^2 + b_3^2 + b_4^2 \end{bmatrix}, \tag{2.9a}$$

with:

$$b_1 = cos(2\epsilon)\ cos(2\theta')\ sin(\delta/2), \tag{2.9b}$$

$$b_2 = cos(2\epsilon)\ sin(2\theta')\ sin(\delta/2), \tag{2.9c}$$

$$b_3 = sin(2\epsilon)\ sin(\delta/2), \tag{2.9d}$$

$$b_4 = cos(\delta/2), \tag{2.9e}$$

Within the scope of this work, the first element of the output Stokes vector, S'_0, representing the detected light intensity I, is measured. By developing the expression for this intensity

as a function of the orientations θ and θ', the following relationship is obtained:

$$\begin{aligned} S_0'(\theta,\theta') = I(\theta,\theta') = {} & M_{00} - M_{01}C_{2\theta}^2 - M_{02}C_{2\theta}S_{2\theta} + M_{03}S_{2\theta} \\ & + (M_{10} - M_{11}C_{2\theta}^2 - M_{12}C_{2\theta}S_{2\theta} + M_{13}S_{2\theta})(b_1^2 - b_2^2 - b_3^2 + b_4^2) \\ & + (M_{20} - M_{21}C_{2\theta}^2 - M_{22}C_{2\theta}S_{2\theta} + M_{23}S_{2\theta})(b_1b_2 - b_3b_4) \\ & + (M_{30} - M_{31}C_{2\theta}^2 - M_{32}C_{2\theta}S_{2\theta} + M_{33}S_{2\theta})(b_2b_4 - b_1b_3)\,. \end{aligned} \tag{2.10}$$

Utilizing the matrix system previously presented in Eq.(2.6), and referencing Eq.(2.10), with taking into consideration $[M_v]$=$[M_{identity}]$, the elements of the 16×16 calculation matrix $[A]$ are functions of the rotation angles θ and θ' (corresponding to the quarter-wave plate and the birefringent plate, respectively), as well as the phase shift (δ) and the ellipticity (ϵ) of the latter. The intensity 16×1 vector of the (MPMVM) is then expressed as follows:

$$[I_N] = [A_{m,n}^N][M_v] = \begin{bmatrix} 1 + A_{0,5} + A_{0,10} + A_{0,15} \\ \vdots \\ 1 + A_{15,5} + A_{15,10} + A_{15,15} \end{bmatrix}. \tag{2.11}$$

$$\begin{bmatrix} I_0 \\ I_1 \\ I_2 \\ I_3 \\ I_4 \\ I_5 \\ I_6 \\ I_7 \\ I_8 \\ I_9 \\ I_{10} \\ I_{11} \\ I_{12} \\ I_{13} \\ I_{14} \\ I_{15} \end{bmatrix} = \begin{bmatrix} S^2\left(\frac{\delta}{2}\right)\cdot\left(S^2(2\epsilon)+1\right) \\ \frac{(S(\delta)+C(\delta)-1)S(2\epsilon)+8C^3(\epsilon)S^2\left(\frac{\delta}{2}\right)S(\epsilon)+C(2\epsilon)S(\delta)+(2-C(\delta))}{2} \\ C(2\epsilon)S(\delta)+1 \\ \frac{(-S(\delta)-C(\delta)+1)S(2\epsilon)+(4C(\delta)-4)C^3(\epsilon)S(\epsilon)+C(2\epsilon)S(\delta)+2-C(\delta)}{2} \\ \left(1+C(\delta)\right)S^2(2\epsilon) \\ \frac{\sqrt{2}\,S^2\left(\frac{\delta}{2}\right)S(4\epsilon)+\left(C^2(2\epsilon)S^2\left(\frac{\delta}{2}\right)+C^2\left(\frac{\delta}{2}\right)-\left(S^2\left(\frac{\delta}{2}\right)S^2(2\epsilon)+S(\delta)S(2\epsilon)\right)\right)}{2}+1 \\ -\left(\sqrt{2}\,C(2\epsilon)S^2\left(\frac{\delta}{2}\right)S(2\epsilon)\right)+\sqrt{2}\,C\left(\frac{\delta}{2}\right)C(2\epsilon)S\left(\frac{\delta}{2}\right)+1 \\ \frac{(-S(\delta)-C(\delta)+1)S(2\epsilon)+(4C(\delta)-4)C^3(\epsilon)S(\epsilon)+C(2\epsilon)S(\delta)+2-C(\delta)}{2} \\ -C(\delta)+1 \\ \frac{S(\delta)S(2\epsilon)+\left(\sqrt{2}C(2\epsilon)S(\delta)-C(\delta)\right)}{2}+1 \\ C(2\epsilon)\left(1-C(\delta)\right)S(2\epsilon)+1 \\ \frac{S(\delta)+(1-C(\delta))S(2\epsilon)+C(2\epsilon)S(\delta)+C(\delta)}{2}+4C^3(\epsilon)S^2\left(\frac{\delta}{2}\right)S(\epsilon)+1 \\ -C(\delta)+1 \\ \frac{(S(\delta)+1-C(\delta))S(2\epsilon)+(-C(2\epsilon)S(\delta)+(2-C(\delta))-8C^3(\epsilon)S^2\left(\frac{\delta}{2}\right)S(\epsilon))}{2} \\ \frac{S(4\epsilon)(C(\delta)-1)}{2}+1 \\ \frac{(-S(\delta)+(C(\delta)-1))S(2\epsilon)+8C^2(\epsilon)S^2\left(\frac{\delta}{2}\right)S(\epsilon)+C(2\epsilon)S(\delta)+(4C(\delta)-4)C^4(\epsilon)+(4-4C(\delta))C^2(\epsilon)+1}{2} \end{bmatrix} \tag{2.12}$$

Using sixteen angular combinations (θ, θ') and incorporating Eq.(2.12) into the calculus model, it is feasible to determine all elements of the $[M_{vmod}]$, as demonstrated in the subsequent analysis.

2.2.3 Calculus Model

To obtain the $[M_{Vmod}]$ and thereby ascertain the various characteristics of the birefringent sample, a calculus model was developed according to the procedures previously described. The angular positions of the birefringent medium and the quarter-wave plate were selected as multiples of 22.5°, with subindices (idt) referring to identity and (Vmod) to vacuum modified. The following steps were undertaken:
$[I_v] = [A_{idt}][M_{idt}]$ when the birefringent medium is a quarter-wave plate ($\epsilon = 0$ and $\delta = 90°$). However, when the quarter-wave plate is substituted with another birefringent medium (ϵ and δ being unknown and differing values), alterations in the detected intensity may occur either in the 16×16 matrix [A] or the 16×1 vector [M], as detailed in the subsequent calculations:

$$[I_{Vmod}] = [A_{idt}][M_{Vmod}]\,, \tag{2.13a}$$

$$[I_{Vmod}] = [A_{Vmod}][M_{idt}]\,, \tag{2.13b}$$

$$[A_{idt}][M_{Vmod}] = [A_{Vmod}][M_{idt}]\,, \tag{2.14}$$

$$[M_{Vmod}] = [A_{idt}]^{-1}[A_{Vmod}][M_{idt}]\,, \tag{2.15}$$

$$[M_{Vmod}] = [A_{idt}]^{-1}[I_N]\,. \tag{2.16}$$

2.2.4 Modified Vacuum Mueller Matrix

The calculus model represented by Equation (2.16) yields sixteen explicit expressions m_{ij} for the Mueller matrix of the birefringent medium under investigation. These expressions are functions of the phase shift δ and ellipticity ϵ. Each expression includes two terms, D

and E, and for simplification, the term B is also considered.

$$D = (cos(\delta) - 1)\,, \tag{2.17a}$$

$$E = sin(4\epsilon)\,, \tag{2.17b}$$

$$B = DE\,. \tag{2.17c}$$

These expressions have been normalised to M_{ij} by being divided by the first element of the Mueller matrix [m_{00}] that holds the maximum value in the hole matrix, as indicated next:

Original expressions

$$m_{00} = (4 - 3\sqrt{2})\ B + 1 \tag{2.18}$$

$$m_{01} = (4 - 3\sqrt{2})\ B + cos(\delta) \tag{2.19}$$

$$m_{02} = (4 - 3\sqrt{2})\ B - sin(\delta)\ sin(2\epsilon) \tag{2.20}$$

$$m_{03} = \frac{-\sqrt{2}+1}{2}\ B \tag{2.21}$$

$$m_{10} = (3\sqrt{2} - 4)\ B \tag{2.22}$$

$$m_{11} = (3\sqrt{2} - 4)B\ - \frac{1}{2}\ (cos(4\epsilon) + 1)D \tag{2.23}$$

$$m_{12} = (3\sqrt{2} - 4)\ B \tag{2.24}$$

$$m_{13} = \frac{\sqrt{2}-2}{2}\ B \tag{2.25}$$

$$m_{20} = \frac{\sqrt{2}}{2}\ B \tag{2.26}$$

$$m_{21} = \frac{\sqrt{2}}{2}\ B \tag{2.27}$$

$$m_{22} = (\frac{5\sqrt{2}-6}{2})\ B - \frac{1}{2}\ (cos(4\epsilon) + 1)D \tag{2.28}$$

$$m_{23} = (3 - 2\sqrt{2})\ B \tag{2.29}$$

$$m_{30} = \frac{4\sqrt{2}-5}{2}\ B \tag{2.30}$$

$$m_{31} = \frac{4\sqrt{2}-5}{2}\ B \tag{2.31}$$

$$m_{32} = -\frac{-\sqrt{2}+1}{2}\ B \tag{2.32}$$

$$m_{33} = \frac{3\sqrt{2}-4}{2}\ B + cos(2\epsilon)\ sin(\delta) \tag{2.33}$$

Normalised expressions

$$M_{00} = 1 \tag{2.34}$$

$$M_{01} = \frac{D}{m_{00}} + 1 \tag{2.35}$$

$$M_{02} = -\frac{sin(\delta)\ sin(2\epsilon) + 1}{m_{00}} + 1 \tag{2.36}$$

$$M_{03} = \frac{m_{00} - B - 1}{6m_{00}} \tag{2.37}$$

$$M_{10} = \frac{1}{m_{00}} - 1 \tag{2.38}$$

$$M_{11} = -\frac{(cos(4\epsilon) + 1)D - 2}{2m_{00}} - 1 \tag{2.39}$$

$$M_{12} = \frac{1}{m_{00}} - 1 \tag{2.40}$$

$$M_{13} = \frac{-m_{00} - 2B + 1}{6m_{00}} \tag{2.41}$$

$$M_{20} = \frac{\sqrt{2}B}{2m_{00}} \tag{2.42}$$

$$M_{21} = \frac{\sqrt{2}B}{2m_{00}} \tag{2.43}$$

$$M_{22} = \frac{-3D(cos(4\epsilon) + 1) + 2B - 5m_{00} - 3}{6m_{00}} \tag{2.44}$$

$$M_{23} = \frac{B-2}{3m_{00}} + \frac{2}{3} \tag{2.45}$$

$$M_{30} = \frac{B+4}{6m_{00}} - \frac{2}{3} \tag{2.46}$$

$$M_{31} = \frac{B+4}{6m_{00}} - \frac{2}{3} \tag{2.47}$$

$$M_{32} = \frac{-m_{00} + B + 1}{6m_{00}} \tag{2.48}$$

$$M_{33} = \frac{2cos(2\epsilon)\ sin(\delta) + 1}{2m_{00}}\ - \frac{1}{2} \tag{2.49}$$

2.2.5 Properties Recovery

The resulting Mueller matrix indicates that for a perfect linear birefringent medium, characterized by an ellipticity of the eigenstates ϵ=0, the first element m_{00} will turn to equal 1. Consequently, the matrix elements are normalized, with the diagonal elements m_{11}, m_{22}, and m_{33}, as well as the element m_{01} of the matrix M_{Vmod}, undergoing corresponding changes. All other elements of the matrix are zero. The expressions for the varying elements are given as follows:

$$M_{01} = cos(\delta)\,, \tag{2.50}$$

$$M_{11} = -cos(\delta) + 1\,, \tag{2.51}$$

$$M_{22} = -cos(\delta) + 1\,, \tag{2.52}$$

$$M_{33} = sin(\delta)\,. \tag{2.53}$$

In this work, the Mueller matrix of the birefringent medium is considered at an azimuthal angle of the fast axis $\theta' = 0°$ relative to the system's vertical axis. Therefore, a positive value of M_{01} indicates that the presumed axis is the fast one; otherwise, it is the slow one. This approach allows for explicitly identifying the rapid and slow axes of the linear birefringent medium.

Also, through the resulting modified vacuum Mueller matrix, the obtainment of other targeted properties δ and ϵ (for a linear birefringent material, in general, $\epsilon \approx 0$) is now a matter of solving a system of two equations with two unknowns, any equation coupled with M_{01}, M_{11}, M_{22} *or* M_{33} from the calculated Mueller matrix will serve the purpose, for example but not limited to:

$$\begin{cases} M_{01} = \dfrac{(cos(\delta) - 1)}{(4 - 3\sqrt{2})\,(cos(\delta) - 1)sin(4\epsilon) + 1} + 1 \\ M_{10} = \dfrac{1}{(4 - 3\sqrt{2})\,(cos(\delta) - 1)sin(4\epsilon) + 1} - 1 \end{cases} \tag{2.54}$$

The solutions to this system of equations correspond to the desired properties consequently:

$$cos(\delta) = \frac{M_{01} + M_{10}}{M_{10} + 1}\,, \tag{2.55}$$

$$sin(4\epsilon) = \frac{-M_{10}}{(3\sqrt{2} - 4)(M_{01} - 1)}\,. \tag{2.56}$$

2.3 Application to the Characterization of Poly(lactic acid) Polymer Properties

2.3.1 Material Choice and Preparation

The Stokes-Mueller formalism is employed in this study to extract the optical properties of birefringent materials, which are crucial for various applications [53, 54], especially in polarimetry. Recent advances in optical technology demand materials that are widely available, easy to process, cost-effective, and versatile. Polymers [55–61], particularly poly(lactic acid) (PLA), meet these criteria and address environmental concerns due to their biodegradable nature [60, 62]. PLA, a semicrystalline polymer, exhibits linear birefringence due to its ordered and anisotropic crystalline regions [63], making it an ideal candidate for our study. This research investigates, in the scope of experimental validation, the changes in PLA's optical properties across a wide temperature range, leveraging its thermoplastic nature, which undergoes compositional, structural, and functional modifications at specific temperatures [64, 65]. Differential Scanning Calorimetry (DSC) is widely recognized for its accuracy and reliability in assessing thermal transitions and phase changes in polymers [66]. Juxtaposing the findings from the newly proposed method with those obtained from Differential Scanning Calorimetry (DSC) ensures a robust evaluation of its effectiveness and accuracy. The comprehensive validation process highlights the potential of this approach to serve as a reliable alternative for characterizing the optical properties of birefringent media, paving the way for broader applications in material science and optical engineering.

Given the inherent complexities in material storage conditions and sample preparation methods, certain approximations are necessary to ensure reliable experimental outcomes. Nonetheless, the reliability of the experimental results is substantially enhanced through the use of multiple samples and a broad range of thermal intervals.

The study utilized Ingeo biopolymer 2003D PLA granules from NatureWorks, characterized by a glass transition temperature (T_g) of approximately 60°C, a cold crystallization temperature (T_{cc}) within the range of 110-130°C, and a typical melt temperature (T_m) spanning 130-160°C [67]. Samples of neat PLA plates, circular in shape with a diameter of 3 mm and a thickness of 1 mm, were prepared by melting the granules and allowing them to

cool at room temperature. Subsequently, each sample was subjected to different temperature conditions within the range of 45-190°C. Post-annealing, quenching was performed at temperatures below zero to preserve the structural and physical properties at the specified temperature. The evolution of optical properties was then systematically studied.

2.3.2 Experiment

The proposed polarimeter, depicted in Figure 2.2, is utilized to determine the polarimetric properties of PLA samples. The experimental setup is mounted on a precisely adjusted table. The light source is a monochromatic, linearly polarized He-Ne laser with a $\lambda = 543.5$ nm wavelength. The polarization of the emerging light is then measured in terms of intensities to determine the modified vacuum Mueller matrix. This allows for the extraction of the modifications induced by the sample on the various elements of the matrix, facilitating the calculation of its optical properties.

For the initial startup of the setup, the target properties were extracted from a reference medium, a quarter wave plate ($\lambda/4$). The phase shift exhibited an angle value of 89.38°, and the ellipticity had an angle value of 0.2°. These satisfactory results provided sufficient confidence to proceed to the next step. In evaluating the findings, a comparison was made with the DSC results obtained from the same PLA granules used in the study.

DSC, a widely used thermal technique, allows for determining heat flow and the temperatures associated with calorimetric transitions as a function of temperature and time [66]. The primary interest lies in the physical and chemical changes during thermal transitions, such as phase changes, cold crystallization, and melting, which are directly related to the optical properties under investigation. The data collected by the differential scanning calorimeter (Q20, TA) are depicted in a graph alongside the phase shift results obtained using the proposed polarimeter, as shown in Figure 2.3.

2.3.3 Discussion:

The DSC curve of semicrystalline PLA typically exhibits three distinct temperatures, represented by sequential peaks and dips, each corresponding to specific thermal transitions experienced by the material during heating [68]. The phase shift changes as the polymer's molecular chains orient in response to these thermal transitions. This is demonstrated by the similarity in the data patterns observed in both curves, as detailed below:

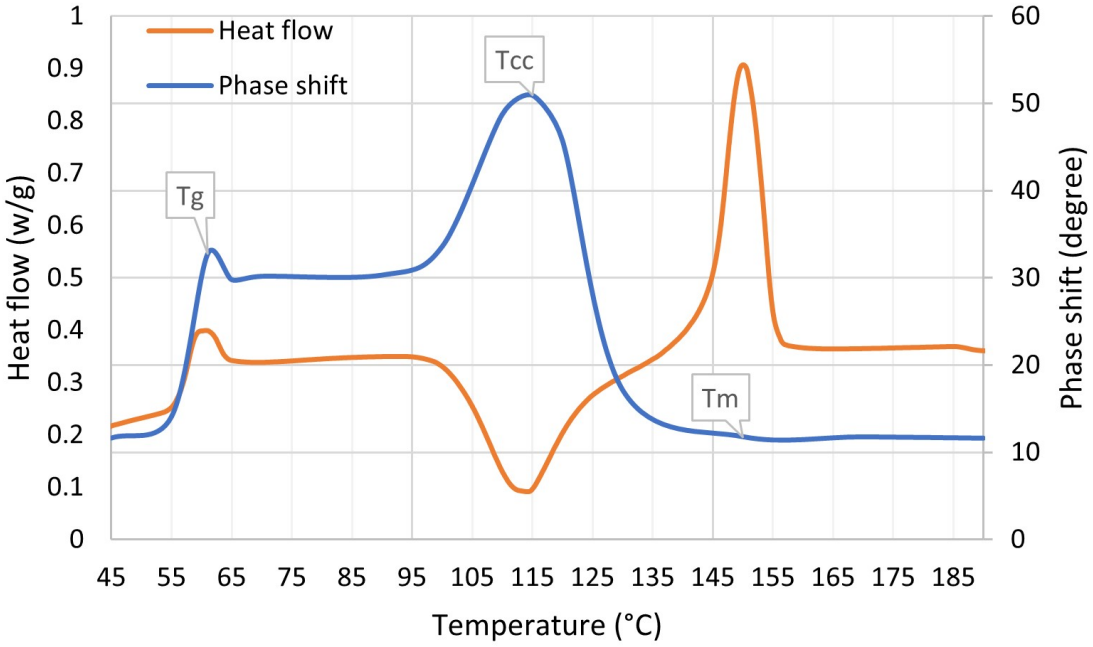

Figure 2.3: Phase shift curve of heated pure PLA plates (blue) compared to DSC heating curve of pure PLA granules at 10°C\min (orange)

1. The glass transition temperature (T_g) is indicated by a slight shift in the baseline of both graphs at 61°C. The phase shift (δ) at this temperature is 32.74°. The phase shift changes from a steady angle of approximately 11° to a higher value of approximately 30° as the heating temperature increases to 100°C. This increase is attributed to the significant mobility gained by some of the amorphous chains or segments at T_g [69], which allows these molecular chains to become oriented, leading to a higher phase shift induced by the material.

2. The cold crystallization temperature (T_{cc}) is reflected as a dip (heat release) in the DSC graph and a peak in the phase shift graph, both observed at 115°C. This phenomenon occurs due to the semicrystalline nature of PLA, indicating that the samples are primarily composed of amorphous, yet crystallizable, material. Cold crystallization takes place because, at a specific heating temperature above T_g, the amorphous molecular chains gain sufficient mobility to arrange into an ordered anisotropic structure, forming crystals through chain folding [63, 70]. This results in the formation of a linear anisotropic medium, exhibiting an ellipticity (ϵ) of 4.58° and a phase shift (δ) of 50.94°.

3. The melting temperature (T_m) is characterized by a peak in the DSC graph and a return to the initial steady behaviour of approximately 11° in the phase shift graph, both occurring at 150°C. At this temperature, both the initial crystalline fraction and the newly developed crystalline segments are melted. The discrepancy between the two curves at the melting point is attributed to the use of plates made from pre-melted moulded granules for phase shift measurements. Consequently, after being melted and cooled for the second time, the sample regains its initial semicrystalline molecular structure, causing the phase shift curve to revert to its original behaviour.

2.4 conclusion

A noovel method based on the Stokes-Mueller formalism was proposed to extract the optical properties of linear birefringent media, specifically their fast and slow axes. This study provided a comprehensive description of the Mueller polarimeter, which utilizes a modified vacuum matrix. The mathematical model and the resulting Mueller matrix expressions were detailed. Experimental validation was conducted using PLA samples, with phase shift and ellipticity measurements confirming the method's validity. These results underscore the method's potential as a powerful tool for optical characterization, materials science, and the study of molecular structures. However, this method has limitations. While it is highly effective in determining the phase shift for materials with low anisotropy, it is less effective for determining the ellipticity of their eigenstates unless the anisotropy is significant. This constraint highlights the need for further refinement. Future research should focus on enhancing the polarimeter's performance and exploring additional optical properties. Addressing the current method's limitations will contribute to its broader applicability and effectiveness in the field of optical characterization.

Chapter 3

Polarimetric Evaluation Of Geometric Phase Elements

La volonté trouve, la liberté choisit.

Trouver et choisir, c'est penser

– Victor Hugo

In recent years, the paradigm of structured light—light defined by a complex spatial arrangement—has garnered significant scholarly interest [71]. In traditional optical imaging, spatial configuration primarily impacts the spread of light intensity. However, an expanding array of studies has concentrated on the control of phase and polarization distributions. The characteristics of light wavefronts, which dictate its propagation behavior, can be modified through phase modulation introduced by optical components. This encompasses not only conventional instruments such as refractive lenses but also contemporary engineered devices, including holograms, spatial light modulators, and metasurfaces [72–74]. This investigation prioritizes the evaluation of optical elements possessing geometric phase (GP) structures, wherein wavefront modification is accomplished through phase retardation phenomena (birefringence), independent of propagation distance. The inaugural identification of the distinctive optical behavior associated with geometric phase was conducted by S. Pancharatnam during his analysis of interference patterns formed by polarized light interacting with crystal plates [8]. It was identified that a phase shift manifests when polarization undergoes a cyclic transformation, equating to half of the solid angle defined by the polarization trajectory on the Poincaré sphere. The Poincaré sphere proved essential to Pancharatnam's comprehension of the geometric characteristics of this phase. Although his research initially attracted minimal focus, it was later revitalized and extensively recognized when M.V. Berry delineated the relationship between Pancharatnam's geometric phase in polarization optics and the more general phenomenon of phase accumulation occurring during the adiabatic evolution of quantum states [9, 75].

Main Objectif

Employing the Mueller matrix polarimetric microscopy and spectroscopy techniques to phase determination and evaluation of the functionality of commercial Geometric Phase (GP) lens and grating.

3.1 General principles about Geometric Phase Optical Elements

3.1.1 Geometric Phase: a universal principle

Geometric phase and holonomy in physics, along with the Foucault pendulum in the real world, all share the same underlying principle: the accumulation of a global change due to transport along a closed path in a curved space. This principle, fundamental to both classical and quantum systems, manifests as the geometric phase in optical and quantum systems, where a phase shift is acquired solely from the path taken in parameter space, independent of the dynamic evolution. Holonomy, in the context of differential geometry, describes the orientation change after parallel transport around a loop in a curved space, which is mathematically and conceptually similar to the geometric phase in physics . The Foucault pendulum, as a real-world example, demonstrates this concept through the gradual rotation of its oscillation plane due to Earth's curvature, analogously exhibiting a form of holonomy. In both cases, whether in abstract parameter spaces or real-world curved surfaces, the path-dependent change reflects the same geometric principle, bridging optical and physical phenomena.

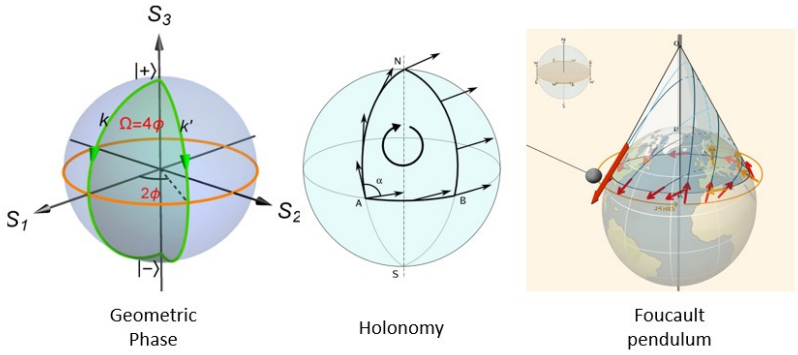

Figure 3.1: Otical geometric phase, Holonomy and Foucault pendulum: same underlying principle.

3.1.2 Fabrication Principle

The optical components exhibiting geometric phase (GP) are fabricated utilizing liquid crystal polymers, which, in conjunction with a photo-alignment layer and various chiral

dopants, are organized into intricate three-dimensional configurations that can be incorporated within a thin film. The manufacturing process is notably complex and has been comprehensively documented in several prior investigations [76–78]. Essentially, these liquid crystal-based Pancharatnam-Berry (PB) optical elements comprise multiple twisted birefringent layers, a configuration that, as will be elaborated upon later and illustrated in Figure (3.2), affects the resultant optical activity. Furthermore, alternative fabrication methods for GP optical components are currently under exploration, including a novel approach involving ultrafast laser inscription within silica glass [79]. The geometric phase is contingent upon the polarization state of the incident light and can be regulated by the alignment of liquid crystals within the optical component, which is accomplished through Linear Photopolymerization (LPP) techniques.

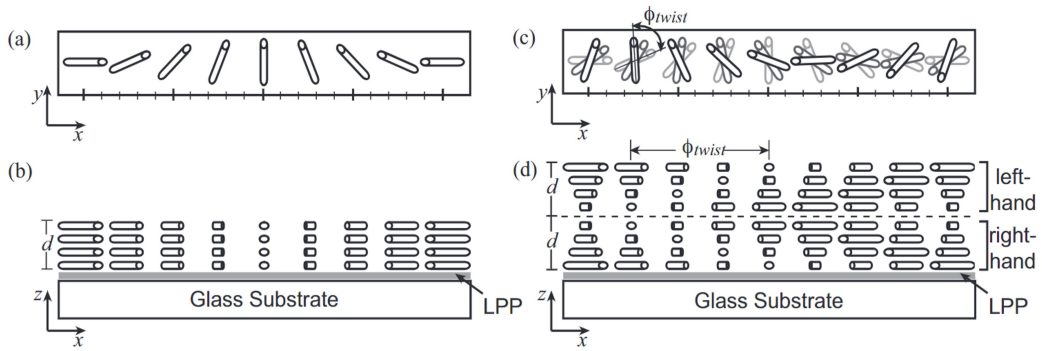

Figure 3.2: Geometric phase elements basic geometry: a) top view, b)side view. The orientation of local linear birefringence is shown as small twisted bars from c) top view and d) side view. image extracted from [80].

3.2 Working Principle of GP elements

To begin, we will examine a half-wave plate's representative Jones matrix (aligning its fast axis horizontally) as a simple and direct approach to explaining the operating principle behind geometric phase (GP) optical elements [81]:

$$J = e^{-i\pi/2} \begin{pmatrix} 1 & 0 \\ 0 & -1 \end{pmatrix} . \tag{3.1}$$

Recall equation (1.33) considering a rotation of the half-wave by an angle ϕ, its Jones matrix is:

$$J' = R(-\phi)JR(\phi) = e^{-i\pi/2}\begin{pmatrix} \cos 2\phi & \sin 2\phi \\ \sin 2\phi & -\cos 2\phi \end{pmatrix}, \tag{3.2}$$

with $R(\phi)$ indicates the 2×2 matrix of rotation expressed earlier by equation (1.33). For an arriving beam of light with circular polarization, it is represented by the Jones vector :

$$E_{\pm} = \begin{pmatrix} 1 \\ \pm i \end{pmatrix}. \tag{3.3}$$

The emerging Jones vector is computed as:

$$J'E_{\pm} = e^{-\pi i/2}\begin{pmatrix} \cos 2\phi & \sin 2\phi \\ \sin 2\phi & -\cos 2\phi \end{pmatrix}\begin{pmatrix} 1 \\ \pm i \end{pmatrix} = e^{-\pi i/2}e^{\pm 2\phi i}\begin{pmatrix} 1 \\ \pm i \end{pmatrix}. \tag{3.4}$$

In this context, the phase factor consists of two components: one is solely determined by the degree of phase delay, while the newly revealed one depends on two times the angle of orientation, ϕ. Now, if the rotation angle ϕ is spatially varying, i.e., $\phi(x, y)$, the resulting light wave experiences a transverse inhomogeneous polarization transformation. This spatial variation leads to a reshaping of the wavefront, which is influenced by the light's state of polarization, thereby allowing the development of what are known as Pancharatnam–Berry phase optical elements. These components were originally introduced by Bharandi[82], with further contributions made by Bomzon et al. [83]. However, experimental implementations of such elements did not emerge until several years later [84, 85].

3.2.1 Not Necessarily Closed Path!

The phase term $\pm 2\phi_i$ presented in Equation (3.4) is commonly Designated as the Pancharatnam–Berry geometric phase. However, the transformation of the vector-matrix described by this equation does not form a closed circuit on the Poincaré sphere, as initially characterized by Pancharatnam [8], since the initial and final polarization states differ (i.e.,perpendicular to each other). Rather, this transformation represents a path connecting the north and south poles (or vice versa) of the Poincaré sphere, traversing a geodesic arc or simply stated a meridian with an azimuth of 2ϕ, as it is shown in Figure (3.3). To complete this path, the transformation defined by the Jones matrix J' could be applied twice,

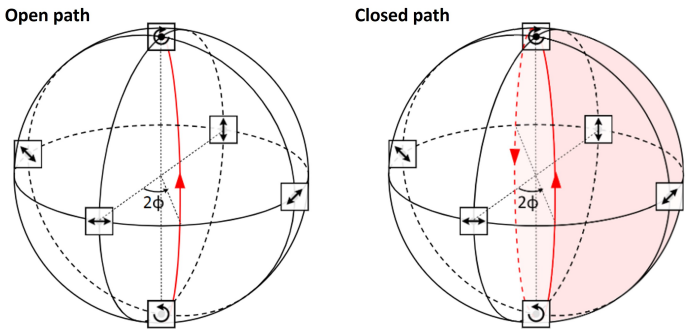

Figure 3.3: The Poincaré sphere pictorial for the transformations $J'E^-$ (Open path) and only $J'J'E^-$ whose panel represents a closed trajectory [81].

yielding [81]:

$$J'J'E_\pm = e^{-\pi i}E_\pm\,, \tag{3.5}$$

(Open path), along with only $J'J'E^-$, whose panel depicts a closed trajectory. The closed trajectory formed by matching the input and output polarization states divides the Poincaré sphere into two hemispheres. In this scenario, the Pancharatnam–Berry phase equals π, while the angular area enclosed by the loop measures 2π, as illustrated in Figure (3.3) (Closed path case). Bhandari's [82] and Roux's [84] seminal work on GP lenses utilized an experimental setup designed to trace a closed loop on the Poincaré sphere, varying with ϕ. In their setup, linearly polarized light at $45°$ is first converted into right-handed circular polarization using a quarter-wave plate, then into left-handed circular polarization through a half-wave plate (the GP lens). Finally, the light is returned to linear polarization via another quarter-wave plate, completing the loop. While additional wave plates are part of their experimental configuration, the effect of GP optical elements can still be observed outside of closed loops. Aharonov and Jeeva Anandan later redefined the geometric phase for non-adiabatic processes [86], with Equation (3.4) demonstrating that two transformations with identical start and end states produce optical phases of opposite signs, depending on the polarization handedness [81].

3.3 Geometric Phase optics in terms of general retarder

In real-world applications, GP optical elements often deviate from the ideal half-wave plate model described in Equation (3.1). For more general cases, Equation (1.48)—the Jones matrix

for a generic retarder—is more appropriate. Therefore, the following section investigates the impact of a general retarder characterized by linear retardance L (with the fast axis horizontal) and circular retardance C [44, 87].

$$J_{gR} = \begin{pmatrix} \cos\frac{T}{2} - \frac{iL}{T}\sin\frac{T}{2} & \frac{C}{T}\sin\frac{T}{2} \\ -\frac{C}{T}\sin\frac{T}{2} & \cos\frac{T}{2} + \frac{iL}{T}\sin\frac{T}{2} \end{pmatrix}.$$

Replicating the steps outlined in equation (3.2), the rotated retarder is expressed as:

$$J'_{gR} = R(-\phi)J_{gR}R(\phi) = \begin{pmatrix} \cos\frac{T}{2} & \frac{C}{T}\sin\frac{T}{2} \\ -\frac{C}{T}\sin\frac{T}{2} & \cos\frac{T}{2} \end{pmatrix} - i\frac{L}{T}\sin\frac{T}{2}\begin{pmatrix} \cos 2\phi & \sin 2\phi \\ \sin 2\phi & -\cos 2\phi \end{pmatrix}. \quad (3.6)$$

The rotated Jones matrix can be expressed as the product of two distinct components. Notably, the first component remains unaffected by the rotation angle ϕ, while all the angular dependence is contained within the second component. The effect of this general rotated retarder on transmitted circularly polarized light can be determined using the following expression:

$$J'_{gR}E_{\pm} = \begin{pmatrix} \cos\frac{T}{2} \pm i\frac{C}{T}\sin\frac{T}{2} \\ -\frac{C}{T}\sin\frac{T}{2} \pm i\cos\frac{T}{2} \end{pmatrix} - e^{\pm 2\phi i}\frac{L}{T}\sin\frac{T}{2}\begin{pmatrix} 1 & \pm i \end{pmatrix}. \quad (3.7)$$

The first term does not induce any phase alteration and, therefore, does not affect the wavefront. This term is typically identified as the zero-order leakage wave. On the other hand, the second term, which carries the opposite handedness to the input, is the only contributor to wavefront modulation due to its association with a Pancharatnam–Berry (PB) phase of $\pm 2\phi$. If $C = 0$ and $L = \pi$, the first term in Equations (3.6) and (3.7) vanishes, leading to the "ideal" scenario described in Equation (3.4), where no leakage wave is present. When $C = 0$ and $L \neq \pi$, a leakage wave still persists; however, it maintains the same polarization as the incident wave. This occurs because the first matrix term in Equation (3.6) reduces to the identity matrix, indicating no change in polarization. This situation is elaborated upon in Ref. [88]. A third case arises when $C \neq 0$ and $L = \pi$. Although similar to the general case, in this instance, a leakage wave is present, and the polarization shifts relative to the incident wave. Further exploration of this case will be presented later.

Next, attention is given to the second term in Equation (3.6), which can be reformulated as:

$$\begin{pmatrix} \cos 2\phi & \sin 2\phi \\ \sin 2\phi & -\cos 2\phi \end{pmatrix} = \frac{e^{-2i\phi}}{2} \begin{pmatrix} 1 & -i \\ i & 1 \end{pmatrix} \begin{pmatrix} 1 & 0 \\ 0 & -1 \end{pmatrix} + \frac{e^{2i\phi}}{2} \begin{pmatrix} 1 & i \\ -i & 1 \end{pmatrix} \begin{pmatrix} 1 & 0 \\ 0 & -1 \end{pmatrix} . \quad (3.8)$$

The original matrix has been decomposed into two separate components, each corresponding to a geometric phase shift of $\pm 2\phi$. Importantly, both terms involve the product of the Jones matrix for either **a right-handed circular polarizer**, $\frac{1}{2}\begin{pmatrix} 1 & i \\ -i & 1 \end{pmatrix}$, or **a left-handed circular polarizer**, $\frac{1}{2}\begin{pmatrix} 1 & -i \\ i & 1 \end{pmatrix}$, along with the Jones matrix representing a half-wave retarder (as given in Equation (3.1)). The presence of these circular polarizer matrices indicates that, regardless of the initial polarization state, the waves undergoing a geometric phase shift of $\pm 2\phi$ will always be circularly polarized. Therefore, the transformation of any general input wave can be mathematically expressed as follows [76, 89]:

$$E_{\text{in}} \rightarrow A_{\text{leak}} E_{\text{leak}} + A_{+} e^{2\phi i} E_{+} + A_{-} e^{-2\phi i} E_{-} . \quad (3.9)$$

The amplitude coefficients A_i determine the distribution of incoming energy among the three resulting waves: the leakage wave, the primary wave (typically corresponding to right-handed circular polarization), and the conjugate wave (typically corresponding to left-handed circular polarization). A distinctive feature of geometric phase (GP) optical elements is the absence of higher-order parasitic diffraction waves. When the GP element operates purely as a lossless retarder, the amplitudes satisfy the relation $A_{\text{leak}}^2 + A_{+}^2 + A_{-}^2 = 1$. Additionally, the circular polarizations associated with E_{+} and E_{-} remain invariant, independent of the input polarization and the retarding characteristics of the optical element. However, the polarization of the leakage wave, E_{leak}, depends on the input polarization E_{in} as well as the parameters C and L. **Equation (3.9) highlights that GP optical elements serve as effective circular polarization beam splitters, separating any incident beam into two circularly polarized beams with opposite handedness**, as depicted schematically in Figure (3.4).

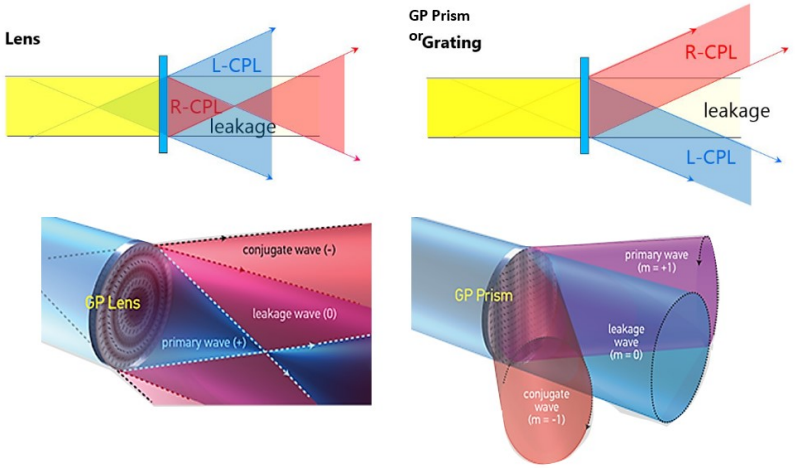

Figure 3.4: A schematic illustration depicting the influence of the GP lens and grating (prism) on an incident wavefront is presented. The labels R-CPL and L-CPL refer to right-circularly polarized light and left-circularly polarized light, respectively [81]. An additional illustration in 3D for both elements is included [90].

3.4 Mathimatical Phase Profiles's expressions of the GP optics

The variation in phase across the plane orthogonal to the propagation axis defines the wavefront or phase profile, which dictates the propagation behavior of the beam. A basic example of an inhomogeneous phase profile is found in polarization gratings, characterized by a linear phase shift described as:

$$\phi_{\text{grating}}(x) = \frac{\pi x}{\Lambda}\,, \tag{3.10}$$

in this context, Λ denotes the grating period. Conversely, polarization lenses are characterized by a quadratic phase function [88]:

$$\phi_{\text{lens}}(r) = \frac{\pi}{\lambda}\left(\sqrt{f^2 + r^2} - f\right)\,, \tag{3.11}$$

here, r represents the radial coordinate, f is the focal length of the lens, and λ is the wavelength. A distinctive property of a GP lens is its behavior with circular polarization: light with one circular polarization converges through the lens (positive focal length), while the opposite polarization causes the light to diverge (negative focal length), as shown in Figure (3.4).

3.5 Experimental Methods and Techniques

The GP optical components analyzed consist of a polarization lens and a polarization grating, both manufactured by ImagineOptix and distributed by Edmund Optics. The polarization lens has a 50 mm focal length, with dimensions of 25 × 25 mm and a thickness of 0.45 mm. The polarization grating shares the same physical size as the lens, featuring a groove density of 286 grooves/mm ($\Lambda = 3.2\,\mu$m), resulting in a diffraction angle of around 10° for light at a wavelength of 550 nm.

3.5.1 Principle of Mesearement

The method employed to assess the performance of the GP elements is Mueller matrix polarimetry, requiring a reevaluation of Equation (1.34).

$$\mathbf{S}^{\text{out}} = \mathbf{M}\mathbf{S}^{\text{in}}\,.$$

The matrix M is referred to as the 4×4 Mueller matrix, consisting of 16 real elements m_{ij}. Typically, Mueller matrices are normalized to the m_{00} element as discussed at great length in chapter 1, ensuring that the matrix elements lie within the range of -1 to 1. The Stokes–Mueller formalism is highly effective for analyzing light interactions with media, particularly in scenarios where the degree of polarization of the output beam may be reduced. However, when depolarization is absent, a direct correspondence exists between Jones and Mueller matrices, allowing the parameters within Jones matrices, as described in Section (3.3), to be extracted from the Mueller matrix [87]. Various decomposition techniques have been developed to analyze experimental Mueller matrices [40], enabling the straightforward extraction of physical properties, such as birefringence, from the data. In practice, Mueller matrix polarimetry can be implemented by incorporating a polarization state generator (PSG) and analyzer (PSA) into the optical paths of existing systems, such as microscopes, allowing for a comprehensive analysis of sample structures.

3.5.1.1 Measurement Techniques

Mueller Matrix Microscope

The polarimetric measurements presented here were performed using two custom-built Mueller matrix polarimeters. The first is a Mueller matrix microscope that uses two rotating compensators in conjunction with a camera for Mueller matrix imaging at micrometric resolution [91, 92]. The Mueller matrix (MM) microscope operates based on the Stokes-Mueller formalism, which provides a systematic approach for describing how light's polarization changes as it passes through various optical elements. In this system (see Figure 3.5), light first enters the Polarization State Generator (PSG), which consists of a polarizer and a rotating compensator. The light is then transmitted through the sample, where its polarization state is altered. After passing through the sample, the light reaches the Polarization State Analyzer (PSA), also made up of a rotating compensator and a polarizer. Both compensators rotate at different speeds, introducing time-dependent changes to the light's polarization [91].

The polarization state of the light after passing through the system is described by a series of matrix multiplications as indicated in equation 1.35:

$$S_{\text{out}}(t) = P_1 M_{C1}(t) M_S M_{C0}(t) P_0 S_{\text{input}} ,$$

where the output Stokes vector is a result of the interactions between the polarization elements and the sample. The final Mueller matrix of the sample contains 16 elements, each corresponding to different optical properties. Specific elements are linked to phenomena such as linear and circular dichroism, as well as linear and circular birefringence. Through careful calibration and analysis, the MM microscope can extract detailed information about the sample's optical properties, making it a powerful tool for characterizing materials with complex anisotropic behaviors. The retrieval of the Mueller matrix microscope elements (MM) allows the identification of the sample's different optical properties. Interestingly, for our study, m_{12} and m_{21} are due to circular birefringence, while linear birefringence is translated by the elements $m_{13}, m_{23}, m_{31},$ and m_{32} [91]. Similar to the study made in chapter2, the calibration is made in the absence of the sample and therefore none of the polarimetric effects is present and the Mueller matrix M_S coincides with the identity matrix.

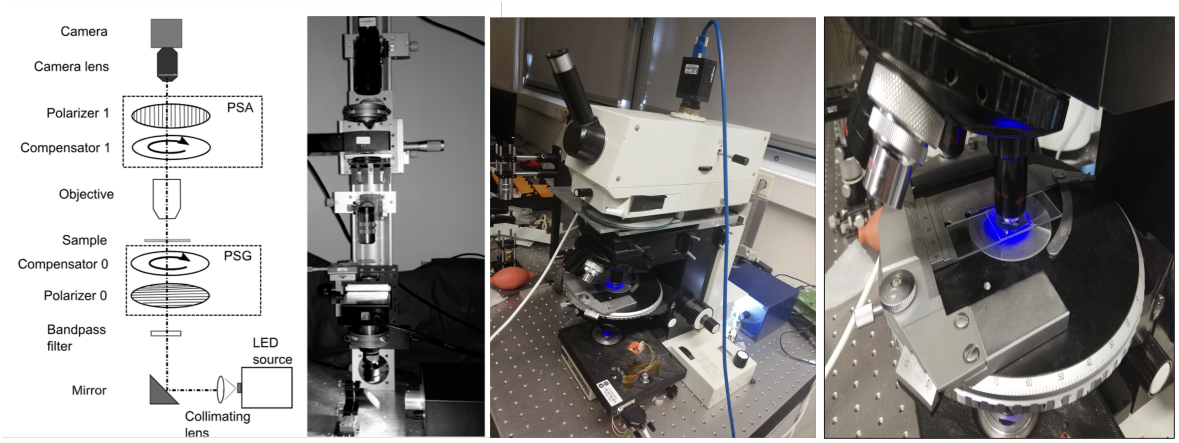

Figure 3.5: scheme of the Mueller Matrix microscope, technical drawing at left, its photos in the middle and the intime GP sample measuring at right [91].

Figures 3.9, 3.10,3.12,3.13 are given by this polarimetric microscope.
This microscope operates in two modes: in the standard or orthoscopic mode, the front focal plane of the objective is focused on the camera sensor, where each point on the sensor corresponds to a point on the sample. In the diffractometer mode, the back focal plane of the objective is imaged onto the camera sensor, where each point corresponds to a direction of light diffraction [93].

Mueller Matrix Spectroscope

The second polarimeter is a spectroscopic device capable of measuring the complete Mueller matrix without any moving components, as it relies on four photoelastic modulators, each operating at distinct frequencies.

This design, as shown in Figure 3.6, enables the simultaneous measurement of all 15 independent components of the normalized Mueller matrix. Using this method, it becomes possible to capture both the optical characteristics of the sample and its depolarization effects in real time. Figure 3.13 is an example of the given images. The working principle of the device follows a mathematical framework similar to previously established methods [94].

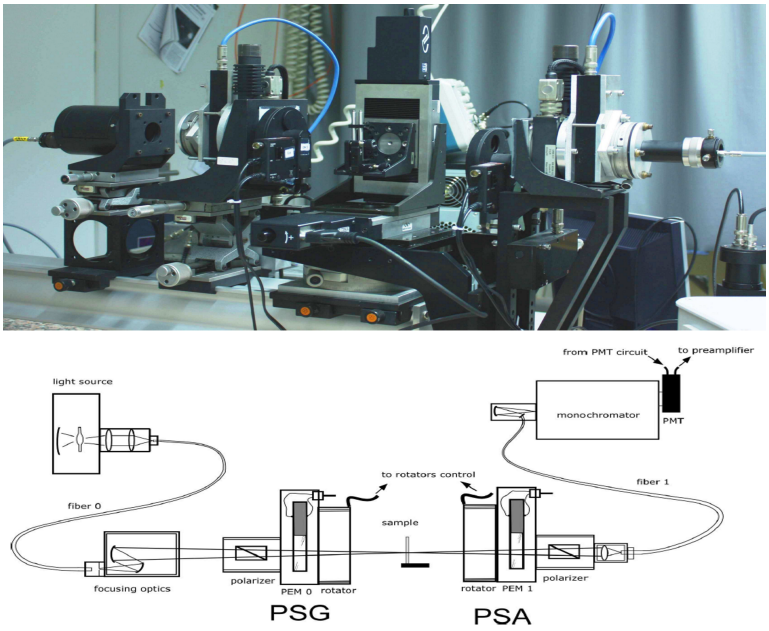

Figure 3.6: A photo and technical depiction of the Mueller Matrix Spectrometer with four photoelastic modulators [94].

3.6 Evaluation and Results

As a first observation made by the naked eye, the GP elements exhibit a high inherent chromatic aberration, clearly present in Figure (3.7). The light spots are the intensity of light emerging from the GP lens under microscopic vision with a green, blue, and red light source. As a result of the chromatic aberration, the distance of the spectral separation is relatively dependent on the wavelength. Color-selective geometric-phase lenses for imaging purposes have recently been reported [95]. The geometric phase profiles are most effectively analyzed through the use of a Mueller matrix microscope. This method is essential because only a polarimeter with exceptionally high spatial resolution can reveal the point-to-point variation in retardation orientation. Figure (3.8) displays the normalized Mueller matrix images taken at the central region of the lens and the polarization grating. For these measurements, a 10× microscope objective was used for the lens, while a 50× objective was applied to the grating, both utilizing green light at 540 nm.

The measured Mueller matrices allow for the determination of the linear retardance orientation (denoted as ϕ) at each pixel, using the analytic inversion technique [87]. The in-plane

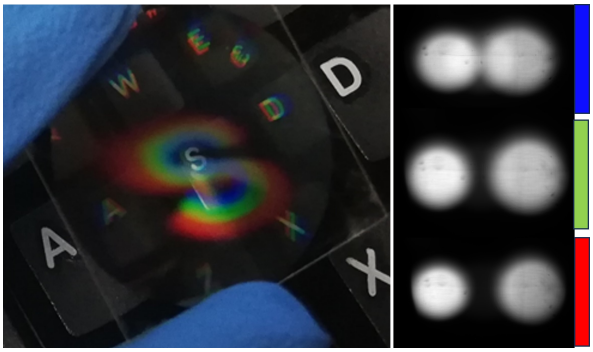

Figure 3.7: live observation from GP lens showing a high spectral dependence of response translated by the different spatial separation distance between the primary and conjugate waves for the microscope's blue, green, and red light source.

orientation angle ϕ is described by:

$$\phi = \frac{1}{2}\text{atan2}(L'_B, L_B)\,, \tag{3.12}$$

where L'_B and L_B are parameters derived from the analytic inversion, and atan2 represents the two-argument arctangent function. The results of this computation are depicted in Figure (3.9). As anticipated, the ϕ phase distribution shows concentric rings of constant phase for the lens, while in the case of the grating, it forms straight lines. The phase values range between $-90°$ and $90°$, and since $\pm 90°$ represent the same physical orientation, the phase plots in Figure (3.9) display discontinuities at these points. If required, these "wrapped" phase profiles can be unwrapped by extending the orientation angles beyond $90°$, which is also demonstrated in Figure (3.9). Additionally, the figure compares the experimentally obtained unwrapped phases with the theoretical predictions based on Equations (3.10)(3.11) for the lens and the grating, respectively [81]. Overall, there is a strong correlation between the experimental data and the theoretical models. Minor discrepancies may arise due to deviations in the manufacturing process of the GP optical elements from their specified values or from distortions introduced by the microscope objective in our Mueller matrix setup. When compared to other techniques for examining the geometrical phase, such as polarization microscopy [96] or optical interferometry [76], Mueller matrix microscopy offers the benefit of maintaining the simplicity of polarization microscopy while also providing fully quantitative and precise measurements [81].

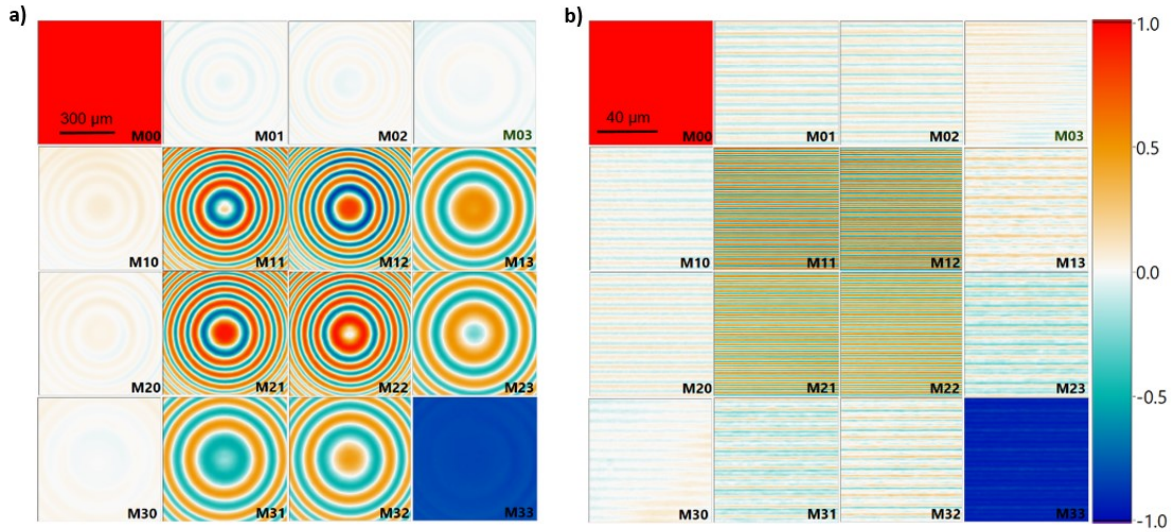

Figure 3.8: Normalized Mueller matrix images are shown for both the lens in panel (a) and the grating in panel (b). The scale bar is provided in the M_{00} element of each image.

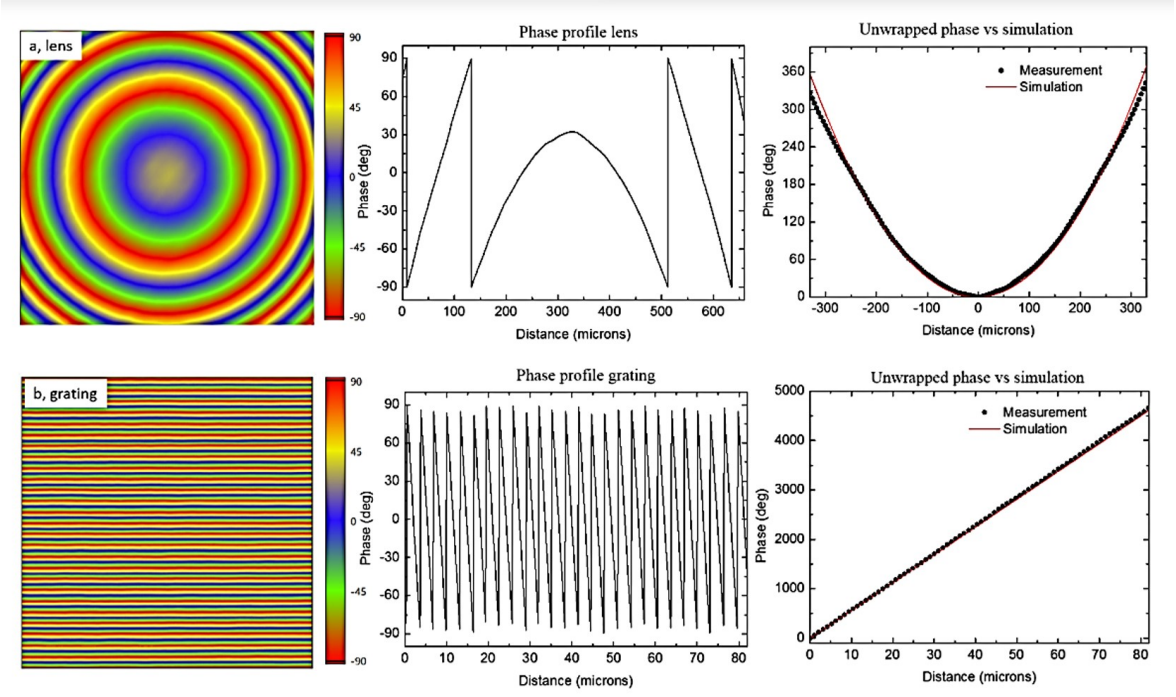

Figure 3.9: Phase profiles, ϕ, are presented for the lens in (a) and the grating in (b). The images on the left display the spatially resolved phase, while the central plots show vertical cross-sections of the phase profiles. The graphs on the right illustrate the comparison between the unwrapped experimental phases and the simulated ones.

3.6.1 Linear and Circular Retardances

The Mueller matrix microscopy data presented earlier not only enable the calculation of phase profiles but also offer insight into the linear and circular retardances of the films. Figure (3.10) illustrates these findings for the GP lens. The linear retardance exhibited a fairly uniform value around 2.85 rad, which is slightly lower than the "ideal" value of π, corresponding to perfect half-wave retardation. At this wavelength, the circular retardance was approximately -0.3 rad and appeared to be somewhat less spatially uniform compared to the linear retardance. Additionally, while the linear retardance remained nearly constant across the visible spectrum, the circular retardance was more dependent on wavelength, even changing sign when comparing blue and red wavelengths. This characteristic, likely associated with the twisted structure of the liquid crystal layers, will be further explored in the following sections [81].

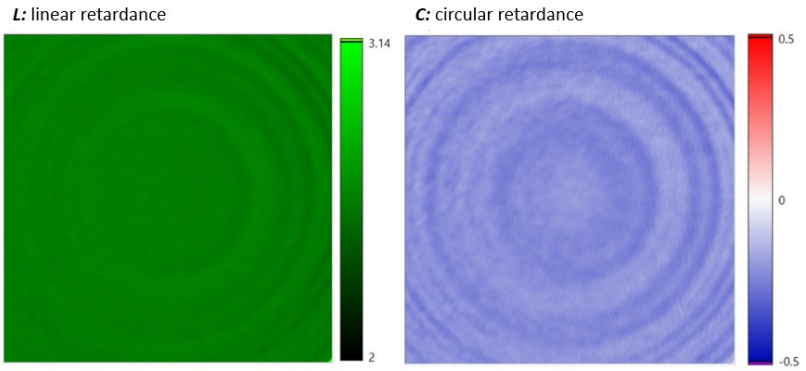

Figure 3.10: Values for both linear and circular retardance magnitudes in the central region of the lens are shown, with an imaged area of 620 μm by 620μm. The scales are presented in radians.

3.6.2 Evaluation of the Primary and Conjugate Waves Through Polarimetric Patterns

A straightforward method for analyzing the polarization behavior of the three waves into which the light incident on a GP optical element is redistributed involves using a Mueller matrix microscope in diffractometer mode. Figure (3.12) depicts the (unnormalized) Mueller

matrix measurements obtained for both the lens and the grating in this mode. Notably, for the lens measurement, the light was directed through a side spot rather than its centre. This approach was chosen because when light is centred, the lens focuses or defocuses it, preventing a clear spatial separation of the waves. However, with a side-incident beam, the separation effect becomes more similar to that of a grating. An illustrative figure is given below, it shows the Mueller matrices obtained by the polarimetric spectroscope for a light spot that passed through the center of the GP lens exhibiting no spatial separation of the light wave components and the second case for a light spot passed through the left side of the GP lens with a resulted in clear spatial separation.

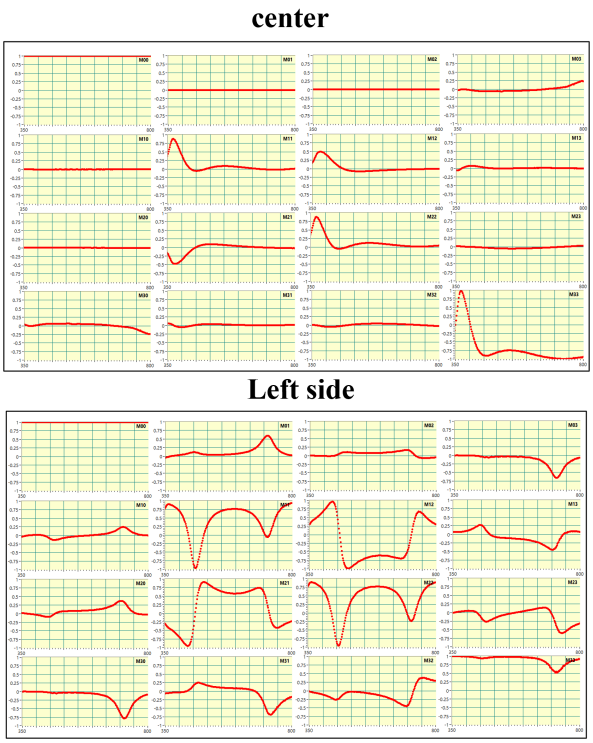

Figure 3.11: Spectroscopic Mueller matrices of the light spot passing through the centre and the left side of the GP sample lens.

In Figure (3.12), the primary and conjugate waves can be distinctly observed as separated spots, while the leakage wave, which lies between the two, is hardly visible due to its significantly weaker intensity. From these images, the Mueller matrices corresponding to the primary and conjugate waves can be approximated as follows:

$$\begin{pmatrix} 1 & 0 & 0 & -1 \\ 0 & 0 & 0 & 0 \\ 0 & 0 & 0 & 0 \\ 1 & 0 & 0 & -1 \end{pmatrix} = \begin{pmatrix} 1 & 0 & 0 & 1 \\ 0 & 0 & 0 & 0 \\ 0 & 0 & 0 & 0 \\ 1 & 0 & 0 & 1 \end{pmatrix} \begin{pmatrix} 1 & 0 & 0 & 0 \\ 0 & 1 & 0 & 0 \\ 0 & 0 & -1 & 0 \\ 0 & 0 & 0 & -1 \end{pmatrix}, \tag{3.13}$$

$$\begin{pmatrix} 1 & 0 & 0 & 1 \\ 0 & 0 & 0 & 0 \\ 0 & 0 & 0 & 0 \\ -1 & 0 & 0 & -1 \end{pmatrix} = \begin{pmatrix} 1 & 0 & 0 & -1 \\ 0 & 0 & 0 & 0 \\ 0 & 0 & 0 & 0 \\ -1 & 0 & 0 & 1 \end{pmatrix} \begin{pmatrix} 1 & 0 & 0 & 0 \\ 0 & 1 & 0 & 0 \\ 0 & 0 & -1 & 0 \\ 0 & 0 & 0 & -1 \end{pmatrix}. \tag{3.14}$$

In the equations above, we demonstrated that the measured Mueller matrix on the left can be expressed as the product of a right- or left-circular polarizer matrix with a half-wave retarder matrix. This corresponds to the result that was previously introduced in Equation (3.8), though now it is represented in terms of Mueller matrices instead of Jones matrices. Moreover, using the spectroscopic polarimeter, we confirmed that these polarization characteristics of the primary and conjugate waves remained consistent across a broad spectral range, extending well beyond the advertised range of 450–650 nm [81].

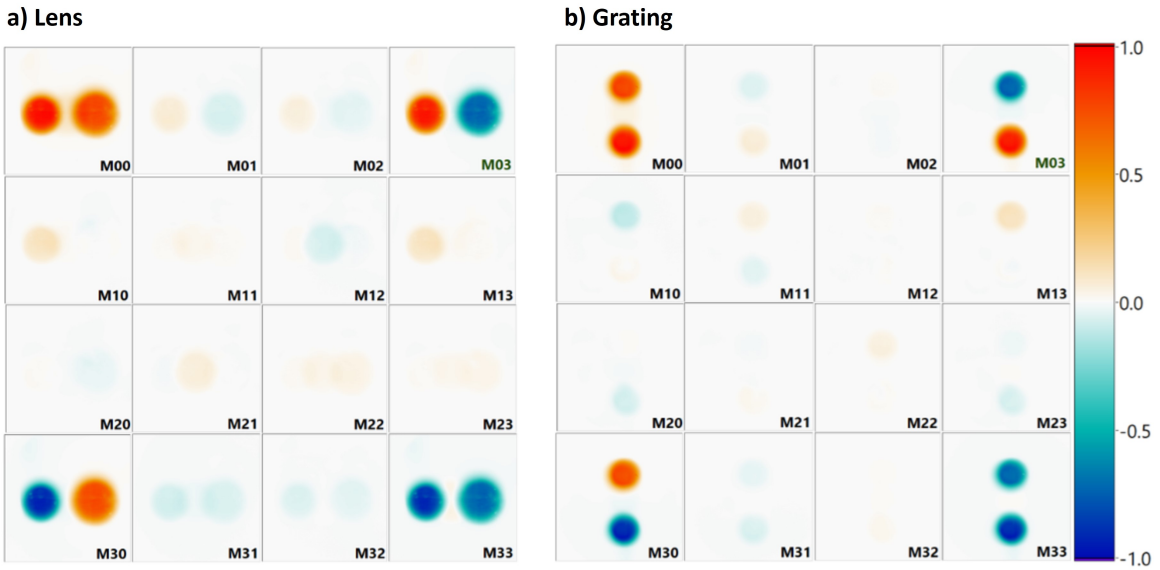

Figure 3.12: Unnormalized Mueller matrix images in diffractometer mode for the lens (a) and the grating (b).

3.6.3 Effenciency in Terms of Leakage Wave

Both the lens and the grating produced a weak yet detectable leakage wave across the entire spectral range that was examined using our polarimeters. This result aligns with the expectation, as indicated by Equation (3.9), since when $L \neq \pi$ and $C \neq 0$ (as observed in our samples, confirmed by Figure (3.10), a leakage wave emerges. The leakage waves for both the grating and the lens were measured in the range from 400 nm to 800 nm using the spectroscopic Mueller matrix polarimeter, and the results are shown in Figure (3.13). (For the lens, measurements were taken near its edge to avoid the superposition of the three waves, which would occur if the light passed through the center.)
As seen in (3.13), the Mueller matrix is not diagonal, suggesting that the leakage wave does not preserve the polarization of the incident beam. The complex optical behavior displayed in the figure is due to the presence of both circular and linear anisotropies. Given the liquid crystal's twisted structure, circular anisotropies dominate, appearing as both circular retardance and circular diattenuation. This latter effect is visible from the non-zero values of the m_{03} and m_{30} elements of the Mueller matrix. We attribute this phenomenon to the differing efficiencies of the primary and conjugate modes (implying that A_+ differs slightly from A_- in Equation (3.9)), which is a topic for future exploration, as this study does not assess the efficiency of the emergent waves. It is worth noting that the relatively small circular retardance observed at the microscopic level (Figure 3.12) is amplified significantly when focusing on the leakage wave alone, as shown in Figure (3.14). This figure presents the circular retardances derived from the analytic inversion of the Mueller matrices in Figure (3.13).

The large circular retardance observed in Figure (3.14) can be understood by further decomposing the first Jones matrix from Equation (3.9) (associated with the leakage wave) into two terms:

$$\begin{pmatrix} \cos\frac{T}{2} & \frac{C}{T}\sin\frac{T}{2} \\ -\frac{C}{T}\sin\frac{T}{2} & \cos\frac{T}{2} \end{pmatrix} = \frac{C}{T}\begin{pmatrix} \cos\frac{T}{2} & \sin\frac{T}{2} \\ -\sin\frac{T}{2} & \cos\frac{T}{2} \end{pmatrix} + \left(\frac{T-C}{T}T - C\cos\frac{T}{2}\right) I\,, \quad (3.15)$$

where I is the 2 × 2 identity matrix. The first term is a pure rotator Jones matrix, while the second term corresponds to an identity matrix. In the presence of circular retardance ($C \neq 0$), the leakage wave results from the combination of two waves: one with a polarization

rotated by $\frac{T}{2}$ relative to the input, and the other maintaining the input polarization. Given that, in GP optical components, T is typically close to π (with $L \approx \pi$ and C being small), the second term of Equation (3.15) becomes negligible, leaving the first rotator term as the main contributor to the leakage wave, even when C is of small values [81].
The presence of linear anisotropies in the leakage wave (i.e., changes in the polarization of the leakage wave upon azimuthal rotation of the GP optical element) was not expected from Equation (3.15), which only accounted for circular anisotropies in the Jones matrix of the leakage wave. The reasons for this behavior remain unclear, though we hypothesize it may be due to slight spatial inhomogeneities in the magnitude of L across the illuminated area, as suggested earlier in Figure (3.12).

From the above analysis, it is evident that polarimetric measurements of the leakage wave provide a highly sensitive and effective method to assess the "ideal" nature of GP optical elements. This approach should be considered in future evaluations of GP optical components, as it involves a simple, non-invasive measurement.

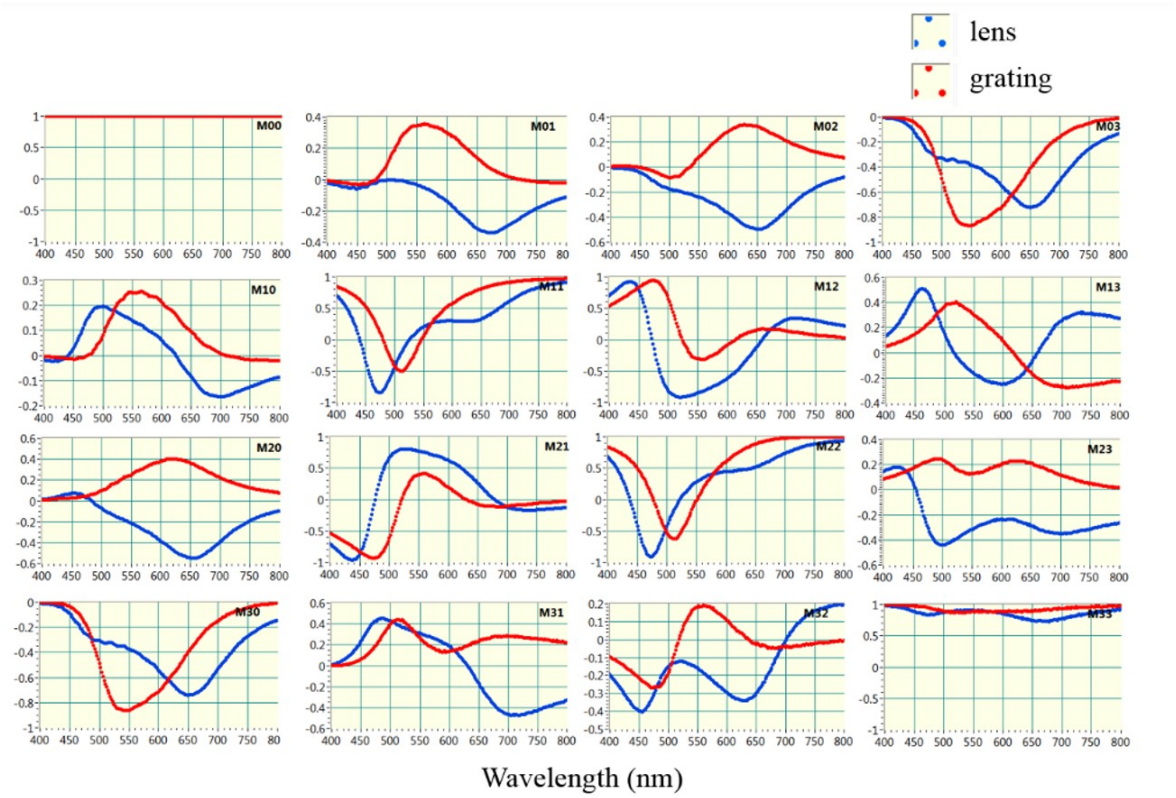

Figure 3.13: The spectroscopic Mueller matrices for the leakage waves of both the lens and the grating were measured. In these matrices, all elements have been normalized with respect to the m_{00} element. The results, displayed herein, provide insights into the polarization characteristics of the leakage waves across the analyzed spectral range. Normalization to m_{00} ensures a consistent comparison of the Mueller matrix elements, emphasizing the relative polarization effects.

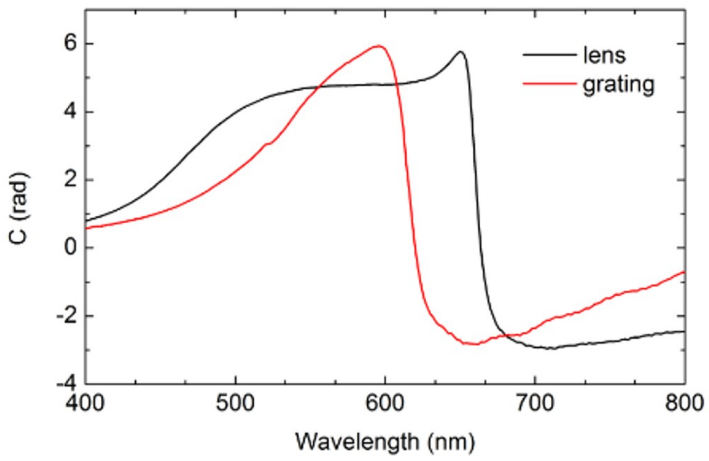

Figure 3.14: The circular retardance derived from the leakage waves of both the lens and the grating was analyzed and presented.

3.7 Conclusion

We have shown that the characteristics of GP optical elements can be effectively analyzed through polarimetric methods, eliminating the need for interferometric techniques typically required to measure dynamic phases. The phase profiles can be extracted directly from Mueller matrix measurements with micrometer-scale spatial resolution. Additionally, our theoretical and experimental results demonstrate that deviations from the half-wave linear retardance and the presence of circular retardance contribute to a significant leakage wave, which in turn affects the optical element's overall efficiency. Despite these effects, the primary and conjugate waves remain fully circularly polarized, independent of the input polarization, due to the space-variant linear retardance functioning as a polarization beam-splitter.

Furthermore, our findings suggest that measuring the Mueller matrix associated with the leakage wave (which is technically straightforward since it does not require wavefront redirection) offers valuable insights into various properties of the optical element. These include the presence of circular retardance, linear and circular diattenuation, and potential disparities in efficiency between the primary and conjugate waves.

With advancements in the manufacturing of GP optical components, enabling the development of physically thin elements with minimal losses, we believe polarimetry is the optimal technique for studying and evaluating these next-generation components.

Chapter 4

Spectrally Modulated Polarimetry

"الْعِلْمُ أَفْضَلُ خَلَفٍ، وَالْعَمَلُ بِهِ أَكْمَلُ شَرَفٍ"

قـال بعض الأدباء

Polarimetry is an effective technique for optical characterization and remote sensing, relying on the analysis of the polarization state of light. While it has broad utility, certain applications require overcoming technical challenges to meet specific demands for accuracy, resolution, speed, and sensitivity. Many contemporary polarimeters encode polarization information in the temporal domain, using time-dependent compensators such as rotating waveplates, photoelastic modulators, and electrically tunable liquid crystals. Polarization data can also be encoded spatially, through methods like splitting the beam or employing polarization-sensitive cameras. Additionally, polarization measurements can be performed in the spectral domain, as initially described in independent works by Oka and Kato [10], Iannarilli et al. [97], and Nordsieck [98]. Over the past few years, spectral modulation in Stokes or Mueller polarimetry has been widely explored by researchers [99–103].

Main objectif

This chapter's main purpose is to develop the wavelength-domain analysis technique based on Stokes polarimeter. This technique addresses some of the limitations associated with channeled polarimetry with Fourier transform-based analysis.

4.1 Spectral-Domain Polarimetry

In polarimetric measurements, the spectral domain offers a powerful approach for capturing the wavelength-dependent behavior of light's polarization state as it interacts with a sample. Unlike traditional time-domain polarimetry, which measures the polarization of light at a fixed wavelength or over time, spectral-domain polarimetry utilizes the variation of light across a range of wavelengths to provide a richer, more detailed picture of the sample's optical properties.

4.1.1 Time-Domain Vs. Spectral-Domain Polarimetry

Time-Domain Polarimetry typically measures the polarization state at a fixed wavelength or over discrete intervals in time. This approach is useful for capturing dynamic changes in the sample's polarization response, but it often lacks the spectral information needed to fully characterize materials with wavelength-dependent properties. The focus is generally on the time evolution of polarization, as explained in the theoretical chapter, which can limit insights into how different wavelengths interact with the sample. **Spectral-Domain Polarimetry**, on the other hand, collects polarization data across a continuous range of wavelengths. This provides a much broader understanding of how the sample behaves across the spectrum, revealing wavelength-specific effects such as birefringence, dichroism, or circular birefringence, which are essential for understanding materials that exhibit complex optical responses.

4.1.2 Spectrally Modulated Polarimetry Applications

Spectrally modulated polarimetry has several real-world applications for which it offers distinct advantages over time-domain polarimetry, depending on the functional role of the measured material. Among others, we site:

- Material characterization in manufacturing because of its High resolution, which allows for high spectral resolution measurements, which can identify subtle

wavelength-dependent effects that time-domain systems may miss. This aspect is what this chapter explores at a great length. [104].

- Biomedical Imaging and Diagnostics such as ophthalmology and cancer detection, precise imaging of tissue optical properties is essential for diagnosis and treatment planning. In this field specifically, Spectrally Modulated Polarimetry offers two features over time-domain analysis. The first is the enhanced contrast images by measuring how light's polarization changes across different wavelengths and improving the detection of specific tissue characteristics. While the second feature relies on the fact that it enables depth profiling and differentiation of tissue layers based on their spectral polarization response, which is crucial for identifying and characterizing different tissue types [105].

- Remote sensing and environmental monitoring: Spectral-domain polarimetry can capture how the polarization state of light changes across the entire visible and near-infrared spectrum, which is essential for assessing various environmental parameters.

- Optical coatings and thin films Spectral-domain polarimetry provides a complete picture of how the coating's optical properties vary with wavelength [106].

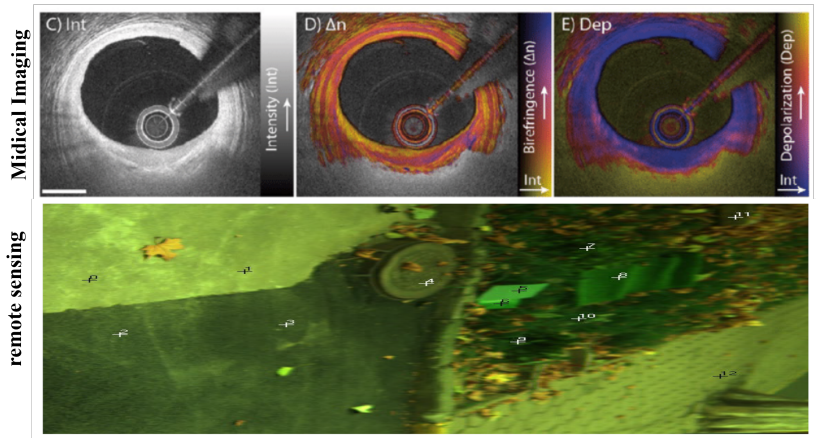

Figure 4.1: Spectrally modulated polarimetry for medical imaging and remote sensing applications. Adapted from [105, 106]

4.1.3 Spectral Resolution Importance

The **spectral resolution** of the system plays a critical role in the accuracy of polarimetric measurements. Spectral resolution refers to the ability of the spectrometer to distinguish between closely spaced wavelengths. Higher spectral resolution allows for more precise measurements of wavelength-dependent changes in the polarization state, enabling the detection of fine optical features. For example, in the study of birefringent materials, high spectral resolution can reveal subtle shifts in polarization due to small variations in the material's refractive index at different wavelengths. In contrast, low-resolution systems may miss these details, leading to incomplete or less accurate characterizations.

4.1.4 Insights into Complex Optical Properties

Spectral-domain polarimetry provides valuable insights into complex optical properties of materials that are not easily captured by time-domain techniques. Some examples include:

- **Birefringence**: By analyzing how the polarization state changes across wavelengths, researchers can determine the wavelength-dependent birefringence of a material, which is crucial in fields like optical communication and material science.
- **Circular Dichroism**: Spectral-domain measurements allow for the precise characterization of circular dichroism in chiral molecules, providing insights into their molecular structure and interactions.
- **Depolarization Effects**: Spectral-domain polarimetry can also detect how light depolarizes across different wavelengths, which is important for studying materials that scatter light or cause multiple reflections within a medium.

Overall, polarimetric measurements in the spectral domain offer a detailed, wavelength-dependent understanding of the optical properties of materials. This approach is particularly useful for studying samples with intricate optical behaviors, where the interaction of light varies significantly across the spectrum. By leveraging the spectral domain, re-

searchers can gain deeper insights into phenomena like birefringence, dichroism, and depolarization.

4.2 Channeled Spectrum vs. Wavelength Domain Analysis

The spectral modulation technique, pioneered by Oka and Kato, is now commonly known as channeled polarimetry. This method is not limited to the spectral domain but can be applied to any system with periodic signal modulation. In the channeled method, the Stokes parameters are retrieved by performing a Fourier transform on the intensity as a function of the wavenumber, isolating each parameter into its respective frequency channel [10, 101, 107]. The resulting amplitude and phase of these frequency channels are used to determine the Stokes parameters, drawing upon concepts rooted in telecommunications and signal processing.

In this work, we propose a spectrally modulated Stokes polarimeter that does not rely on the channeled spectrum approach, as it bypasses periodic modulation and avoids Fourier transform-based analysis. Instead, our method utilizes an algebraic matrix inversion technique. This approach addresses some of the limitations associated with channeled polarimetry. For instance, channeled analysis requires evenly sampled signals in wavenumber, which is often not the case when using dispersive spectrometers that measure intensity as a function of wavelength $I(\lambda)$. While resampling methods can be applied, our algebraic method eliminates this necessity. Additionally, the wavelength-dependent birefringence of the retarding crystal, which is typically overlooked in channeled polarimetry [108–110], can be easily accounted for with our method. A related approach using a linear operator was previously proposed by Sabatke et al. [111, 112], though their method was implemented in the wavenumber domain.

Polarimeters are used in a wide range of scientific and industrial applications across fields such as chemistry, biology, physics, astronomy, and materials science. As a result, the diverse range of measurement environments and needs cannot be met by a single type of polarimeter. The spectral polarimeter developed in this work offers advantages over time-modulated systems, such as compactness, no moving components, fast acquisition

times, and low manufacturing cost. However, it does have the drawback of limited spectral resolution, restricting its application to studying properties with gradual wavelength variation.

4.3 Theoretical Basing

A Stokes polarimeter utilizing spectral modulation can be constructed using two retarders with differing thicknesses, arranged such that the fast axis of the second retarder is rotated by 45° relative to the first, followed by a polarizer whose transmission axis aligns with the fast axis of the first retarder. In the context of Stokes-Mueller formalism, this configuration is described by the equation:

$$\mathbf{S}_{out} = \mathbf{M}_P \mathbf{M}_{R2} \mathbf{M}_{R1} \mathbf{S}_{in}, \tag{4.1}$$

where $\mathbf{S}_{in}$ represents the unknown input Stokes vector $(S_0, S_1, S_2, S_3)^T$, $\mathbf{M}_{R1}$ and $\mathbf{M}_{R2}$ are the Mueller matrices for the two retarders, which are oriented 45° apart, and $\mathbf{M}_P$ is the Mueller matrix of the polarizer.

A polychromatic light source is employed, with a spectrometer capturing the intensity as a function of wavelength (λ). The polarimeter does not cause time-dependent variations in intensity; any such fluctuations would likely be from the light source itself. Nevertheless, these variations typically have minimal impact on the polarimetric measurement as it is not dependent on time-domain analysis. From equation (4.1), substituting the known Mueller matrices for the polarizer and retarders, the detected intensity as a function of wavelength is given by [10]:

$$(\lambda) = S_0 + S_1 \cos(\delta_{2\lambda}) + S_2 \sin(\delta_{1\lambda}) \sin(\delta_{2\lambda}) - S_3 \cos(\delta_{1\lambda}) \sin(\delta_{2\lambda}), \tag{4.2}$$

where $\delta_{1\lambda}$ and $\delta_{2\lambda}$ are the wavelength-dependent retardances of the first and second retarders, respectively. It is assumed here that the polarizer has negligible wavelength dependence, which is reasonable given the availability of high-quality achromatic polarizers. According to this model, the detected spectral intensity is influenced by $\delta_{1\lambda}$ and $\delta_{2\lambda}$, as well as the emission spectrum of the light source and the detector's spectral response, although these effects can be calibrated.

The retardance for each retarder is expressed as:

$$\delta_{i\lambda} = \frac{2\pi \Delta n_\lambda d_i}{\lambda}, \tag{4.3}$$

where Δn_λ denotes the birefringence of the retarders, defined as the difference between the extraordinary and ordinary refractive indices ($\Delta n = n_e - n_o$), and d_i is the thickness of the crystal. The subscript λ emphasizes that birefringence is wavelength-dependent, although this dependence is typically smaller than the explicit $1/\lambda$ relationship seen in equation (4.3), and is often neglected in channeled spectral polarimetry.

Assuming the Stokes parameters in equation (4.2) are wavelength-independent, the equation can be recast as a scalar product between a vector containing the spectral modulation, $\mathbf{B}$, and the input Stokes vector $\mathbf{S}_{in}$:

$$I(\lambda) = \begin{bmatrix} 1 \\ \cos(\delta_{2\lambda}) \\ \sin(\delta_{1\lambda})\sin(\delta_{2\lambda}) \\ -\cos(\delta_{1\lambda})\sin(\delta_{2\lambda}) \end{bmatrix}^T \begin{bmatrix} S_0 \\ S_1 \\ S_2 \\ S_3 \end{bmatrix} = \mathbf{B}^T \mathbf{S}_{in}. \tag{4.4}$$

As the spectrometer provides a series of N intensity measurements, this equation can be generalized as:

$$\mathbf{I}_\lambda = \overline{\mathbf{B}}^T \mathbf{S}_{in}, \tag{4.5}$$

where $\mathbf{I}_\lambda$ is a vector containing the N intensity values, and $\overline{\mathbf{B}}$ is a $4 \times N$ matrix. By applying the Moore-Penrose pseudoinverse of $\overline{\mathbf{B}}$, the input Stokes vector $\mathbf{S}_{in}$ can be retrieved:

$$\mathbf{S}_{in} = (\overline{\mathbf{B}\mathbf{B}}^T)^{-1}\overline{\mathbf{B}}\mathbf{I}_\lambda, \tag{4.6}$$

where $\overline{\mathbf{B}\mathbf{B}}^T$ is a 4×4 matrix. A similar approach is used in time-modulated polarimeters [91, 94, 113, 114], where the system is overdetermined, and the pseudoinverse minimizes error. This method recovers the Stokes vector without decomposing the intensities into separate channels based on carrier frequencies, as done in channeled polarimetry. The ability of the spectral modulation technique to accurately determine $\mathbf{S}_{in}$ depends on how well-conditioned the system is, particularly in relation to the calculation in Equation((4.6)). Specifically, the performance degrades when $\overline{\mathbf{B}\mathbf{B}}^T$ approaches singularity. Numerous authors have examined the optimization of this process, particularly in the context of time-modulated systems. For spectrally modulated systems, the success of the matrix inversion

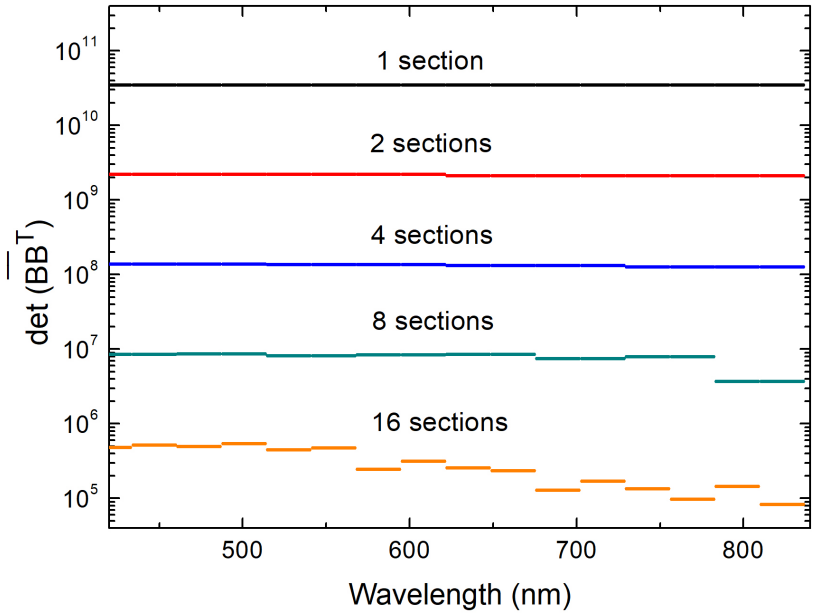

Figure 4.2: Determinant values $|\overline{\mathbf{B}}\overline{\mathbf{B}}^T|$ as a function of the number of sections n [104].

in Equation (4.6) hinges on the retardance characteristics of the crystals, as given by Equation (4.3), as well as the spectral range and resolution provided by the detecting spectrometer [104].

If $\mathbf{S}_{in}$ varies with the wavelength, the analysis in equation (4.6) can be applied to smaller spectral segments instead of the entire set of N intensities recorded by the spectrometer. Typically, the intensity spectrum is divided into n sections ($n \ll N$), each containing N/n intensities. This enables constructing a $\overline{\mathbf{B}}$ matrix with dimensions $4 \times (N/n)$, which is then used in equation (4.6) to calculate the Stokes vector for each spectral section. Increasing n enhances the spectral resolution of the Stokes vector measurements but negatively impacts the conditioning of the computation in (4.6).

Figure 4.2 presents the determinant values $|\overline{\mathbf{B}}\overline{\mathbf{B}}^T|$ as a function of the increasing number of sections for our spectral polarimeter. The polarimeter's specific configuration is discussed in the next section. The figure illustrates how well-conditioned the measurements are and helps assess noise tolerance and error susceptibility. The data is based on a spectral range from 420 nm to 820 nm, with intensity samples every 0.5 nm ($N = 800$). As n increases to 1, 2, 4, 8, and 16, the determinant values decrease, especially in the infrared region for $n = 16$, where smaller sections (with around 50 intensities) are less well-conditioned

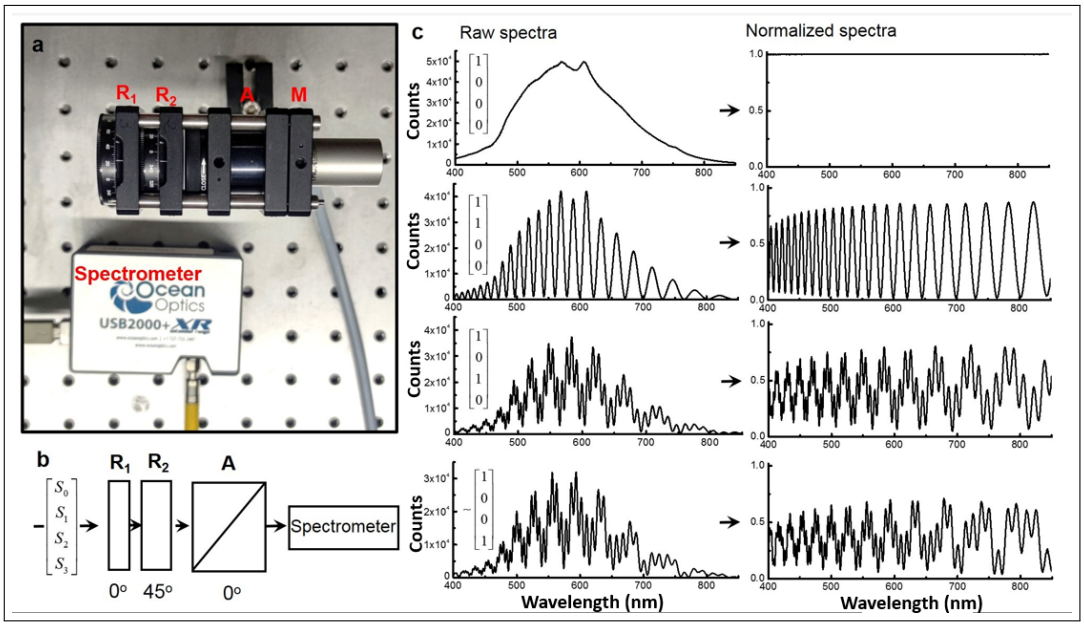

Figure 4.3: a. Photograph of the spectral polarimeter setup. R_1 and R_2 denote the first and second retarders, respectively, mounted on rotation stages to establish a $45°$ misalignment. A is the analyzer, while M is a parabolic mirror focusing light into the optical fiber connected to the spectrometer. b. Schematic diagram of the polarimeter. c. Measured spectra for different input Stokes vectors. The normalized spectra are obtained by normalizing each spectrum to that corresponding to the Stokes vector $(1, 0, 0, 0)^T$ [104] .

due to fewer modulation cycles caused by the reduced retardance of the crystals at longer wavelengths. The results in Figure 4.2 imply a trade-off between spectral resolution and signal-to-noise ratio for spectrally modulated polarimeters. Consequently, applications that require both high spectral resolution and a high signal-to-noise ratio would benefit from employing a spectrometer with very high resolution paired with thick retarders to enable the use of narrow spectral sections [104].

4.4 Material and Experimental Conditions

A key advantage of spectrally modulated polarimeters over traditional time-modulated systems is their potential for compact designs without the need for any moving components. This also makes them more affordable, with the primary expense stemming from the spectrometer. When designing a spectral polarimeter, careful consideration must be given to the material and thickness of the retarders, which should be aligned with the spectral res-

olution of the chosen spectrometer.

Our polarimeter, depicted in Figure 4.3, utilizes Y-cut sapphire crystal retarders (Photon-Export), where the optical axis runs parallel to the plane of the crystal. Synthetic sapphire is known for its excellent transparency over a wide wavelength range, spanning from 150 nm (ultraviolet) to 5500 nm (mid-infrared), and its hardness allows it to be polished with high precision. Additionally, sapphire has strong thermal stability. In the visible region, the birefringence of sapphire is approximately $|n_e - n_o| \simeq 0.008$ [115], but small wavelength-dependent variations in birefringence must be accounted for, as will be detailed in the calibration section. We experimented with sapphire crystals of nominal thicknesses of 1 mm, 2 mm, and 3 mm, with different combinations of these retarders available for use in the polarimeter. In the results reported here, we used the 3 mm retarder as the first element and the 2 mm retarder as the second. A Glan-Taylor calcite polarizer served as the analyzer, and a parabolic mirror was used to focus the light into an optical fiber that guides it to the spectrometer.

The spectrometer employed in this setup is the Ocean Optics USB2000+XR, equipped with a 2048-element CCD array detector. This spectrometer covers a range from 200 nm to 1100 nm and achieves a resolution up to 1.5 nm at full width at half maximum. The spectral resolution of the spectrometer effectively dictates the allowable thickness of the retarders, as it must be able to clearly resolve the modulation introduced by the crystals. Hence, the retarder thickness should ideally be chosen based on the spectrometer's resolution. However, due to the wavelength-dependent nature of retardance, following an inverse relationship with wavelength as shown in equation (4.3), higher spectral resolution is required for shorter wavelengths. Without access to a high-resolution spectrometer, it may be difficult to identify retarders that can function effectively over a wide spectral range. For instance, retarders that are well-suited for the visible range may lead to suboptimal modulation in the near-infrared, while introducing excessive high-frequency modulation in the ultraviolet that exceeds the spectrometer's resolution. These effects are visible in Figure 4.3c, where fewer modulation cycles can be observed around 800 nm, and at wavelengths shorter than ~ 450 nm, the spectrometer struggles to resolve the rapid oscillations.

The light source's emission spectrum is also a significant factor in spectral polarimetry.

Typically, broadband light sources impose additional modulation on the detected spectra, as shown in Figure 4.3c. It is often advantageous to normalize the measured spectrum with respect to the emission spectrum of unpolarized light, i.e., when the retarders introduce no polarization modulation, and the spectrum is purely a reflection of the light source's emission profile. This normalization has been applied to the data in the second column of Figure 4.3c [104].

4.5 Calibration configuration

The primary goal of the calibration is to identify the characteristics of the spectral modulation, which relies on the retardance of the crystals as expressed by (4.3). This process allows us to determine the values of d and Δn_λ for each retarder. The birefringence Δn_λ varies with wavelength and can be described using the following Sellmeier dispersion relation:

$$\Delta n_\lambda = A + \frac{B\lambda^2}{\lambda^2 - C} + \frac{E\lambda^2}{\lambda^2 - F^2}\,. \tag{4.7}$$

The calibration of this full dispersion relation, which includes five parameters in total, is most effectively carried out over the broadest spectral range available based on the combined capabilities of the spectrometer and the light source. However, when focusing on a narrower spectral range, such as 100 nm, one can truncate equation (4.7) and use just the first three parameters. In extreme cases where a very narrow spectral band is of interest (likely requiring thicker retarders), Δn_λ can be treated as a constant with only a single parameter.

In our system, the calibration is completed by acquiring two sets of normalized intensity spectra [104]:

- First, an achromatic polarizer is aligned to set a Stokes vector $(1, 1, 0, 0)^T$, generating an intensity $I(\lambda) = 1 + \cos(\delta_{2\lambda})$, which depends solely on the second retarder. The parameters of this retarder, including d_2, A_2, B_2, C_2, D_2, E_2, and F_2, are then determined using an iterative optimization algorithm, specifically the differential evolution method.
- Next, the polarizer is rotated by $45°$ to produce a Stokes vector $(1, 0, 1, 0)^T$, resulting

in an intensity $I(\lambda) = 1 + \sin(\delta_{1\lambda})\sin(\delta_{2\lambda})$. With the parameters for the second retarder fixed from the previous step, another optimization algorithm is applied to find the calibration parameters for the first retarder, which includes d_1, A_1, B_1, C_1, D_1, E_1, and F_1.

Figure 4.4 shows the birefringence values obtained for both retarders during the calibration process. Since both retarders are constructed from the same material (sapphire), their birefringence would be expected to be identical in theory. However, calibrating the polarimeter is more robust when the birefringence values for the retarders are treated as independent parameters, which results in slightly different values for each retarder, as shown in Figure 4.4. These minor discrepancies may arise due to small misalignments or stresses introduced during the cutting and polishing of the crystals. The thickness values obtained were close to their nominal values, with $d_2 = 2.00 \pm 0.01$ mm and $d_1 = 3.02 \pm 0.01$ mm [104].

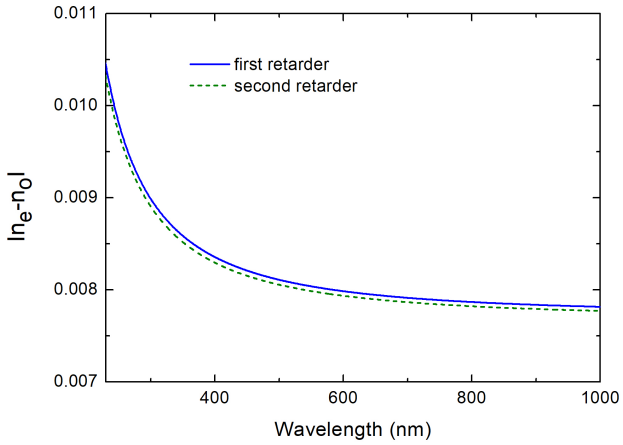

Figure 4.4: Wavelength dependence of the birefringence of sapphire, determined during the calibration of the first and second retarders [104].

4.6 Application to the Measurement of Optical Rotation

In this part of the work, we demonstrate the use of the spectral polarimeter in measuring the optical rotation of chiral substances, a classic application of polarimetry dating back to the 19th century. Despite its historical origins, optical rotation remains highly relevant today with key applications across industries such as pharmaceuticals, food, cosmetics, chemistry,

and forensics. Commercial optical rotation polarimeters typically rely on time-modulated techniques, using either high-precision rotary encoders or Faraday rotators, and perform measurements at specific wavelengths. Due to its historical importance, the sodium D line at 589 nm is still commonly used. While our spectral polarimeter does not measure at exact wavelengths, it is well-suited for optical rotation experiments because the optical rotatory dispersion of most transparent materials in the visible range (above 450 nm) is small and varies smoothly. As previously mentioned, increasing the spectral resolution of our system would require thicker retarders and a higher-resolution spectrometer [104]. One

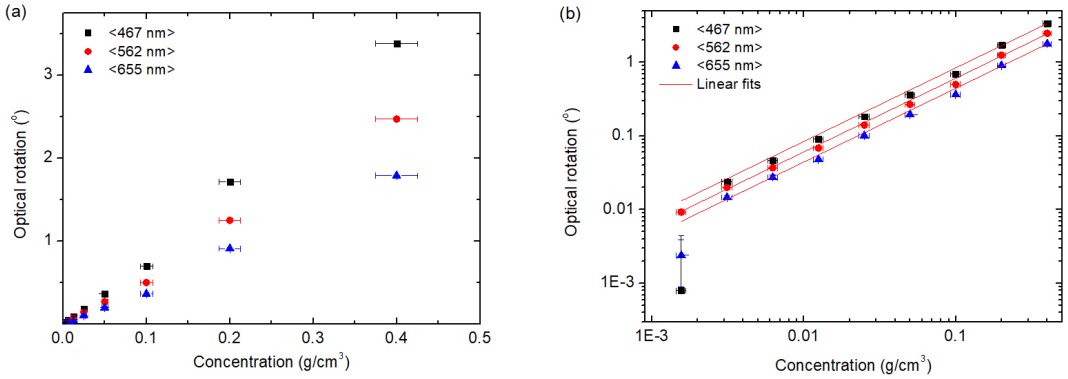

Figure 4.5: Optical rotation of a sucrose solution at varying concentrations: linear scales (a) and logarithmic scales (b)[104].

of the primary challenges in optical rotation measurements is the detection of very small polarization rotations, which occur in solutions with low concentrations of chiral solutes. Specialized polarimeters are designed for measuring small rotation angles, with the best commercial devices achieving accuracies of approximately $\pm 0.002°$, often using precision mechanical components [116]. To measure optical rotation using the spectral polarimeter described in Fig. 4.3, linearly polarized light with a known azimuthal angle, ψ, is directed through the system. The azimuth is calculated from the Stokes vector components using the following equation:

$$\psi = \frac{1}{2}(\mathrm{atan2}(S_2, S_1)), \tag{4.8}$$

where $\mathrm{atan2}$ represents the four-quadrant inverse tangent function. When a cuvette containing an optically active solution is placed in the light path, it induces a small rotation

in the polarization angle. The optical rotation of the chiral solution is then determined by measuring the change in the azimuthal angle.

For this experiment, we selected a spectral range from 420 nm to 700 nm, divided into three sections, providing a spectral resolution of around 100 nm. The optical rotation values measured in each section were associated with the central wavelength of that section. Although this approximation averages the rotation over the entire section, it is reasonable given the minimal dispersion of optical rotation in the visible spectrum.

An initial sucrose solution was prepared by dissolving 40 grams of table sugar in 100 ml of water. Measurements were carried out in a quartz cuvette with a 10 mm pathlength. At the highest concentration, the measured optical rotation exceeded 3° for the section centered at 467 nm. The main goal of this experiment was to determine the lowest optical rotation detectable by the polarimeter. The solution was diluted stepwise by 1:1 with water in each subsequent step, and the optical rotation was measured after each dilution. After eight dilutions, the lowest concentration tested was approximately 0.0015 g/cm^3. Figure 4.5 displays the results of the optical rotation measurements for the three spectral regions with central wavelengths at 467 nm, 562 nm, and 655 nm. The expected linear relationship between optical rotation and concentration was observed. The low-concentration results are best visualized using the logarithmic scale in Figure 4.5b. At 562 nm, the polarimeter reliably resolved rotations below 0.01° at the lowest tested concentration. However, for the regions at 467 nm and 655 nm, reliable measurements were obtained only down to the second-to-last concentration. For the shortest wavelengths, the limited resolution of the spectrometer was likely unable to fully capture the high-frequency spectral oscillations caused by the retarders, as seen earlier in Figure 4.3c. For longer wavelengths, the poorer performance is likely due to the suboptimal conditioning of equation (4.6) in that spectral range, where fewer modulation cycles are available. When using more spectral sections to increase resolution, the inversion process became noisier, as expected from Figure 4.2. For example, with six sections (a resolution of around 50 nm), accurate measurements were only obtained for concentrations above 0.03 g/cm^3. In contrast, with three sections, concentrations as low as 0.003 g/cm^3 were successfully measured, as seen in Figure 4.5 [104].

4.7 Conclusions

This work demonstrates that spectral modulation in polarimetry can be effectively analyzed without the need for a channeled approach, such as Fourier transform techniques. We introduced a novel method that enables spectral domain analysis to be performed directly in the wavelength domain, eliminating the need for conversion to wavenumber. This approach, commonly applied in time-domain analysis, relies purely on linear algebra, utilizing a least-squares estimator through the pseudoinverse to achieve the optimal fit to the experimental data. The method's implementation is straightforward, making it particularly suitable for use with dispersive spectrometers that record intensity as a function of wavelength.

We illustrated this approach with a compact, cost-effective Stokes polarimeter, which is an excellent choice for applications requiring both high sensitivity and precision, but not necessarily high spectral resolution. The instrument was successfully applied to measure the small polarization rotations induced by highly diluted solutions of chiral molecules, showcasing its capabilities in sensitive optical measurements.

General Conclusion and Future Perspectives

Final Conclusion

The general conclusion of this dissertation reflects the culmination of extensive research and development in the field of light polarization, particularly in its application to material characterization. From its origins in the 17th century, the study of light polarization has evolved significantly, laying the groundwork for modern optical sciences. This dissertation not only traces the historical progression of polarization but also advances its practical applications through innovative polarimetric techniques. By bridging the gap between theory and application, the work presented here makes meaningful contributions to both the understanding and practical use of polarization in contemporary optics and materials science.

The research presented in this thesis began with a comprehensive historical review of light polarization, documenting the evolution of the field from its early discoveries to the development of modern theoretical frameworks. This historical exploration highlighted how each scientific advancement contributed to a greater understanding of polarization, likening the process to assembling the intricate pieces of a puzzle. Over the past 70 years, a significant shift from theoretical studies to practical, data-driven applications has occurred, setting the stage for the contributions made in this work.

In the core of this thesis, a novel method based on the Stokes-Mueller formalism was proposed and validated for characterizing linear birefringent media. By focusing on the extraction of optical properties such as fast and slow axes, the study provided a robust description of the Mueller polarimeter and its modified vacuum matrix. Experimental validation using PLA samples confirmed the effectiveness of this approach, particularly in phase shift measurements. However, limitations were identified in the method's ability to determine ellipticity in media with low anisotropy, highlighting an avenue for future improvements. Addressing these limitations would broaden the applicability of the

technique, making it an even more powerful tool for material characterization.

Further research explored the utility of polarimetric methods in studying geometric phase (GP) optical elements. Through both theoretical and experimental work, it was demonstrated that the Mueller matrix can be effectively employed to assess the phase profiles of these elements, providing micrometric spatial resolution without the need for traditional interferometric techniques. The study also shed light on the effects of circular and linear retardance deviations, particularly in generating leakage waves that influence optical element efficiency. Despite these challenges, the study confirmed that space-variant linear retardation could still function as a highly efficient polarization beam-splitter, with potential applications in the development of next-generation GP optical elements, including gratings and lenses with minimal losses.

Additionally, this thesis introduced a new method for performing spectral domain polarimetric analysis without resorting to the typical channeled approach or Fourier transforms. Instead, a linear algebra-based approach using a least-squares estimator was employed, simplifying the analysis of spectrally modulated polarimetry. This innovative approach proved particularly effective in measuring polarization effects in solutions of chiral molecules, demonstrating the potential for compact, low-cost polarimetric instruments in high-sensitivity applications.

In conclusion, this dissertation contributes significantly to the fields of optics and materials science by advancing polarimetric techniques and showcasing their potential across a range of applications. From the historical study of polarization to the development of novel methodologies for optical characterization, the work presented here not only enhances our understanding of light-matter interactions but also sets the stage for future innovations in both fundamental and applied optics. The findings underscore the importance of polarimetry as a versatile and precise tool, with far-reaching implications for material science, molecular studies, and the development of advanced optical components.

Potential Perspectives

Perspectives The work presented in this dissertation opens several avenues for future research and development in the field of polarimetry and optical characterization. One of the immediate goals is to refine the proposed Stokes-Mueller method to overcome its current limitations in analyzing materials with low anisotropy. By enhancing the method's sensitivity, particularly in measuring ellipticity, it could become a more versatile tool for characterizing a broader range of materials, from biological tissues to advanced metamaterials.

Another promising direction involves the continued exploration of geometric phase (GP) optical elements. The insights gained from this study on leakage waves and phase profiles can be extended to optimize the design and fabrication of next-generation GP components, such as highly efficient and compact optical gratings and lenses. Further, integrating these elements into emerging optical systems may provide new applications in telecommunications, imaging, and quantum optics.

The development of new polarimetric techniques, such as the direct spectral analysis approach introduced in this thesis, also offers great potential for future work. By applying these methods to more complex media, such as chiral molecules in biological systems, researchers can gain deeper insights into the molecular structure and dynamics that govern various optical properties. The continued miniaturization and cost-efficiency of polarimeters will also drive their adoption in fields where high precision and sensitivity are critical, including biomedical diagnostics and material science.

Finally, as technology advances, interdisciplinary applications of polarimetry are likely to expand. By integrating polarimetric methods with computational approaches and machine learning, future research can further unlock the potential for real-time, automated analysis of material properties, enhancing both the accuracy and efficiency of optical characterization techniques.

Appendix

Spectrally modulated polarimetry with wavelength domain analysis

HANA BENDADA[1,2], BELKACEM BAKHOUCHE[2], LUIS OSCAR GONZÁLEZ-SIU[3], NEIL C. BRUCE[4], AND ORIOL ARTEAGA[1,5,*]

[1] Dep. Física Aplicada, Feman Group, Universitat de Barcelona, Barcelona 08028, Spain
[2] Institute of Optics and Precision Mechanics, laboratory of photonic systems and nonlinear optics, Ferhat Abbas University of Setif, Setif 19000, Algeria
[3] School of Engineering and Information Technology, University of New South Wales, Canberra, ACT 2610, Australia
[4] Instituto de Ciencias Aplicadas y Tecnología, Universidad Nacional Autónoma de México, Ciudad Universitaria, 04510, Mexico City, Mexico
[5] Institute of Nanoscience and Nanotechnology (IN2UB), Universitat de Barcelona, Barcelona 08028, Spain
[*] Corresponding author: oarteaga@ub.edu

Compiled September 19, 2024

Spectrally modulated Stokes polarimeters use a pair of high order crystal retarders to generate a spectrally-depending modulation of the polarization of light. In these systems, the detected intensity vs wavenumber spectrum is usually referred to as a channeled spectrum and the Fourier inversion of this spectrum allows the determination of Stokes parameters of light without needing any other mechanical or active device for polarization control. This work proposes a spectrally modulated polarimeter beyond the concept of a channeled wavenumber spectrum, so effectively detaching the spectral modulation from the Fourier analysis technique. The wavelength domain analysis we use is best suited for dispersive spectrometers offering intensity vs wavelength measurements. The technique is illustrated with the measurement of very small optical rotations produced by sucrose solutions. The proposed technique is easily extendable to spectrally modulated Mueller polarimeters.

http://dx.doi.org/10.1364/ao.XX.XXXXXX

1. INTRODUCTION

Polarimetry is a powerful optical characterization technique and remote-sensing method that is based on measuring the polarization characteristics of light. For some applications, its implementation can be technically challenging to achieve a desired level of accuracy, resolution, speed and sensitivity. Most usual modern polarimeters store the polarization information in the temporal domain by using time-varying compensators such as rotating retarders, photoelastic modulators, electrically controlled liquid crystals, etc. The polarization information can also be stored in the spatial domain by, for example splitting light into different beams or using polarization sensitive cameras. Lastly, it is also possible to obtain the polarization information from analysis in the spectral domain, as was reported independently by Oka and Kato [1], Iannarilli et al. [2] and Nordsieck [3]. In recent years, the application of the spectral modulation in Stokes or Mueller polarimeters has been considered by many authors [4–8].

The method of spectral modulation, as presented and developed by Oka and Kato is usually referred today as channeled polarimetry, although a channeled treatment is applicable not only in the spectral domain, but to any system involving a periodic modulation of the signal. In the channeled approach, the measurement algorithm uses the Fourier transform of the intensity as a function of the wavenumber to recover the Stokes parameters by separating them into channels based on their carrier frequencies [1, 6, 9]. The values of the Stokes parameters are obtained from the amplitude and phase of the carrier frequency, using concepts and strategies developed in the fields of telecommunications and signal processing.

In this work, we will introduce a spectrally modulated Stokes polarimeter not using a channeled spectrum approach, i.e., without requiring a periodic modulation because the algebraic analysis we propose is not based on the Fourier transform. As we shall show, this new method can address some of the problems associated with a channeled treatment. One example is that to apply Fourier transform analysis of the channeled approach one needs to consider an evenly sampled signal in wavenumber, but systems using dispersive spectrometers do not fulfil this condition as they measure the intensity as a function of the wavelength $I(\lambda)$, although resampling strategies can be used. Another example, is that the dispersion of birefringence of the retarding crystal, often not accounted for in the channeled approach [10–12], can be effortlessly taken into account in our algebraic matrix inversion method. The new method to perform the spectral domain analysis is the main result of this work. A similar method, also based on a linear operator, was proposed

by Sabatke and coauthors [13, 14], although their method was implemented in the wave-number domain.

Polarimeters are applied both for scientific research and industrial metrology in many different fields such as chemistry, biology, physics, astronomy, material science, etc. This gives a large number of measurement environments and requirements that cannot possibly be covered with a single type of polarimeter. The spectral polarimeter presented in this work has advantages with respect to the more common time-modulated systems, such as having compact size, no moving parts, fast measurement time, and low fabrication cost. However, the main disadvantage is that the spectral resolution of the final measurements is low, which limits the application to the study of properties that do not vary sharply with wavelength. As an illustration of a possible application of this system, we show how this spectral polarimeter can be used to measure the optical rotation in very diluted sucrose solutions.

2. THEORY

A spectral Stokes polarimeter can be realized by a pair of retarders of different thickness with the fast axis of the second retarder making a relative angle of 45° and a polarizer with the transmission axis aligned with the fast axis of the first retarder. In the Stokes-Mueller calculus this is presented as:

$$\mathbf{S}_{out} = \mathbf{M}_P \mathbf{M}_{R2} \mathbf{M}_{R1} \mathbf{S}_{in} \tag{1}$$

Where $\mathbf{S}_{in}$ is the unknown incoming Stokes vector $(S_0, S_1, S_2, S_3)^T$, $\mathbf{M}_{R1}$ and $\mathbf{M}_{R2}$ are the Mueller matrices of the retarders that are misaligned by 45° and $\mathbf{M}_P$ is the Mueller matrix of a polarizer.

A polychromatic light source is used and a spectrometer detects the intensity as a function of the wavelength (λ). This polarimeter will not introduce variations of the detected intensity with time and, if they were present, they would most likely come from fluctuations of the light source. However, in general these variations will not substantially affect the result of the polarimetry measurement as no time-domain analysis is done. From Eq. (1), substituting the well-known Mueller matrices for retarders and polarizers, the intensity detected as a function of wavelength is [1]:

$$\begin{aligned} I(\lambda) = {} & S_0 + S_1 \cos(\delta_{2\lambda}) + S_2 \sin(\delta_{1\lambda}) \sin(\delta_{2\lambda}) \\ & - S_3 \cos(\delta_{1\lambda}) \sin(\delta_{2\lambda}), \end{aligned} \tag{2}$$

where $\delta_{1\lambda}$ and $\delta_{2\lambda}$ are respectively the retardances of the first and second retarders, which are a function of λ. Note this calculation assumes that the polarizer has no dependence in λ, as good achromatic polarizers are widely available. According to this result, the spectrally detected intensity will depend on the values of $\delta_{1\lambda}$ and $\delta_{2\lambda}$, but it will be also affected by the emission spectrum of the light source and the spectral response of the detector, although these effects can be calibrated. The retardance can be written as

$$\delta_{i\lambda} = \frac{2\pi \Delta n_\lambda d_i}{\lambda}, \tag{3}$$

where Δn_λ is the birefringence of the retarders, defined as the difference between the extraordinary and ordinary refractive indices ($\Delta n = n_e - n_o$) and d is the crystal thickness. We include the subscript λ in Δn_λ to emphasize that the birefringence of a crystal is unavoidably a function of the wavelength. This dependence is generally small if compared with the $1/\lambda$ dependence that is explicit in Eq. (3), and it has been often neglected in spectral polarimetry using the channeled spectrum approach.

We consider now that the Stokes parameters in Eq. (2) do not depend on the wavelength; later we will discuss how their possible dependency in λ can be treated. Eq. (2) can be then written as the scalar product of a vector containing the spectral modulation, $\mathbf{B}$, and the incoming Stokes vector $\mathbf{S}_{in}$:

$$I(\lambda) = \begin{bmatrix} 1 \\ \cos(\delta_{2\lambda}) \\ \sin(\delta_{1\lambda}) \sin(\delta_{2\lambda}) \\ -\cos(\delta_{1\lambda}) \sin(\delta_{2\lambda}) \end{bmatrix}^T \begin{bmatrix} S_0 \\ S_1 \\ S_2 \\ S_3 \end{bmatrix} = \mathbf{B}^T \mathbf{S}_{in} \tag{4}$$

As the measurement obtained by the spectrometer consists of a collection of N intensity measurements this equation can be rewritten as:

$$\mathbf{I}_\lambda = \overline{\mathbf{B}}^T \mathbf{S}_{in} \tag{5}$$

where $\mathbf{I}$ is a vector that includes the N intensities and $\overline{\mathbf{B}}$ is a matrix with dimension $4 \times N$. This equation can be inverted using the Moore–Penrose pseudo inverse of $\overline{\mathbf{B}}$ allowing to obtain $\mathbf{S}_{in}$ as

$$\mathbf{S}_{in} = (\overline{\mathbf{B}\mathbf{B}}^T)^{-1} \overline{\mathbf{B}} \mathbf{I}_\lambda, \tag{6}$$

where $\overline{\mathbf{B}\mathbf{B}}^T$ is a matrix of dimension 4×4. An equation analog to this one is widely used to analyze intensities of time-modulated polarimeters [15–18], as to reduce noise the data acquisition is usually adjusted to produce overdetermined systems and the pseudoinverse solves the system in the least-square error perspective: it finds the solution that minimizes the error. Note that this equation allows the recovery of the Stokes vector without specifically separating each parameter into channels with different carrier frequencies, as is done in channeled polarimeters.

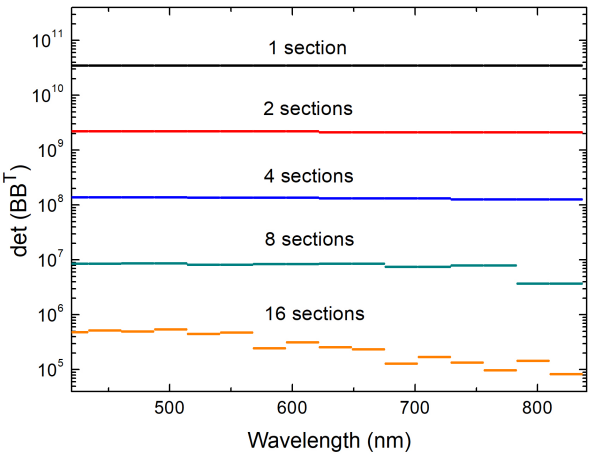

Fig. 1. Values of the determinant $|\overline{\mathbf{B}\mathbf{B}}^T|$ as a function of the number of sections n considered.

The ability of the spectral modulation method to measure $\mathbf{S}_{in}$ will depend on how well conditioned the calculus is in Eq. (6); in particular one needs to avoid situations where $\overline{\mathbf{B}\mathbf{B}}^T$ is close to a singular matrix. The optimization of the calculus based on the pseudoinverse has been discussed by many authors, particularly for time-modulated systems. For spectrally modulated systems the performance of the matrix inversion in Eq. (6) will depend on the retarding properties of the crystals, as obtained from Eq. (3), and the resolution and spectral range offered by the detecting spectrometer.

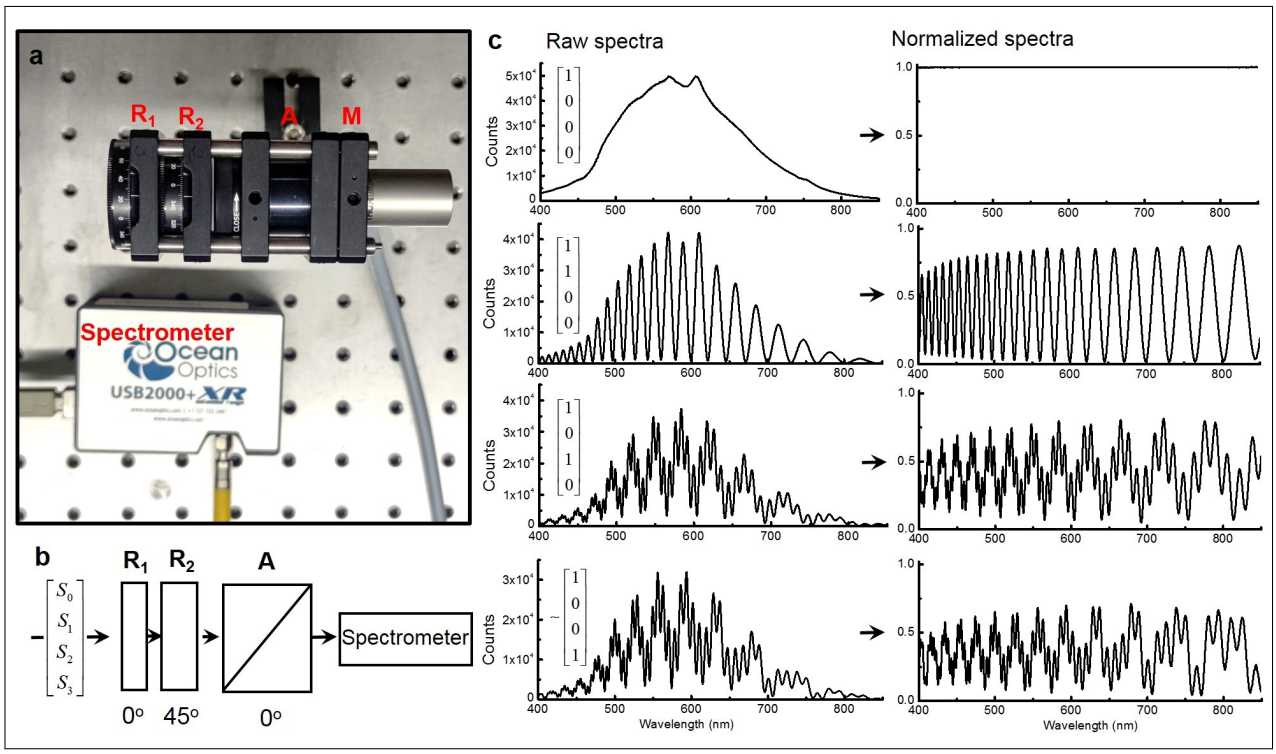

Fig. 2. a. Photo of the spectral polarimeter. R_1 and R_2 are respectively the first and second retarders mounted on rotation stages to set a misalignment of 45°. A is the analyzer and M is a parabolic mirror that focuses light on the core of the optical fiber that connects to the spectrometer. b. Schematic representation of the polarimer. c. Measured spectra for several different input Stokes vectors. The normalized spectra are generated by normalizing each acquired spectra by the spectrum corresponding to the Stokes vector $(1,0,0,0)^T$.

If $\mathbf{S}_{in}$ is a function of the wavelength, the analysis given in Eq. (6) can be performed in reduced spectral sections instead of considering all N intensities provided by the spectrometer. Usually we cut up the intensity spectrum in n sections ($n \ll N$) so that the intensity vector for each section contains N/n intensities. Therefore, a matrix $\overline{\mathbf{B}}$ with dimension $4 \times (N/n)$ can be built to find, with the help of Eq. (6) the Stokes vector for each spectral section. Increasing n will enhance the spectral resolution in the measurement of the Stokes vector, but it will be detrimental for the conditioning of the calculus in Eq. (6). Fig. 1 shows the values of the determinant $|\overline{\mathbf{B}}\overline{\mathbf{B}}^T|$ for an increasing number of sections in our spectral polarimeter (the specific characteristics of this polarimeter will be discussed in the next section), which can serve to evaluate how well conditioned the measurement is, to determine the resilience towards noise and errors. In this figure, we considered a usable spectral range from 420 nm to 820 nm with intensities obtained every 0.5 nm ($N = 800$) and it can be seen how the determinant decreases with increasing values of $n = 1, 2, 4, 8, 16$. Note also that for a small number of sections the whole spectral range is analyzed with similar values of the determinant, but for $n = 16$ there is a substantial decrease of conditioning in the IR, indicating that, in this region, the small sections (that have ~ 50 intensities) are not very well conditioned as they do not include enough modulation cycles due to the decreasing retardance of the crystals at these longer wavelengths. Fig. 1 suggests that for spectrally modulated polarimeters there is a trade-off between spectral resolution and the signal-to-noise of the polarimetric measurement. Therefore, for applications demanding both high spectral resolution and high signal-to-noise, it would be essential to have a very high-resolution spectrometer to equip the polarimeter with thick retarders that would permit using spectrally narrow sections.

3. EXPERIMENT

One of the main advantages of spectrally modulated polarimeters with respect to the more common time-modulated systems is that they can have a very compact design and without any moving part. The overall cost of the instrument is low and it is mainly determined by the cost of the spectrometer. The most relevant aspect to consider when designing a polarimeter with spectral modulation is the material and thickness of the retarders in relation to the spectral resolution of the spectrometer that is going to be used.

In our polarimeter, shown in Fig. 2, we use sapphire crystal retarders with a Y-cut (PhotonExport), meaning that the optical axis of the material is parallel to the plane of the crystal. Synthetic sapphire is highly transparent to wavelengths of light between 150 nm (ultraviolet) and 5500 nm (mid-infrared) and, because of its hardness, it can be polished to a high standard. Sapphire also has a good thermal stability. In the visible range sapphire has a birefringence $|n_e - n_o| \simeq 0.008$ [19], but the subtle variation of the birefringence with wavelength needs to be taken into account, as will be discussed in the calibration section. For our implementation, we have tried crystals with nominal thicknesses of 1 mm, 2 mm and 3 mm. Any combination of two of these retarders can be used for the polarimeter. The results

that we report in this work use the 3 mm crystal as first retarder and the 2 mm crystal as second retarder. As analyzing polarizer we use a Glan-Taylor calcite polarizer and a parabolic mirror focuses the light beam into an optical fiber that guides light to the spectrometer.

The spectrometer used is an Ocean Optics USB2000+XR that disperses light on a 2048-element CCD array detector. This spectrometer is responsive from 200 to 1100 nm and can reach a resolution up to 1.5 nm with full width at half maximum. Generally speaking, the resolution of the spectrometer is what limits the thickness of the retarders that can be used in the polarimeter, as the spectrometer needs to clearly resolve the spectral modulation created by the crystals. This means that, in principle, one should chose the thickness of the retarders depending on the spectral resolution of the spectrometer. However, as the retardance of crystals is heavily dependent on the wavelength and with a dependence $\sim 1/\lambda$ (Eq. (3)), higher spectral resolutions will be needed for measurements at shorter wavelengths. Unless a very high resolution spectrometer is available, it can be difficult to find retarders able to cover a large spectral range: for example, a set of retarders giving a "suitable" modulation in retardance in the VIS range, will typically introduce a sub-optimal modulation in the near IR, while in the UV they will most likely introduce a high frequency modulation that exceeds the spectral resolution of the spectrometer. These effects can be qualitatively seen in Fig. 2c as one can observe the low number of modulation cycles around 800 nm, while below $\sim$ 450 nm the spectrometer cannot resolve well the narrow oscillations.

The emission spectrum of the light source is also important for spectral polarimeters, as the usual emission spectra of broadband light sources further modulate the measured spectra as shown in Fig. 2c. If possible, it is beneficial for measurements to normalize the acquired spectrum by the raw spectrum measured for unpolarized light, i.e. when the retarders cannot introduce any polarization modulation and the measured spectrum only corresponds to the emission spectrum. This normalization has been applied to the graphs in the second column of Fig. 2c.

4. CALIBRATION

The objective of the calibration is to determine the characteristics of the spectral modulation, which depends on the retardance of the crystals as given by Eq. (3). Therefore, the calibration is used to determine d and Δn_λ for each of the retarders, Δn_λ is a function of the wavelength that we parameterize with the following Sellmeier dispersion relation:

$$\Delta n_\lambda = A + \frac{B\lambda^2}{\lambda^2 - C} + \frac{E\lambda^2}{\lambda^2 - F^2}. \quad (7)$$

The calibration of this complete dispersion relation (a total of 5 parameters) is best performed using the largest spectral range offered by the combination of the spectrometer and light source. However, if one is interested in a narrower spectral range, e.g. 100 nm, one can safely truncate Eq. (7) and use only the first 3 parameters. In the limit case where one is interested in a very narrow spectral band (in which case very thick retarders would be most likely needed) one can treat Δn_λ as a constant with only one parameter.

In our system, the calibration in completed with two successive spectrum acquisitions, using normalized light intensities:

- An achromatic polarizer is used to set a Stokes vector $(1,1,0,0)^T$ producing an intensity $I(\lambda) = 1 + \cos(\delta_{2\lambda})$ that depends only on the properties of the second retarder. An iterative optimization algorithm (differential evolution method) is then used to determine the calibration parameters of the second retarder (d_2, A_2, B_2, C_2, D_2, E_2 and F_2).
- The polarizer is rotated by 45° to set a Stokes vector $(1,0,1,0)^T$ producing, for this orientation, an intensity $I(\lambda) = 1 + \sin(\delta_{1\lambda})\sin(\delta_{2\lambda})$. The parameters of the second retarder are fixed to those determined in the previous step and an optimization algorithm is used again to determine the calibration parameters of the first retarder (d_1, A_1, B_1, C_1, D_1, E_1 and F_1).

Fig. 3 shows the birefringence obtained for the first and second retarders during calibration. As both retarders are made from the same material (sapphire), in principle the same values would be expected for both retarders. However, the calibration of our polarimeter is more robust when the birefringence values of the retarders are treated independently, so that slightly different birefringence values are obtained for each retarder, as shown in Fig. 3. These small differences are likely justifiable by small misaligments or stresses that can be introduced during the cut and polish of the crystals. The thickness values obtained were close to the nominal values, with $d_2 = 2.00 \pm 0.01$ mm and $d_1 = 3.02 \pm 0.01$ mm.

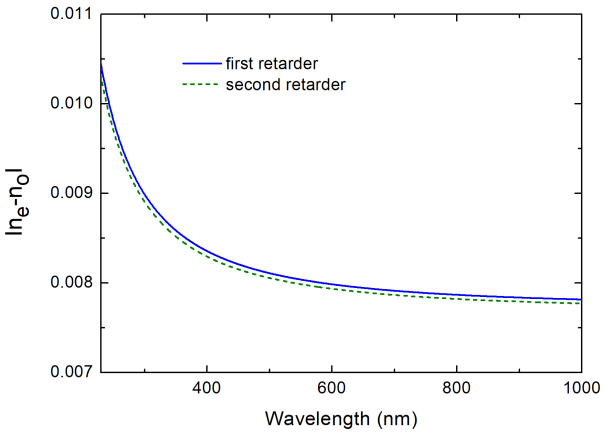

Fig. 3. Wavelength dispersion of the birefringence of Sapphire obtained from the calibration of the first and second retarders.

5. APPLICATION TO THE MEASUREMENT OF OPTICAL ROTATION

We will illustrate the utilization of the spectral polarimeter in the measurements of the optical rotation of chiral solutions. This is one of the earliest applications of polarimetry (dating back to the XIX century) and still remains popular as it has important applications in the pharmaceutical industry, food industry, the cosmetics industry, chemical science, forensic science, etc. Commercial polarimeters used in the measurements of optical rotation typically use a time-dependent approach by either using high-resolution rotary encoders or Faraday rotators and offer measurements on some selected wavelengths. For historical reasons, 589 nm light (the sodium D line) is the most-used wavelength for optical rotation measurements. Our spectral polarimeter cannot offer measurements at sharply defined wavelengths, but it is well-suited for this type of measurements as for most transparent substances or materials optical rotatory

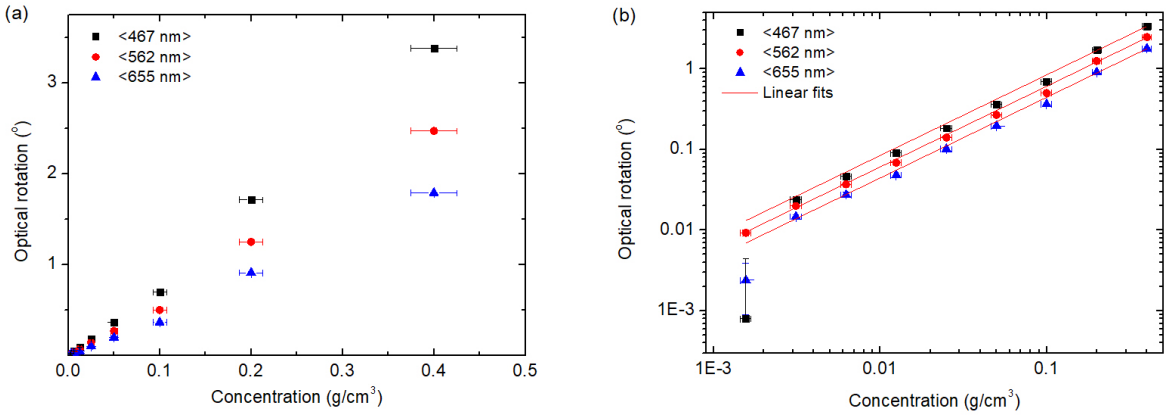

Fig. 4. Optical rotation of a sucrose solution at varying concentrations: linear scales (a) and logarithmic scales (b).

dispersion in the visible range (above 450 nm) is relatively small and smoothly varying. As discussed above, if we wanted to increase the spectral resolution of our polarimeter we should use thicker retarders and a higher-resolution spectrometer.

The main challenge for optical rotation measurements is being able to detect the small optical rotations generated by solutions with low concentrations of chiral solutes. Therefore, polarimeters working in this field specialize in small angles of polarization rotation. The best commercial instruments report a measurement accuracy around $\pm 0.002^\circ$ and, in most cases, the measurement involves moving optical components with very high-quality motors [20].

To measure optical rotation with the spectral polarimeter shown in Fig. 2, one can simply send linearly polarized light with a certain known azimuth, ψ, to the device. The azimuth can be obtained from the Stokes components as:

$$\psi = \frac{1}{2}(\text{atan2}(S_2, S_1)), \tag{8}$$

where atan2 is the four-quadrant inverse tangent that uses two arguments. Then, when a cell or a cuvette with an optically active solution is introduced in the beam path there will be a small rotation of the polarization direction. By measuring the change in the azimuth direction, the spectral polarizer will determine the optical rotation produced by the chiral solution.

The spectral range was chosen between 420 nm and 700 nm and it was divided into three sections so that the spectral resolutions of the final measurements were $\sim$ 100 nm. We associate the measured optical rotation in each section with the central wavelength of the section. This association is an approximation since what we are effectively measuring is the averaged optical rotation for the whole section but, given the relatively small dispersion of optical rotation in the visible range, we consider this association to be reasonable enough for this illustrative experiment. We prepared an initial sucrose solution by dissolving 40 gr of table sugar (sucrose) in 100 ml of water. Measurements were done in a quartz cuvette of 10 mm pathlength. At this initial concentration, the measured optical rotation was more than 3° for the section with lowest wavelength (central value of 467 nm). The main objective of this prospective experiment was to search for the smallest amount of optical rotation that the polarimeter could detect. Next, we started to dilute the solution in several successive steps, making in each step a 1:1 dilution in water with the solution resulting from the previous step. For the solutions obtained at each, step we measured the new optical rotation. After 8 dilutions, the lowest concentration we tested was around 0.0015 g/cm^3.

Fig. 4 shows the results of the optical rotation experiment for the three wavelength regions examined (that had central wavelengths of 467 nm, 562 nm and 655 nm). The plots of optical rotation vs concentration show the expected linear trend. The results for the low-concentration solutions are better visualized with the logarithmic scales shown in Fig. 4b. In the region with central wavelength 562 nm, the method was able to properly resolve optical rotations below 0.01°, for the solution with the lowest concentration. However, for the regions with central wavelengths 467 nm and 655 nm, the polarimeter could only offer reliable measurements until the concentration second to last. For the section with shortest wavelengths this is probably due to the limited spectral resolution of our spectrometer, that cannot fully resolve the high-frequency spectral oscillations introduced by the retarders, as was already visible in Fig. 2c. For the section corresponding to longer wavelengths, the reduced resolution in optical rotation detection is probably produced by the non-optimal conditioning of Eq. (6) in this spectral range, as less modulation cycles are analyzed. We also performed the same measurements using a higher number of sections, which resulted in a better spectral resolution of the optical rotation values. However, as suggested by Fig. 1, this was detrimental for the matrix inversion process, leading to more noise and errors. For example, when using 6 sections (spectral resolution of $\sim$ 50 nm) we only obtained physically consistent results in all 6 sections for concentrations above 0.03 g/cm^3, while when using 3 sections we could still measure well concentrations around 0.003 g/cm^3, as it is shown in Fig. 4.

6. CONCLUSIONS

In this work, we have shown that spectrally modulated polarimetry can be easily analyzed without necessarily using a channeled approach, i.e., without doing any Fourier transform. We have presented a new method to perform the spectral domain analysis directly in the wavelength domain without the need to do any conversion to wavenumber. This method, which

is also of common application in the time-domain, only uses linear algebra with a least-squares estimator, the pseudoinverse, to find the best match to the data. The implementation of this approach is very simple and it is particularly well suited for dispersive spectrometers that measure the intensity as function of wavelength. This method has been illustrated with a compact and low-cost Stokes polarimeter that is an ideal instrument for applications that require a high sensitivity and accuracy but that do not demand a high spectral resolution. We have used this instrument to measure the small polarization rotation generated by very diluted solutions of chiral molecules.

Funding. Ministerio de Ciencia Innovación y Universidades RYC2018-024997-I and RTI2018-098410-J-I00 (MCIU/AEI/FEDER, UE). Dirección General de Asuntos del Personal Académico, Universidad Nacional Autónoma de México PAPIIT IG100121.

Acknowledgments. Luis Oscar González-Siu acknowledges a grant provided under the Programa Nacional de Posgrados de Calidad (PNPC) of Consejo Nacional de Ciencia y Tecnología (CONACYT) and Programa de Maestría y Doctorado en Ingeniería (PMDI) from the National Autonomous University of Mexico (UNAM).

Disclosures. The authors declare no conflicts of interest.

Data Availability. Data underlying the results presented in this paper are not publicly available at this time but may be obtained from the authors upon reasonable request.

REFERENCES

1. K. Oka and T. Kato, "Spectroscopic polarimetry with a channeled spectrum," Opt. letters **24**, 1475–1477 (1999).
2. F. J. Iannarilli Jr, S. H. Jones, H. E. Scott, and P. L. Kebabian, "Polarimetric-spectral intensity modulation (p-sim): enabling simultaneous hyperspectral and polarimetric imaging," in *Infrared technology and applications XXV,* vol. 3698 (International Society for Optics and Photonics, 1999), pp. 474–481.
3. K. Nordsieck, "A simple polarimetric system for the lick observatory image-tube scanner," Publ. Astron. Soc. Pac. **86**, 324 (1974).
4. M. W. Kudenov, N. A. Hagen, E. L. Dereniak, and G. R. Gerhart, "Fourier transform channeled spectropolarimetry in the mwir," Opt. express **15**, 12792–12805 (2007).
5. Y. Otani, T. Wakayama, K. Oka, and N. Umeda, "Spectroscopic mueller matrix polarimeter using four-channeled spectra," Opt. communications **281**, 5725–5730 (2008).
6. A. S. Alenin and J. S. Tyo, "Generalized channeled polarimetry," JOSA A **31**, 1013–1022 (2014).
7. M. W. Kudenov, M. J. Escuti, E. L. Dereniak, and K. Oka, "White-light channeled imaging polarimeter using broadband polarization gratings," Appl. optics **50**, 2283–2293 (2011).
8. G. Zhou, Y. Li, and K. Liu, "Reconstruction and calibration methods for a mueller channeled spectropolarimeter," Opt. Express **30**, 2018–2032 (2022).
9. K. Oka and T. Kaneko, "Compact complete imaging polarimeter using birefringent wedge prisms," Opt. express **11**, 1510–1519 (2003).
10. L. O. González-Siu and N. C. Bruce, "Error analysis of channeled stokes polarimeters," Appl. Opt. **60**, 4511–4518 (2021).
11. L. O. González-Siu and N. C. Bruce, "Analysis of experimental errors in mueller matrix channeled polarimeters," Appl. Opt. **60**, 5456–5464 (2021).
12. A. Taniguchi, K. Oka, H. Okabe, and M. Hayakawa, "Stabilization of a channeled spectropolarimeter by self-calibration," Opt. letters **31**, 3279–3281 (2006).
13. D. S. Sabatke, A. M. Locke, E. L. Dereniak, and R. W. McMillan, "Linear calibration and reconstruction techniques for channeled spectropolarimetry," Opt. express **11**, 2940–2952 (2003).
14. D. S. Sabatke, A. M. Locke, E. L. Dereniak, and R. W. McMillan, "Linear operator theory of channeled spectropolarimetry," JOSA A **22**, 1567–1576 (2005).
15. R. A. Chipman, "Polarimetry," in *Handbook of Optics,* vol. 2 M. Bass, ed. (McGraw-Hill, Cambridge, 1995), chap. 22.
16. O. Arteaga, M. Baldrís, J. Antó, A. Canillas, E. Pascual, and E. Bertran, "Mueller matrix microscope with a dual continuous rotating compensator setup and digital demodulation," Appl. Opt. **53**, 2236–2245 (2014).
17. S. Bian, C. Cui, and O. Arteaga, "Mueller matrix ellipsometer based on discrete-angle rotating fresnel rhomb compensators," Appl. Opt. **60**, 4964–4971 (2021).
18. O. Arteaga, J. Freudenthal, B. Wang, and B. Kahr, "Mueller matrix polarimetry with four photoelastic modulators: theory and calibration," Appl. optics **51**, 6805–6817 (2012).
19. H. Li, C. Cui, S. Bian, J. Lu, X. Xu, and O. Arteaga, "Model-free determination of the birefringence and dichroism in c-cut crystals from transmission ellipsometry measurements," Appl. Opt. **59**, 2192–2200 (2020).
20. A. J. Harvie, T. Phillips, and J. C. deMello, "A high-resolution polarimeter formed from inexpensive optical parts," Sci. reports **10**, 1–12 (2020).

Responding to the Reviewer's comments

As the work presented in this chapter has been published as a scientific paper, it led to a productive discussion with a specialist in the field of polarimetry. This exchange, which included insightful questions and comments, addressed key points of the study. We deemed it valuable to include this discussion here to address potential common inquiries and further clarify important aspects of the work.
The reviewer's comments are put first (R), followed by our answers (A).

R: The authors divide the spectrum into three sections whose central wavelengths are 467nm, 562nm, and 655nm. The authors consider the Stokes vector in each section to be constant and obtain the optical rotation for a certain wavelength region. The optical rotation is wavelength-depended, but in Fig.4.4, the authors use the central wavelength to describe the optical rotation for a certain wavelength region, does the experimental result actually reflect the optical rotation of the central wavelength? Or there may be a relation or approximation between them, please give the explanation. Please explain the physics meaning of the optical rotation for a wavelength region to make this process more convincing.

A: In our demonstration experiment, we split the visible spectrum into three sections, and we associate the measured optical rotation with the central wavelength of each section. As suggested by the reviewer, this association is an approximation, but we think it is reasonable enough for this application. What we are effectively measuring is the "averaged" optical rotation in the whole section that, for example, would coincide with the optical rotation of the central wavelength if the variation of optical rotation with wavelength within the section was a linear function, but not necessarily for other line shapes. However, as the dispersion of optical rotation for transparent materials in the visible range is rather small and the sections relatively narrow, we consider that this approximation is sufficient. For applications demanding a higher spectral resolution it would be advisable to use a higher number of sections combined with thicker retarders.

R: The spectral resolution of the experimental result might be too low, the reconstruction method in Ref. [8] can obtain the Stokes spectra and may improve the spectral resolution.

A: We agree that the reconstruction method in Ref [8] may improve the spectral resolution. We also think, as it is shown in Fig. 1, that for a given system there is always a trade-off between spectral resolution and signal-to-noise of the polarimetry measurement. Therefore, for applications demanding both high spectral resolution and high signal-to-noise it would be essential to have a very high-resolution spectrometer what would permit the use of thick retarders. We have added a sentence right before section 3 to explain this point.

R: Equation (2) may lose 1/2 and there is minus not plus sign before S3, please check Ref.[1]
Equation (4) loses minus sign before the fourth component.

A: We thank reviewer for pointing the sign errors. We have corrected the signs in equation (2) and in equation (4). The overall 1/2 multiplying factor coming from the polarizer is just a scale factor that has no influence in the results and analysis shown, therefore we have opted to omit it for simplicity.

R: The 'minimization algorithm' mentioned in the third paragraph section.4, may cause confusion, and a specific explanation might be required.

A: We thank reviewer 1 for this remark, we have changed the expression of minimization algorithm in section 4 by "optimization algorithm" and we have given more details on the specific algorithm used (differential evolution method.)

Bibliography

[1] Eugene Frankel. "Corpuscular optics and the wave theory of light: the science and politics of a revolution in physics". In: *Social studies of science* 6.2 (1976), pp. 141–184.

[2] Bart Kahr and Oriol Arteaga. "Arago's best paper". In: *ChemPhysChem* 13.1 (2012), pp. 79–88.

[3] Theresa Levitt. *The Shadow of Enlightenment: Optical and Political Transparency in France 1789-1848*. Oxford University Press, 2009.

[4] George Gabriel Stokes. "On the composition and resolution of streams of polarized light from different sources". In: *Transactions of the Cambridge Philosophical Society* 9 (1852), pp. 399–416.

[5] R Clark Jones. "A new calculus for the treatment of optical systemsi. description and discussion of the calculus". In: *Josa* 31.7 (1941), pp. 488–493.

[6] H Müeller. "The foundations of Optics". In: *J. Opt. Soc. Am* 38 (1948), p. 661.

[7] Jose Carlos del Toro Iniesta. *Introduction to spectropolarimetry*. Cambridge university press, 2003, pp. 2–5.

[8] Shivaramakrishnan Pancharatnam. "Generalized theory of interference, and its applications: Part I. Coherent pencils". In: *Proceedings of the Indian Academy of Sciences-Section A*. Vol. 44. 5. Springer. 1956, pp. 247–262.

[9] Michael V Berry. "The adiabatic phase and Pancharatnam's phase for polarized light". In: *Journal of Modern Optics* 34.11 (1987), pp. 1401–1407.

[10] Kazuhiko Oka and Takayuki Kato. "Spectroscopic polarimetry with a channeled spectrum". In: *Optics letters* 24.21 (1999), pp. 1475–1477.

[11] Pierre Cuvelier. "Les Experimenta crystalli Islandici disdiaclastici d'Erasme Bartholin. Traduction française commentée". In: *Revue d'histoire des sciences* 30.3 (1977), pp. 193–224.

[12] Christiaan Huygens. *Traité de la lumière: avec un Discours de la cause de la pesanteur*. Gressner & Schramm, 1966, pp. 48–100.

[13] Isaac Newton. *Opticks, or, a treatise of the reflections, refractions, inflections & colours of light*. Courier Corporation, 1952.

[14] Jean-Louis Basdevant. "Famous optician: Augustin Fresnel and the wave theory of light". In: *Photoniques* (2019), pp. 18–22.

[15] Bob Guenther. "Etienne Louis Malus". In: *Optics and Photonics News* 10.7 (1999), p. 24.

[16] Gábor Horváth. "Polarization Patterns in Nature: Imaging Polarimetry with Atmospheric Optical and Biological Applications : Thesis to Obtain the Degree Doctor of Hungarian Academy of Sciences". PhD thesis. Biooptics Laboratory Department of Biological Physics Loránd Eötvös University, 2003, pp. 1–7.

[17] Giuseppe Pelosi. "Etienne-Louis Malus: The Polarization of Light by Refraction and Reflection is Discovered [Historical Corner]". In: *IEEE Antennas and Propagation Magazine* 51.4 (2009), pp. 226–228.

[18] Edward Collett. *Field guide to polarization*. eng. SPIE field guides ; v. FG05. Bellingham, Wash: SPIE Press, 2005. ISBN: 0819458686.

[19] Frédéric Leclercq. "Arago, Biot, and Fresnel elucidate circular polarization". In: *Revue dhistoire des sciences* 66.2 (2013), pp. 395–416.

[20] T Martin Lowry. "Optical rotatory power". In: *Journal of the Society of Chemical Industry* 54.20 (1935), pp. 477–483.

[21] GP Konnen. *Polarized light in nature*. CUP Archive, 1985, pp. 1–21.

[22] Frédéric Leclercq. "Biot, Chromatic Polarization, and the Theory of Fits". In: *Revue dhistoire des sciences* 64.1 (2011), pp. 121–156.

[23] T. Martin (Thomas Martin) Lowry. *Optical rotatory power*. Dover, 1964.

[24] Shane Cloude. *Polarisation: applications in remote sensing*. OUP Oxford, 2009.

[25] Dennis H Goldstein. *Polarized light*. CRC press, 2017.

[26] A Fresnel. *Oeuvres complètes d'Augustin Fresnel (HH Sénarmont, E. Verdet, & L. Fresnel, Eds.). Paris: Imprimerie Impériale*. 1866.

[27] Subrahmanyan Chandrasekhar. *Radiative transfer*. Courier Corporation, 1960.

[28] Michael I Mishchenko and Larry D Travis. "Maxwell's equations, electromagnetic waves, and Stokes parameters". In: *Photopolarimetry in remote sensing*. Springer, 2004, pp. 1–44.

[29] Oriol Arteaga. *P. Soleillet*. URL: https://www.mmpolarimetry.com/historic-biography-remarks/. (accessed: 31.07.2024).

[30] Paul Soleillet. "Sur les paramètres caractérisant la polarisation partielle de la lumière dans les phénomènes de fluorescence". In: *Annales de physique*. Vol. 10. 12. 1929, pp. 23–97.

[31] RS Krishnan. "Scattering of light in optical glasses". In: *Proceedings of the Indian Academy of Sciences-Section A*. Vol. 3. 1. Springer. 1936, pp. 211–220.

[32] RS Krishnan. "The reciprocity theorem in colloid optics and its generalisation". In: *Proceedings of the Indian Academy of Sciences-Section A*. Vol. 7. 1. Springer India New Delhi. 1938, pp. 21–34.

[33] Francis Perrin. "Polarization of light scattered by isotropic opalescent media". In: *The Journal of Chemical Physics* 10.7 (1942), pp. 415–427.

[34] William A Shurcliff. *Polarized light: production and use*. Harvard University Press, 1962.

[35] Nathan Grier Parke. "Matrix optics". PhD thesis. Massachusetts Institute of Technology, 1948.

[36] SSS Group. *Polarization Image Sensor Technology*. URL: https://www.sony-semicon.com/en/feature/2021052801.html. (accessed: 22.08.2024).

[37] Douglas B. Murphy et. al. *Principles of Birefringence*. URL: https://www.microscopyu.com/techniques/polarized-light/principles-of-birefringence. (accessed: daily updated).

[38] Edmund Optics. *Introduction to Polarization.* URL: https://www.edmundoptics.com/knowledge-center/application-notes/optics/introduction-to-polarization/. (accessed: 29.08.2024).

[39] S. Ohsuka and H. Takamoto. *Photon terrace : Let's learn about light.* URL: http://photonterrace.net/en/photon/category/. (accessed: 24.08.2024).

[40] José J Gil and Razvigor Ossikovski. *Polarized light and the Mueller matrix approach.* CRC press, 2022.

[41] Oriol Arteaga. *study of the geometrical phase using geometrical phase lenses and polarization diffraction gratings.* Lab practice, University of Barcelona. 2020.

[42] Ramonika Sengupta, Brijesh Tripathi, and Asha Adhiya. "Explicit Reconstruction of Polarization Ellipse using Rotating Polarizer". In: *arXiv preprint arXiv:2211.15244* (2022).

[43] Yutao Sang et. al. *Circularly Polarized Luminescence in Nanoassemblies: Generation, Amplification, and Application.* URL: https://www.researchgate.net/figure/A-The-relationship-between-unpolarized-light-and-linearly-and-circularly-polarized_fig2_335073108. (accessed: daily updated).

[44] Oriol Arteaga Barriel. "Mueller matrix polarimetry of anisotropic chiral media". PhD Thesis. Barcelona, Spain: Universitat de Barcelona, 2010.

[45] Eugene Hecht. *Optics.* Pearson Education Limited, 2017.

[46] George R Bird and WA Shurcliff. "Pile-of-plates polarizers for the infrared: improvement in analysis and design". In: *JOSA* 49.3 (1959), pp. 235–237.

[47] P. Schattschneider, S. Rubino, and C. Hébert. "Circular Dichroism in the Transmission Electron Microscope". In: *Reference Module in Materials Science and Materials Engineering*. Elsevier, 2016. ISBN: 978-0-12-803581-8.

[48] Colman Buckley. "Conception et réalisation d'un endomicroscope polarimétrique de Mueller à fibre en vue d'une application à l'aide au diagnostic médical in vivo". PhD thesis. Université de Limoges, 2020.

[49] Grant Sanderson. *The Sugar Water Barber Pole Effect | Optical Puzzles 1.* URL: https://www.youtube.com/watch?v=QCX62YJCmGk. (accessed: 01.09.2023).

[50] Thorlabs groupe. *Using the Poincare Sphere to Represent the Polarization State*. URL: https://www.thorlabs.com/newgrouppage9.cfm?objectgroup_id=14200. (accessed: 11.09.2020).

[51] Chandroth Pannian Jisha, Stefan Nolte, and Alessandro Alberucci. "Geometric phase in optics: from wavefront manipulation to waveguiding". In: *Laser & Photonics Reviews* 15.10 (2021), p. 2100003.

[52] José J Gil and Eusebio Bernabeu. "Obtainment of the polarizing and retardation parameters of a non-depolarizing optical system from the polar decomposition of its Mueller matrix". In: *Optik (Stuttgart)* 76.2 (1986), pp. 67–71.

[53] Orlando Frazão, José M Baptista, and José L Santos. "Recent advances in high-birefringence fiber loop mirror sensors". In: *Sensors* 7.11 (2007). [doi:10.3390/s7112970], pp. 2970–2983.

[54] Martin W McCall, Ian J Hodgkinson, and Qihong Wu. *Birefringent thin films and polarizing elements*. World Scientific, 2014, pp. 283–347.

[55] Kishore Bhowmik and Gang-Ding Peng. "Polymer optical fibers". In: *Handbook of optical fibers* (2019), pp. 1–51.

[56] Arnaldo G Leal-Junior et al. "Polymer optical fiber sensors in healthcare applications: A comprehensive review". In: *Sensors* 19.14 (2019), p. 3156.

[57] Sneha Bhagyaraj, Oluwatobi Samuel Oluwafemi, and Igor Krupa. "Polymers in optics". In: *Polymer Science and Innovative Applications*. Elsevier, 2020, pp. 423–455.

[58] A Tagaya et al. "Polymer optical fiber amplifier". In: *Applied physics letters* 63.7 (1993), pp. 883–884.

[59] Le Zhou et al. "Advancements and Applications of Liquid Crystal/Polymer Composite Films". In: *ACS Materials Letters* 5.10 (2023), pp. 2760–2775.

[60] Chen Wang and Zhi-yi Zhou. "Optical Properties and Lampshade Design Applications of PLA 3D Printing Materials." In: *BioResources* 18.1 (2023).

[61] Dana Ortansa Dorohoi et al. "Review on Optical Methods Used to Characterize the Linear Birefringence of Polymer Materials for Various Applications". In: *Molecules* 28.7 (2023).

[62] Juliene Oliveira Campos de França et al. "Polymers based on PLA from synthesis using D, L-lactic acid (or racemic lactide) and some biomedical applications: a short review". In: *Polymers* 14.12 (2022), p. 2317.

[63] Akihiro Tagaya. "Birefringence of Polymer". In: *Encyclopedia of Polymeric Nanomaterials*. Ed. by Shiro Kobayashi and Klaus Müllen. Berlin, Heidelberg: Springer Berlin Heidelberg, 2021, pp. 1–6.

[64] C Amendola et al. "Use of 3D printed PLA for diffuse optics". In: *Clinical and Translational Biophotonics*. Optica Publishing Group. 2020, JTh2A–16.

[65] Alexandra Bîrcă et al. "Chapter 1 - Introduction in thermoplastic and thermosetting polymers". In: *Materials for Biomedical Engineering*. Ed. by Valentina Grumezescu and Alexandru Mihai Grumezescu. Elsevier, 2019, pp. 1–28. ISBN: 978-0-12-816874-5.

[66] Nagihan Varol. "Advanced thermal analysis and transport properties of stereocomplex polylactide". PhD thesis. Normandie Université, 2019, p. 64.

[67] Rafael A Auras et al. *Poly (lactic acid): synthesis, structures, properties, processing, and applications*. Vol. 10. John Wiley & Sons, 2011, pp. 113–124.

[68] C Schick. "Differential scanning calorimetry (DSC) of semicrystalline polymers". In: *Analytical and bioanalytical chemistry* 395 (2009), pp. 1589–1611.

[69] Lin Li and Greg Curran. "Determination of Rigid and Mobile Amorphous Content of Semicrystalline Polymers Using DSC". In: *Thermal Analysis Application Note, Perkin Elmer Inc* (2006).

[70] Takashi Yamamoto. "Molecular dynamics simulations of polymer crystallization in highly supercooled melt: Primary nucleation and cold crystallization". In: *The Journal of Chemical Physics* 133.3 (2010).

[71] Andrew Forbes. "Structured light: tailored for purpose". In: *Opt. Photon. News* 31.6 (2020), pp. 24–31.

[72] Gun-Yeal Lee, Jangwoon Sung, and Byoungho Lee. "Recent advances in metasurface hologram technologies". In: *ETRI Journal* 41.1 (2019), pp. 10–22.

[73] Burak Gerislioglu et al. “Monolithic metal dimer-on-film structure: New plasmonic properties introduced by the underlying metal”. In: *Nano letters* 20.3 (2020), pp. 2087–2093.

[74] Burak Gerislioglu et al. “The role of Ge2Sb2Te5 in enhancing the performance of functional plasmonic devices”. In: *Materials Today Physics* 12 (2020), p. 100178.

[75] Michael Berry. “Pancharatnam, virtuoso of the Poincaré sphere: an appreciation”. In: *Current Science* 67.4 (1994), pp. 220–223.

[76] Jihwan Kim et al. “Fabrication of ideal geometric-phase holograms with arbitrary wavefronts”. In: *Optica* 2.11 (2015), pp. 958–964.

[77] Xiao Xiang, Jihwan Kim, and Michael J Escuti. “Far-field and fresnel liquid crystal geometric phase holograms via direct-write photo-alignment”. In: *Crystals* 7.12 (2017), p. 383.

[78] Ravi K Komanduri, Kristopher F Lawler, and Michael J Escuti. “Multi-twist retarders: broadband retardation control using self-aligning reactive liquid crystal layers”. In: *Optics Express* 21.1 (2013), pp. 404–420.

[79] Masaaki Sakakura et al. “Ultralow-loss geometric phase and polarization shaping by ultrafast laser writing in silica glass”. In: *Light: Science & Applications* 9.1 (2020), p. 15.

[80] Chulwoo Oh and Michael J Escuti. “Achromatic polarization gratings as highly efficient thin-film polarizing beamsplitters for broadband light”. In: *Polarization science and remote sensing III*. Vol. 6682. SPIE. 2007, pp. 317–328.

[81] Oriol Arteaga and Hana Bendada. “Geometrical phase optical components: measuring geometric phase without interferometry”. In: *Crystals* 10.10 (2020), p. 880.

[82] Rajendra Bhandari. “Polarization of light and topological phases”. In: *Physics Reports* 281.1 (1997), pp. 1–64.

[83] Ze’ev Bomzon et al. “Space-variant Pancharatnam–Berry phase optical elements with computer-generated subwavelength gratings”. In: *Optics letters* 27.13 (2002), pp. 1141–1143.

[84] Filippus S Roux. “Geometric phase lens”. In: *JOSA A* 23.2 (2006), pp. 476–482.

[85] Lorenzo Marrucci, C Manzo, and D Paparo. "Pancharatnam-Berry phase optical elements for wave front shaping in the visible domain: switchable helical mode generation". In: *Applied Physics Letters* 88.22 (2006).

[86] Yakir Aharonov and J Anandan. "Phase change during a cyclic quantum evolution". In: *Physical Review Letters* 58.16 (1987), p. 1593.

[87] Oriol Arteaga and Adolf Canillas. "Analytic inversion of the Mueller-Jones polarization matrices for homogeneous media". In: *Optics letters* 35.4 (2010), pp. 559–561.

[88] Hao Yu et al. "Pancharatnam–Berry optical lenses". In: *JOSA B* 36.5 (2019), pp. D107–D111.

[89] Erez Hasman et al. "Polarization beam-splitters and optical switches based on space-variant computer-generated subwavelength quasi-periodic structures". In: *Optics Communications* 209.1-3 (2002), pp. 45–54.

[90] Michael J Escuti, Jihwan Kim, and Michael W Kudenov. "Controlling light with geometric-phase holograms". In: *Optics and Photonics News* 27.2 (2016), pp. 22–29.

[91] Oriol Arteaga et al. "Mueller matrix microscope with a dual continuous rotating compensator setup and digital demodulation". In: *Applied optics* 53.10 (2014), pp. 2236–2245.

[92] Ertan Kuntman et al. "Conversion of a polarization microscope into a Mueller matrix microscope. Application to the measurement of textile fibers." In: *Óptica pura y aplicada* 48.4 (2015).

[93] Oriol Arteaga, Shane M Nichols, and Joan Antó. "Back-focal plane Mueller matrix microscopy: Mueller conoscopy and Mueller diffractrometry". In: *Applied Surface Science* 421 (2017), pp. 702–706.

[94] Oriol Arteaga et al. "Mueller matrix polarimetry with four photoelastic modulators: theory and calibration". In: *Applied optics* 51.28 (2012), pp. 6805–6817.

[95] Lingshan Li et al. "Color-selective geometric-phase lenses for focusing and imaging based on liquid crystal polymer films". In: *Opt. Express* 30.2 (Jan. 2022), pp. 2487–2502.

[96] Bruno Piccirillo et al. “Flat polarization-controlled cylindrical lens based on the Pancharatnam–Berry geometric phase”. In: *European Journal of Physics* 38.3 (2017), p. 034007.

[97] Frank J Iannarilli Jr et al. “Polarimetric-spectral intensity modulation (P-SIM): enabling simultaneous hyperspectral and polarimetric imaging”. In: *Infrared technology and applications XXV*. Vol. 3698. International Society for Optics and Photonics. 1999, pp. 474–481.

[98] KH Nordsieck. “A simple polarimetric system for the lick observatory image-tube scanner”. In: *Publications of the Astronomical Society of the Pacific* 86.511 (1974), p. 324.

[99] Michael W Kudenov et al. “Fourier transform channeled spectropolarimetry in the MWIR”. In: *Optics express* 15.20 (2007), pp. 12792–12805.

[100] Yukitoshi Otani et al. “Spectroscopic Mueller matrix polarimeter using four-channeled spectra”. In: *Optics communications* 281.23 (2008), pp. 5725–5730.

[101] Andrey S Alenin and J Scott Tyo. “Generalized channeled polarimetry”. In: *JOSA A* 31.5 (2014), pp. 1013–1022.

[102] Michael W Kudenov et al. “White-light channeled imaging polarimeter using broadband polarization gratings”. In: *Applied optics* 50.15 (2011), pp. 2283–2293.

[103] Guodong Zhou, Yanqiu Li, and Ke Liu. “Reconstruction and calibration methods for a Mueller channeled spectropolarimeter”. In: *Optics Express* 30.2 (2022), pp. 2018–2032.

[104] Hana Bendada et al. “Spectrally modulated polarimetry with wavelength domain analysis”. In: *Applied Optics* 61.19 (2022), pp. 5608–5613.

[105] Kenichiro Otsuka et al. “Intravascular Polarimetry for Tissue Characterization of Coronary Atherosclerosis”. In: *Circulation Reports* 1 (Nov. 2019).

[106] Fengqi Guo et al. “Multi-Dimensional Fusion of Spectral and Polarimetric Images Followed by Pseudo-Color Algorithm Integration and Mapping in HSI Space”. In: *Remote Sensing* 16 (2024).

[107] Kazuhiko Oka and Toshiaki Kaneko. “Compact complete imaging polarimeter using birefringent wedge prisms”. In: *Optics express* 11.13 (2003), pp. 1510–1519.

[108] Luis Oscar González-Siu and Neil C Bruce. “Error analysis of channeled Stokes polarimeters”. In: *Applied Optics* 60.16 (2021), pp. 4511–4518.

[109] Luis Oscar González-Siu and Neil C Bruce. “Analysis of experimental errors in Mueller matrix channeled polarimeters”. In: *Applied Optics* 60.18 (2021), pp. 5456–5464.

[110] Atsushi Taniguchi et al. “Stabilization of a channeled spectropolarimeter by self-calibration”. In: *Optics letters* 31.22 (2006), pp. 3279–3281.

[111] Derek S Sabatke et al. “Linear calibration and reconstruction techniques for channeled spectropolarimetry”. In: *Optics express* 11.22 (2003), pp. 2940–2952.

[112] Derek S Sabatke et al. “Linear operator theory of channeled spectropolarimetry”. In: *JOSA A* 22.8 (2005), pp. 1567–1576.

[113] R. A. Chipman. “Polarimetry”. In: *Handbook of Optics*. Ed. by M. Bass. Vol. 2. Cambridge: McGraw-Hill, 1995. Chap. 22.

[114] Subiao Bian, Changcai Cui, and Oriol Arteaga. “Mueller matrix ellipsometer based on discrete-angle rotating Fresnel rhomb compensators”. In: *Applied Optics* 60.16 (2021), pp. 4964–4971.

[115] Huihui Li et al. “Model-free determination of the birefringence and dichroism in c-cut crystals from transmission ellipsometry measurements”. In: *Appl. Opt.* 59.7 (Mar. 2020), pp. 2192–2200.

[116] Andrew J Harvie, TW Phillips, and John Christian deMello. “A high-resolution polarimeter formed from inexpensive optical parts”. In: *Scientific reports* 10.1 (2020), pp. 1–12.


الحمد لله الذي بنعمته تتم الصالحات

ملخص:

ان فهم تفاعلات الضوء عند التقائه مع المادة الفيزيائية هو أمر بالغ الأهمية نظرا للمعلومات التي يسمح باستخلاصها عن تلك المادة، و التي تؤسس لتعزيز و تطوير الخصائص البصرية والهيكلية للمواد، و بخاصة المواد المخصصة لمهمات وظيفية حساسة. و من هذا المنطلق فان خاصية استقطاب الضوء و التقنيات التي تعتمد عليها توفر نهجًا فريدًا ومفصلًا لهذ التحدي. تركز هذه الأطروحة على تطبيق مبدأ ستوكس-مولر الرياضي لدراسة وسائط مختلفة، بهدف استخدام استقطاب الضوء كأداة دقيقة لتوصيف الخصائص البصرية لأنواع مختلفة من المواد. من خلال تطوير وتأكيد منهجيات مبتكرة، تسلط هذه الدراسة الضوء على إمكانيات التنوع في القياس القطبي كأداة لتقدم علم المواد الوظيفية، لا سيما في دراسة الوسائط مزدوجة الانكسار، الوسائط ذات الأطوار البصرية الهندسية وأيضا الجزيئات اللولبية. تحتوي هذه الأطروحة على جزء نظري غني بالمعلومات المتعلقة بالموضوع و 3 أجزاء منفصلة: الأول حول تقديم طريقة جديدة وتأسيس مبادئها الرياضية، والثاني حول استخدام أدوات الاستقطاب لتقييم أداء مواد تم تطويرها مؤخرًا؛ بينما يقدم الجزء الثالث النظر في طريقة استقطاب موجودة بمبدأ علمي مختلف. و في النهاية خلصنا إلى أن هذه الطريقة الاستقطابية المبنية على صيغة ستوكس-مولر تمثل حلاً ناجعا وقد أثبتت فعاليتها وفائدتها العالية في ميادين مختلفة.

Résumé:

La compréhension des interactions lumière-matière est essentielle pour améliorer les propriétés optiques et structurelles des matériaux, et les techniques polarimétriques offrent une approche unique et détaillée de ce défi. Cette thèse se concentre sur l'application du formalisme de Stokes-Mueller pour étudier divers milieux, dans le but d'utiliser la polarimétrie comme un outil précis pour caractériser les propriétés optiques de différents types de matériaux. Grâce au développement et à la validation de méthodologies innovantes, le travail met en évidence le potentiel de la diversité polarimétrique pour faire progresser la science des matériaux, en particulier dans l'étude des milieux biréfringents, des éléments optiques de phase géométrique (la phase de Pancharatnam-Berry) et des molécules chirales.

Abstract:

Understanding light-matter interactions is critical to enhancing the optical and structural properties of materials, and polarimetric techniques offer a unique and detailed approach to this challenge. This thesis focuses on the application of Stokes-Mueller formalism to investigate various media, with the goal of using polarimetry as a precise tool for characterizing optical properties across different material types. Through the development and validation of innovative methodologies, the work highlights the potential of polarimetric diversity in advancing material science, particularly in the study of birefringent media, Pancharatnam–Berry phase optical elements, and chiral molecules.